JPRS L/10088

3 November 1981

USSR Report

METEOROLOGY AND HYDROLOGY

No. 5, May 1981

FBIS FOREIGN BROADCAST INFORMATION SERVICE

FOR OFFICIAL USE ONLY

APPROVED FOR RELEASE: 2007/02/09: CIA-RDP82-00850R000400070003-7

NOTE

JPRS publications contain information primarily from foreign newspapers, periodicals and books, but also from news agency transmissions and broadcasts. Materials from foreign-language sources are translated; those from English-language sources are transcribed or reprinted, with the original phrasing and other characteristics retained.

Headlines, editorial reports, and material enclosed in brackets [] are supplied by JPRS. Processing indicators such as [Text] or [Excerpt] in the first line of each item, or following the last line of a brief, indicate how the original information was processed. Where no processing indicator is given, the information was summarized or extracted.

Unfamiliar names rendered phonetically or transliterated are enclosed in parentheses. Words or names preceded by a question mark and enclosed in parentheses were not clear in the original but have been supplied as appropriate in context. Other unattributed parenthetical notes within the body of an item originate with the source. Times within items are as given by source.

The contents of this publication in no way represent the policies, views or attitudes of the U.S. Government.

APPROVED FOR RELEASE: 2007/02/09: CIA-RDP82-00850R000400070003-7

JPRS L/10088

3 November 1981

USSR REPORT

METEOROLOGY AND HYDROLOGY

No. 5, May 1981

Translation of the Russian-language monthly journal METEOROLOGIYA I GIDROLOGIYA published in Moscow by Gidrometeoizdat.

CONTENTS

UDC 551.577.21(217.17)

CLIMATIC VARIABILITY OF TOTAL MONTHLY PRECIPITATION IN THE NORTHERN HEMISPHERE

Moscow METEOROLOGIYA I GIDROLOGIYA in Russian No 5, May 81 pp 5-16

[Article by Professor G. V. Gruza, Candidate of Geographic Sciences Ye. G. Apasova, All-Union Scientific Research Institute of Hydrometeorological Information--World Data Center, manuscript received 16 Sep 80]

[Text] Abstract: A study is made of variability characteristics of total monthly precipitation anomalies with respect to individual regions and latitudinal belts of the northern hemisphere in January and July 1891-1979 in the 0-85° north latitude zone.

The quality of the initial data on the precipitation anomalies obtained by visual interpolation to the nodes of the geographic coordinate grid with 2.5° grid intervals is estimated.

The statistical parameters of the anomalies were calculated with respect to several segments of the instrument observation period. It is demonstrated that depending on the scale of the area averaging and the time period, the magnitude and sign of the linear trend vary significantly. On the whole, over an 89-year period throughout the hemisphere the anomalous nature of the January precipitation is increasing, and July, decreasing.

By comparison with the temperature, the total monthly precipitation is characterized by much greater spatial variability. Accordingly, and for other generally known reasons, climatic conditions have long been studied by station observation data. However, the necessity for evaluating the precipitation climate for an entire hemisphere, similarly to how this has been done in a number of global temperature studies (the last of which [1], also contains recommendations on the forms of representation of empirical characteristics), leads to the conclusion of expendiency of using a data which are smoother and more regular in space. In the present paper, the original maps of [4] have been selected as the source of information from which by visual interpolation, an archive of precipitation anomalies has been created for January and July 1891 to 1960 in percentages of the long-term mean (the norm) at the nodes of a coordinate grid of points with parallel and meridian intervals of 2.5°. The data for 1961-1975 were prepared at the GGO [Main Geophysical Observatory] by the procedure of [4], and maps of the anomalies in percentages of the "Clino" norms (1931-1960) compiled at the USSR Hydrometeorological Center were used for 1976-1979.

By comparison with the total precipitation field, the anomaly field is more uniform in space inasmuch as the division by the "norm" smooths the regional singularities. Additional smoothing is accomplished by visual interpolation. On the whole, the quality of the archive data varies as a function of the method of measuring the precipitation and processing the measurement results, the accuracy of which is determined by the methods of calculating the norms, reproduction of the uniformity of the series, anomaly mapping, and also visual interpretation from the maps, and so on. Without discussing the measurement procedure, which has been sufficiently discussed in the specialized literature, let us try to evaluate the quality of the preparation of the archive which will naturally be approximate inasmuch as it does not appear possible to define exact quality criteria as yet. The precision of the interpolated anomaly fields depends primarily on the density of the network, approximately characterized by the number of stations used when preparing the maps (Figure 1).

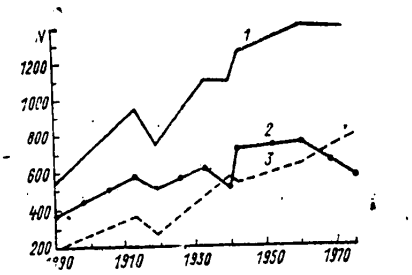

Figure 1. Variation of the number of stations in 1891-1979.
1 -- northern hemisphere, 2 -- foreign territory, 3 -- USSR

Until 1910 the network was two or three times smaller than at the present time, and during the world wars, the number of stations diminished abruptly. On the whole throughout the hemisphere 1400 stations have been recently used. Is this many or few? Obviously, it is not so simple to answer this question, for calculation of the required number of observations is complicated by the anisotropicity of the spatial correlation function which is still unknown to us.

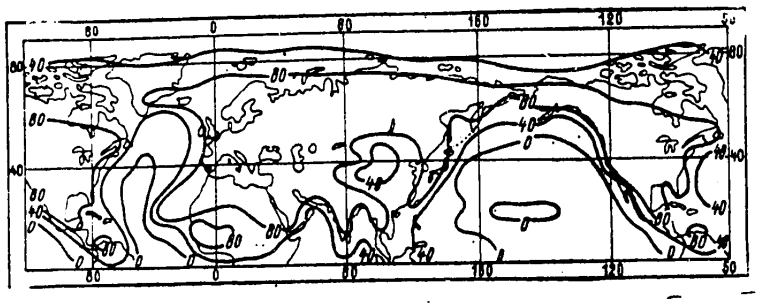

Figure 2. Quantity of data at the nodes of the coordinate grid, 1891-1979

Let us use a map of the number of observations at each node for 89 years to characterize the completeness of the data (Figure 2). Its distribution with respect to the hemisphere is far from uniform. The blank spots are the central parts of the oceans; the series is insufficiently long in the polar and equatorial regions and in the Tibetian Highlands. The existing gaps, generally speaking, can be filled in, as has been done, for example, in [10] for precipitation over the Pacific Ocean. At the present time it is possible to use satellite observations for this purpose. Establishment of this type of relation is a subject for independent research.

As for uniformity of the series, an indirect characteristic of which can be the value of $\delta R = R - 100$ characterizing the difference between the ideal anomaly norm (100%) and the actual long-term mean $\bar{R}$ for the investigated period, judging by the maps of δR the uniformity is disturbed in the American sector of the Arctic, the oceans and at the boundaries of arid zones which have different locations in January and July. The latter include regions where precipitation does not fall annually (Africa, Central Asia). In the temperate latitudes of both continents δR does not exceed $\pm 5\%$, including the territory of the USSR where, as is known, the measurement procedure and norms have changed many times. Thus, it is possible that the norms calculated over 50 or more years do not depend on the limits of the period [8]. The procedure for processing the initial data for anomaly maps is discussed in more detail in [4].

An idea of the accuracy of the interpolation can be obtained when comparing the spatial correlation of the total monthly precipitation in the central regions of the European part of the USSR with interrelation between the anomalies in Moscow and the grid node closest to it, the distance between which was 174 km (Table 1). In the first column of the table the autocorrelation of the station observations is presented for this distance (according to the data of [6, 7]). In the winter this autocorrelation turned out to be higher, and in the summer, lower, then the precipitation correlation at Moscow Station and at the nearest node of the grid included in the investigated archive (the second column). It is possible that the summer precipitation is smoothed to a higher degree by visual interpolation than the winter precipitation.

Table 1. Correlation Coefficients of the Total Monthly Precipitation

Precipitation at the stations according to the data of [6, 7]		Precipitation at the node $\phi=55°$ north latitude, $\lambda=40°$ east and at Moscow Station	
January	July	January	July
0.75	0.54	0.73	0.62

In order to check the correspondence of the archive data to the actual fields, a comparison was also made between the behavior of the deviations from the norm of the long-term average precipitation for America taken from [9] with the curves in Figure 6, which demonstrates their similarity.

Considering the rounding (10%) used when preparing the archive and the maps of δR that we obtained, the conclusion must be drawn that the errors connected with nonuniformity of the series and other errors do not go outside this limit in the temperate zone. Over the American sector of the Arctic and the shipping lanes

of the oceans the errors increase, and the data become unreliable. On the whole it is possible to consider that the archive data reflect the basic laws of precipitation and can be used in the first approximation to estimate the climatic parameters.

The statistical precipitation characteristics, including smoothed over large territories, have been investigated many times, but the global field is the initial subject only in a small number of papers [3, 5, 9]. The University of Colorado is conducting a planned study of the precipitation conditions over the continental zones -- American, Eurasia, Africa [9]. The precipitation spectra averaged over 10-degree latitudinal zones in the Northern and Southern Hemispheres are presented in [11].

Having more complete data over a longer period of time than in [9] and data that is more reliable than in [11], we are able to obtain a number of important variability parameters, the procedure for the calculation of which was developed in [2] and used in [3] to process part of the archive. All further conclusions pertain to precipitation anomalies in January and July characterizing the degree of disturbance with respect to the long-term mean monthly total precipitation field. Let us remember that these values, just as the total precipitation, have positive asymmetry of distribution (the mean is greater than the mode), and the lower limit of the anomalies is zero.

The trend of the anomalies over many years can be characterized approximately by the linear trend factor β, that is, the tangent of the slope of the approximating straight line calculated by the time series data at each point of the grid (Figure 3). A visual estimate of the areas indicates insignificant predominance of the regions with increased precipitation in January and decreased in July. On the whole, β does not exceed 1% per year. The β field calculated by the data for the last 19 years looks different (Figure 4). The order of the values increases to 4%/year, and alternation of the regions of opposite signs takes place more frequently. Let us remember that in accordance with the value of δR the information is reliable everywhere with the exception of the oceans. It is also necessary to consider that on the equidistant projection maps in the polar regions, the scale with respect to the parallels is enlarged, and in the equatorial regions, reduced by comparison with the actual scale, which distorts the representation of the proportion of the corresponding areas on the maps.

In order to obtain a more definite idea of the secular variability, let us calculate the mean anomalies over enlarged regions distinguished by certain typical features. The averaging over two continental zones of the hemisphere, as was done in [9], appears to be too generalized, for along with the continental precipitation it is useful to have information about precipitation in individual regions of Asia which have at the present time been distinguished with respect to predominant direction of river runoff and also with respect to the central area where the rivers flow into inland bodies of water. In Table 2 a list of regions is presented, and the number of nodes, by the data of which the weighted mean (weight -- cosine of the latitude) was calculated, is indicated. The information at the nodes falling in the arid zones (in Asia, America, Africa) where $\Delta R=0$ is excluded from the analysis. Analyzing the variability by individual segments of the 89-year period (the data for 1976-1979 calculated short-series and therefore unrepresentative "Clino" norms are excluded from them in the first four intervals) in the regions with most reliable data (Table 3), it is possible to arrive at the following conclusions.

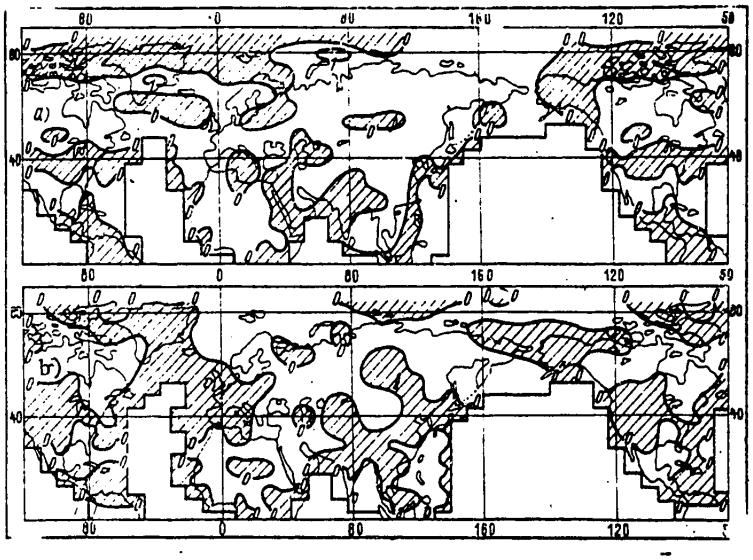

Figure 3. Linear trend factor (%/year), 1891-1979.
a -- January, b -- July

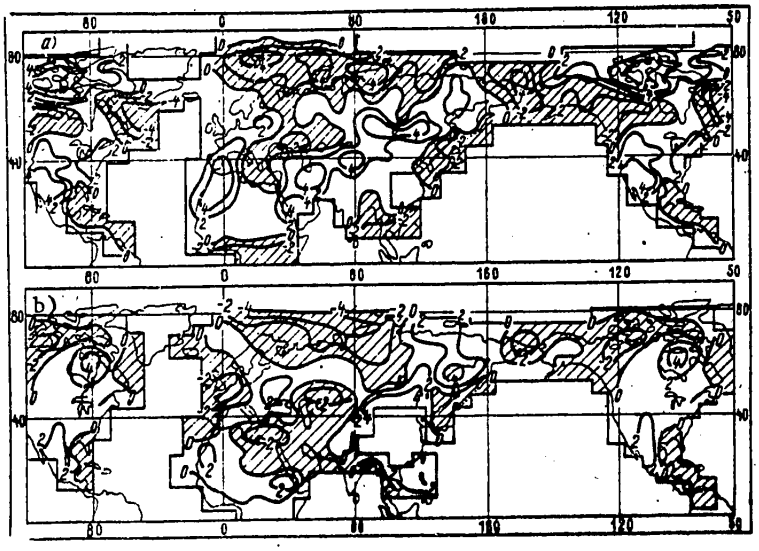

Figure 4. Linear trend factor (%/year), 1961-1979.
a -- January, b -- July

Table 2. Regions of the Northern Hemisphere for Calculating the Mean Precipitation Anomalies

Region	No of points
Eurasia	1098
Northern Asia	391
Central Asia	180
Southern Asia	205
Eastern Asia	145
Europe	235
Africa	285
North America	414

1. The long-term average precipitation anomalies are, as a rule, $<100\%$, which is probably connected with reducing the local maxima during interpolation (Southern and Eastern Asia in January, Central Asia in July, Africa). If we assume that the reduction is systematic, then the conclusion can be drawn that the fluctuations of the means reflect the actual variations in the precipitation conditions.

2. The data for 1976-1979 obtained by the 30-year "Clino" norms are included in the analysis only in two periods out of nine to avoid distortions caused by the nonuniformity. At the same time it is possible to propose that the sharp increase in the precipitation anomalies in the last 16 years and, especially, the last 10 years, is connected with a decrease in the long-term average participation during the 1931-1960 period by comparison with 1891-1975.

3. On the whole in January data is larger than in July for all periods, including for the last decade, when a sharp increase in the anomlies took place in both months.

4. In two periods (1956-1975 and 1966-1975) a decrease in the January precipitation is noted in the Eastern Hemisphere, and an increase in the Western Hemisphere. In July, on the other hand, a negative trend is observed for the greater part of Asia.

5. The relative dispersion α (the contribution of the linear trend to the total dispersion) increases with a decrease in length of the series, but it is on the whole small and obviously reflects the fact that there is no significant, well-defined linear trend in the precipitation over the 85-year period.

Confirmation of some of the indicated singularities can be found on the graphs of the behavior over many years of the anomalies in a number of regions and for the 0-85° N belt as a whole matched with the third-order trend lines (Figure 5). It is difficult to distinguish any regularity in the alternation of the maxima and minima; therefore the conclusions of [11] of insignificant guarantee of the spectral frequencies of the mean zonal precipitation within the limits of 2 to 6 years appears to be convincing. Returning to the problem of uniformity of the series, let us note that in the long-term behavior of the January anomlies in Northern Asia, including the greater part of the territory of the USSR, there

is a positive discontinuity in the 1950's after which the norm turned out to be low. It is possible that this is a consequence of changing instruments, the effect of which could not be avoided, in spite of the carefully developed method of preparing the initial data [4]. The stable increase in anomalous nature was reflected in the largest of all the regions in the 85-year period of positive linear trend (β=2.9%/10 years) and also in the value of α=16% corresponding to it. It is obvious that in order to obtain reliable estimates of the variability, the uniformity of the time series has primary significance, and from this point of view retaining the initial method of measuring the precipitation, in spite of its imperfection, would be more useful.

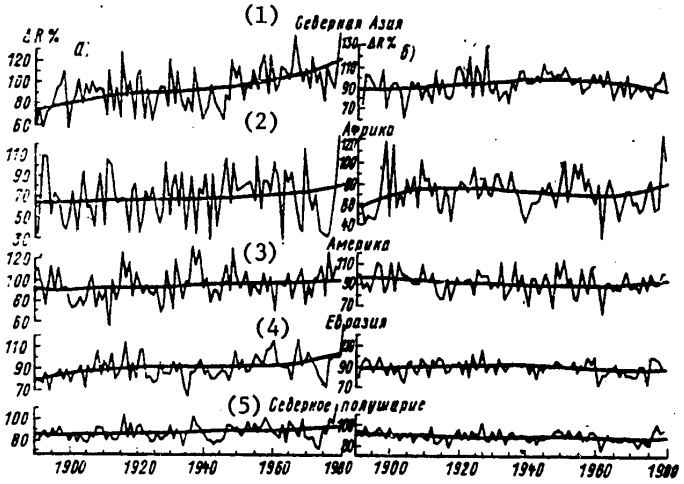

Figure 5. Long-term behavior of the third-order trend and anomalies. a -- January, b -- July.

Key:
1. Northern Asia
2. Africa
3. America
4. Eurasia
5. Northern Hemisphere

As has already been pointed out above, in reference [1] recommendations are presented with respect to the uniform representation of the empirical data on climate variability. Accordingly, in Table 4 estimates are presented for the trend in the precipitation anomalies with respect to five latitudinal zones, including, in addition to the precipitation over the dry land, data on the oceans where they exist, that is, in the coastal zone and regions of intense shipping. It is possible to see that the variation of the sign of β takes place to some degree comparatively with respect to all zones. Thus, in January against a background of insignificant positive trends, there was an increase in precipitation for the entire period in 1940-1964, after which came a decrease in 1946-1975* and a sharp increase at the end of the period. In July the pattern of the sign

*[(sic) -- translator's note: probably 1964.]

Table 3. Estimates of the linear trend parameters of the total monthly precipitation anomalies by regions of the Northern Hemisphere for various parts of the time series

Region	Parameters	1891—1975 (85 yrs)	1946—1975 (30 yrs)	1956—1975 (20 yrs)	1966—1975 (10 yrs)	1970—1979 (10 yrs)	1891—1940 (50 yrs)	1940—1964 (25 yrs)	1964—1979 (16 yrs)
					January				
Eurasia	β%/10 yrs	1,2	—1,4	—9,5	—27,0	33,5	0,8	5,5	7,2
	$\overline{R}$%	91	96	96	94	96	89	94	97
	α%	8	1	24	44	42	2	17	6
Northern Asia	β%/10 yrs	2,9	3,0	—3,6	—28,9	22,2	1,1	12,3	—0,6
	$\overline{R}$%	93	104	107	107	106	88	96	108
	α%	16	4	2	27	15	1	32	0
Central Asia	β%/10 yrs	0,9	—0,1	—0,2	3,7	36,6	—0,3	—6,7	6,5
	$\overline{R}$%	94	97	97	96	103	91	98	104
	α%	1	0	0	0	30	0	6	2
Southern Asia	β%/10 yrs	—0,1	—7,1	—16,4	—6,0	61,9	1,1	—7,8	23,4
	$\overline{R}$%	78	77	75	69	79	78	84	78
	α%	0	7	12	0	47	0	6	16
Eastern Asia	β%/10 yrs	—0,2	—10,2	—14,6	—22,0	40,4	2,3	3,2	6,3
	$\overline{R}$%	82	83	78	75	75	83	83	77
	α%	0	12	11	7	19	2	1	2
Europe	β%/10 yrs	0,4	—2,0	—15,3	—49,4	27,5	0,2	9,7	5,8
	$\overline{R}$%	101	103	104	99	102	100	102	102
	α%	0	1	18	38	12	0	14	1
Africa	β%/10 yrs	0,1	—13,2	—19,2	—25,7	84,6	0,7	4,1	22,5
	$\overline{R}$%	68	71	65	54	72	67	75	71
	α%	0	24	20	10	29	0	2	7
North America	β%/10 yrs	0,5	—2,7	3,9	14,8	31,8	1,9	—1,4	9,6
	$\overline{R}$%	93	95	92	93	96	93	93	96
	α%	1	4	4	15	40	3	1	12

FOR OFFICIAL USE ONLY

APPROVED FOR RELEASE: 2007/02/09: CIA-RDP82-00850R000400070003-7

[Table 3, continued]

July

Eurasia	β%/10 yrs	—0,1	—3,5	—5,1	—7,2	15,9	1,0	—0,6	4,5
	R%	94	93	92	90	94	94	94	93
	α%	0	26	20	16	36	5	0	11
Northern Asia	β%/10 yrs	0,7	—5,2	—5,7	—8,6	9,3	1,8	—3,5	4,6
	R%	97	98	96	93	95	95	102	94
	α%	2	33	19	14	20	4	12	9
Central Asia	β%/10 yrs	—0,4	—8,7	—17,4	—51,5	32,7	1,1	5,2	—4,4
	R%	82	83	80	75	72	84	85	78
	α%	0	10	14	59	22	1	3	1
Southern Asia	β%/10 yrs	—0,4	—5,6	—7,7	—6,1	20,5	0,7	0,5	—0,8
	R%	93	92	90	88	90	94	93	92
	α%	0	12	8	4	19	0	0	0
Eastern Asia	β%/10 yrs	—0,8	1,3	11,9	24,0	2,0	0,7	—9,6	11,4
	R%	97	94	92	101	105	99	91	100
	α%	1	0	7	29	0	0	10	19
Europe	β%/10 yrs	0,1	1,1	—2,4	4,5	16,7	0,4	1,6	9,4
	R%	96	96	97	95	102	96	95	99
	α%	0	1	2	2	16	0	2	14
Africa	β%/10 yrs	0,2	—5,6	—2,3	17,8	50,2	1,4	3,4	20,3
	R%	74	75	71	68	77	74	76	74
	α%	0	11	1	24	41	1	3	24
North America	β%/10 yrs	—0,3	—0,3	2,8	2,3	13,6	—1,0	—0,7	6,6
	R%	96	95	94	96	98	96	94	97
	α%	0	0	3	1	36	2	0	21

Table 4. Estimates of the Linear Trend Parameters of the Total Monthly Precipitation Anomalies of the Primary Latitudinal Zones of the Northern Hemisphere for Different Parts of the Time Series

January

North latitude, deg	Parameters	1891—1975 (85 yrs)	1946—1975 (30 yrs)	1956—1975 (20 yrs)	1966—1975 (10 yrs)	1970—1979 (10 yrs)	1891—1940 (50 yrs)	1940—1964 (25 yrs)	1964—1978 (15 yrs)
85,0—17,5	β%/10 yrs	0,6	—2,3	—6,8	—10,7	29,8	0,7	4.2	0,6
	$\bar{R}$%	92	95	95	92	95	91	94	94
	α%	4	9	26	53	53	2	18	0
85,0—72,5	β%/10 yrs	0,3	—4,1	—17,5	—25,9	10,4	—0,5	6,9	—18,5
	$\bar{R}$%	89	92	92	84	79	88	92	85
	α%	0	4	29	30	8	0	8	25
72,5—57,5	β%/10 yrs	1,2	—0,4	—10,1	—12,2	21,4	0,7	12,1	—0,8
	$\bar{R}$%	95	101	102	97	98	93	97	99
	α%	6	0	24	11	21	1	42	0
57,5—37,5	β%/10 yrs	0,8	—0,8	—1,8	—17,0	16,5	0,9	1,4	—6,0
	$\bar{R}$%	97	100	100	100	100	96	98	100
	α%	4	1	1	35	22	2	1	9
37,5—17,5	β%/10 yrs	—0,4	—5,8	—9,3	—0,2	53,4	0,1	—0,7	9,4
	$\bar{R}$%	85	84	82	78	88	85	87	82
	α%	1	15	14	0	43	0	0	6

[Table 4, continued]

North latitude, deg	Parameters	1891—1975 (85 yrs)	1946—1975 (30 yrs)	1956—1975 (20 yrs)	1966—1975 (10 yrs)	1970—1979 (10 yrs)	1891—1940 (50yrs)	1940—1964 (25 yrs)	1964—1978 (15 yrs)
July									
85,0—17,5	β%/10 yrs	—0,2	—3,2	—2,9	—6,6	13,0	—0,1	—0,5	4,2
	$\bar{R}$%	92	92	90	90	92	92	92	91
	α%	1	32	15	37	42	0	1	15
85,0—72,5	β%/10 yrs	1,3	0,9	5,5	—7,4	—32,8	—2,5	2,5	—15,0
	$\bar{R}$%	93	100	99	102	91	89	97	97
	α%	2	0	9	6	44	2	1	28
72,5—57,5	β%/10 yrs	0,3	—2,2	—1,6	—7,5	—0,8	—0,2	0,1	—0,0
	$\bar{R}$%	97	98	97	96	96	96	99	96
	α%	1	8	2	12	0	0	0	0
57,5—37,5	β%/10 yrs	—0,4	—3,4	—5,5	—9,8	23,5	0,2	—0,0	4,9
	$\bar{R}$%	91	90	89	87	92	92	91	91
	α%	2	21	22	37	46	0	0	8
37,5—17,5	β%/10 yrs	—1,3	—6,5	—4,2	0,8	23,5	—0,3	—3,7	13,0
	$\bar{R}$%	84	80	76	75	82	86	83	78
	α%	14	36	10	0	37	0	12	27

alternation and magnitude of β with respect to zones and periods becomes more spotty. Analyzing the long-term behavior of the anomalies by the graphs matched with the five-year sliding means (Figure 6), it is possible to distinguish approximately the same features as in Figure 5.

The basic experimental results consist in the following.

1. The archive of precipitation anomalies created by visual interpolation by the originals maps of [4] has precision sufficient for estimation of the climatic variability of the precipitation on the continents.

2. The representation of the precipitation data in the form of anomalies in percentages of the norm permits us to achieve spatial smoothing and thus convert from analysis of the point observations to a study of the precipitation field in the hemisphere.

3. The parameters of the field variability vary significantly in space and time; therefore in order to distinguish the characteristic features it is recommended that the anomalies be smoothed on the scales of the subcontinents.

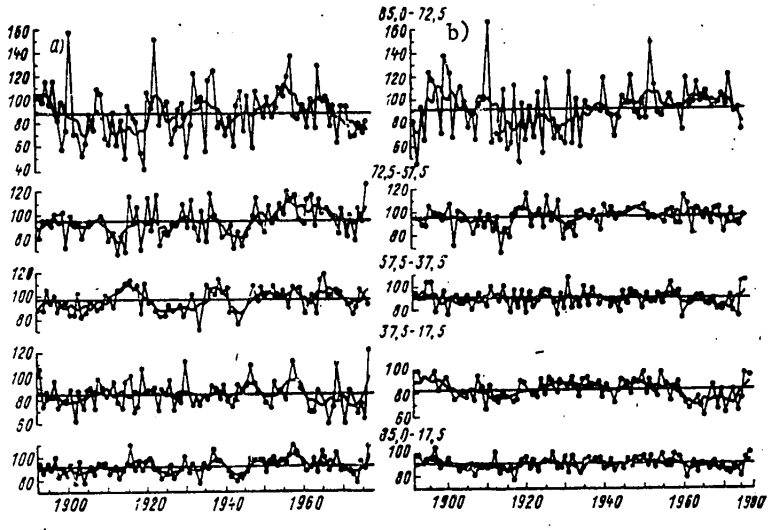

Figure 6. Long-term behavior of anomalies by latitudinal zones and 5-year sliding means (%).
a -- January, b -- July.

4. The growth of the anomalous nature in January and insignificant decrease in July are observed on the whole for the hemisphere in 1891-1975.

5. The primary problems of future research must be restoration of the uniformity of the series by converting to a united long-term norm and calculation of the climatic characteristics of the total precipitation. It is also possible to note the necessity for analyzing the trends of the continuous (in contrast to monthly)

normalized precipitation series and to calculate the interrelations with the air pressure and temperature variations.

In conclusion, the authors express their sincere appreciation to G. T. Gnevko for the organization and performance of the work of creating the archive and E. Ya. Ran'kova for the library of computer programs put at our disposal for the calculations.

BIBLIOGRAPHY

1. Vinnikov, K. Ya., et al. "Modern Climate Variations of the Northern Hemisphere," METEOROLOGIYA I GIDROLOGIYA [Meteorology and Hydrology], No 6, 1980.

2. Gruza, G. V.; Ran'kova, E. Ya. "Empirical-Statistical Analysis of the Structure and Variations of the Observed Climate," TRUDY VNIIGMI-MTSD [Works of the All-Union Scientific Research Institute of Hydrometeorological Information -- World Data Center], No 68, 1980.

3. Gruza, G. V.; Ran'kova, E. Ya.; Apasova, Ye. G. "Statistical Characteristics of the Anomaly Field of the January Precipitation in the Northern Hemisphere," TRUDY VNIIGMI-MTSD, No 77, 1980.

4. KARTY MESYACHNYKH I GODOVYKH SUMM OSADKOV V OTNOSHENII K MNOGOLETNIM SREDNIM SEVERNOGO POLUSHARIYA [Maps of the Monthly and Annual Total Precipitation with Respect to the Long-Term Mean for the Northern Hemisphere], Nos 1-3, 1964, Leningrad, Main Geophysical Observatory.

5. Kuznetsova, L. P.; Nekhocheninova, V. I. "Time Variations of Temperature and Precipitation Averaged for the Continents (Europe and North America)," METEOROLOGIYA I GIDROLOGIYA, No 4, 1977.

6. Polishchuk, A.I. "Problem of the Statistical Structure of the Winter Precipitation Field," TRUDY GGO [Works of the Main Geophysical Observatory], No 215, 1968.

7. Polishchuk, A.I. "Statistical Structure of Summer Precipitation," TRUDY GGO, No 268, 1972.

8. SREDNIYE MNOGOLETNIYE MESYACHNYYE I GODOVYYE SUMMY ATMOSFERNYKH OSADKOV PO ZARUBEZHNOY TERRITORII SEVERNOGO POLUSHARIYA [Long-Term Mean Monthly and Annual Total Atmospheric Precipitation over the Foreign Territory of the Northern Hemisphere], Leningrad, Gidrometeoizdat, 1972.

9. Corona, T. J. "Further Investigation of the Interannual Variability of Northern Hemisphere Continental Precipitation," ENVIRON. RES. PAPER COLOR STATE UNIV., No 20, 1979.

10. Dorman, C. E.; Bourke, R. H. "Precipitation Over the Pacific Ocean, 30°S to 60°N," MON. WEATHER REV., Vol 107, No 7, 1979.

11. Xanthakis, J.; Tritakis, B. "Analytical Expression of the Mean Annual Variation of the Precipitation within Various Latitude Zones of the Earth," PRACTICA OF THE ACADEMY OF ATHENS, Vol 51, No 47, 1976 (1977).

UDC 551.(510.522:553:554)(47+57)

CLIMATIC CHARACTERISTICS OF VERTICAL WIND SHIFTS IN THE GROUND LAYER OF THE ATMOSPHERE OVER THE USSR

Moscow METEOROLOGIYA I GIDROLOGIYA in Russian No 5, May 81 pp 17-23

[Article by F. F. Bryukhan', Professor I. G. Guterman, All-Union Scientific Research Institute of Hydrometeorological Information -- World Data Center, manuscript received 18 Aug 80]

[Text] On the basis of the data from four-time radiosonde observations in the boundary layer at 146 stations in the USSR for the period from 1961 to 1970, the climatic characteristics of the vertical wind shifts were calculated. The spatial climatic pattern of the wind shifts was obtained. An analysis is made of the shifts on the scale of the USSR in the 0-100 meter layer and over individual stations vertically. The diurnal behavior and probability characteristics of the shifts are considered.

The consideration of the vertical wind shifts in the ground layer of the atmosphere, as emphasized in the resolutions of the Fourth Meeting of the Committee on Aviation Meteorology of the World Meteorological Organization (KAM-IV VMO) [16], is very important to supporting safe takeoff and landing of aircraft. The study of the vertical wind shifts is also important for more thorough representation of the wind conditions in the ground layer of the atmosphere inasmuch as the magnitude of the wind shifts depends both on the thermal stratification of the atmosphere and the interaction of the air currents with the relief of the underlying surface.

The study of wind shifts is the subject of a comparatively small number of papers, for interest in this problem began to be shown only 10-20 years ago. The study of the wind shift in the ground layer has been primarily based on the measurement data on a meteorological tower at one station (in particular, on the meteorological tower in Obninsk) [1-2, 12, 18, and so on]. Balloon data which permit a detailed study of the wind shift conditions in individual regions have been used more rarely [9]. In references [14, 15], generalized data from temperature-wind sounding in the boundary layer for one station were used to analyze the wind profiles and shifts. In [8] a detailed analysis is made of the wind shift distribution in the free atmosphere by radiosonde data. In reference [10] an analysis was made of the shifts in the territory of the USSR based on the results of radiosonde observations in the 1000 to 850 mb layer. However, maps constructed in [10] for the indicated layer are of no practical significance in view of the great thickness of the layer, although they are of interest in climatological respects.

In order to study the shift distribution laws and methods of predicting these shifts to promote flight safety it is first necessary to investigate the basic climatic features of the wind shift distribution. Such a study is made in this paper.

In the paper four-time radiosonde observations over a 10-year period (from 1961 to 1970) at 146 stations distributed uniformly throughout the territory of the USSR, were used. On the average approximately 250 observations were made at each station at one time of day over the entire 10-year period. Multiplying by four we have a total of 1000. The initial wind data were taken on the windvane level (8-12 meters), at altitudes of 100, 200, 300, 500, 600 and 900 meters reckoned from the station level and at altitudes of 200, 500, 1000, 1500, 2000, and 3000 meters reckoned from sea level.

The described data take up significant space, and for effective use at the VNIIGMI-MTsD, an archive of observations with respect to the boundary layer was created on magnetic tapes on the Minsk-32 computer and the unified system of computers. Information is packed on these tapes with maximum recording density, which permits the data from three stations to be recorded on one tape. In the phase of formation of the archive, a rough check was made of the initial data by the procedure described in [3]. By cooperation between the Arctic and Antarctic Scientific Research Institute and the Moscow Division of the VNIIGMI [All-Union Scientific Research Institute of Hydrometeorological Information], under the direction of K. Ye. Chernin, a set of programs was written for processing the indicated data, in particular, the programs for calculating the characteristics of the vertical wind shifts.

As a result of the fast rise of the radiosonde, the accuracy between the wind speed and direction is greatly inferior to the accuracy of measuring the wind on meteorological towers and masts. During mast or tower measurements it is possible to obtain a detailed vertical structure of the wind at several points in the USSR. Although the radiosonde data are less accurate, they offer the possibility of obtaining a three-dimensional picture of the wind in the boundary layer of the atmosphere. A large number of observations and a quite large set of altitudes obviously permit us to obtain reliable climatic characteristics of the wind shifts.

The calculation of the characteristics of the vertical wind shifts based on the velocity differences of two adjacent levels contains a double random error. Therefore, the magnitude of the shift is calculated with less accuracy than the values of the velocities themselves on the levels. In addition, the accuracy of determining the wind shift depends on the thickness of the layer for which it is determined. Thus, the shifts calculated for layers of different thickness can not be compared to each other. Thus, by the results of the calculations presented below, a maximum shift is easily detected in the 500-600 meter layer comparable to the values in the lower (300-500 meters) and higher (600-900 meters) layers. The problem of the relation of the layer thickness to the wind shift in the ground layer is investigated in detail in [4], and in the free atmosphere, in [8].

The most important of the characteristic shifts used in aviation is $\overline{\gamma}$ -- the mean value of the modulus of the vector shift. Therefore in the given paper basically a study is made of the characteristics γ (the monthly mean over many years) and the recurrence of individual values of the modulus of the vector shifts.

In Figure 1 the climatic maps of the modulus of the vector shifts in January and July are presented for the 0-100 meter layer over the USSR. In January and also in July the maximum shifts are observed over Northern Kazakhstan and Western Siberia, over the Central part of the European Territory of the USSR, and over the Northern part of Kamchatka. The minimum shift regions in January are traced west of the Urals, over the Eastern Ukraine and Eastern Siberia.

In July on the whole throughout the USSR, the wind shifts are less than in January. The peaks are located almost in the same regions as in the winter, over Central Asia and Western Siberia. Over the other regions the wind shifts are basically minimal.

A comparison of the maximum and minimum shift zones both in January and in July indicates that relief has the predominant significance in their formation. In the annual behavior the latter acts on the nature of variation of the wind with altitude in practice uniformly in contrast to circulation or, in particular, the horizontal nonuniformity of the temperature field. Both the latter factors, as is known, have significant annual variation.

The powerful shift maximum over Northern Kazakhstan in January is connected with the influence of the Ural Mountains and the exit of the air currents to the Western Siberian Plain. The Southwestern Currents, which prevail over the European territory of the USSR, flow around the Ural Mountains, change direction to the south and partially cross over the mountain range. Additional turbulence with unstable stratification or lee waves with lifted inversions can occur depending on the thermal stratification of the air after the mountain obstacles [17]. In the case of stable thermal stratification the current lines on the lee side of the mountains are clustered toward the ground surface. The indicated factors lead to large wind shifts.

An analogous phenomenon occurs in July. The difference consists only in the fact that the winds blow from the north and northwest and flow takes place around the Urals from north to south. During movement of the air current toward the south over the Western Siberian Plain and Northern Kazakhstan the wind intensifies, as a result of which powerful shifts are observed over this region. The powerful shift maximum in July is also caused by mesoscale circulation.

In the center of the zone of greatest mean monthly shifts over Northern Kazakhstan they reach $7 \cdot 10^{-2}$ sec^{-1} in January; over the central regions of the European Territory of the USSR they reach $5 \cdot 10^{-2}$ sec^{-1}. In the minimum shift zones, for example, in the foothills of Central Asia, the Baykal region, over the northeastern part of the USSR in the center of the Siberian winter maximum (Verkhoyansk, Yakutsk) they amount to only $2 \cdot 10^{-2}$ sec^{-1}.

The field of the modulus of the vector wind shifts in July, as can be determined by Figure 1b is less uniform with respect to territory, and the values of $\bar{\gamma}$ themselves are smaller. In the region of maximum shifts over the northern part of Kazakhstan they reach only $5 \cdot 10^{-2}$ sec^{-1}. Over the central regions of the European Territory of the USSR in July their values decrease to $4 \cdot 10^{-2}$ sec^{-1} in January. At the same time it is characteristic that in Transbaykal, the belt of increased shifts $5 \cdot 10^{-2}$ sec^{-1} is retained in both January and July.

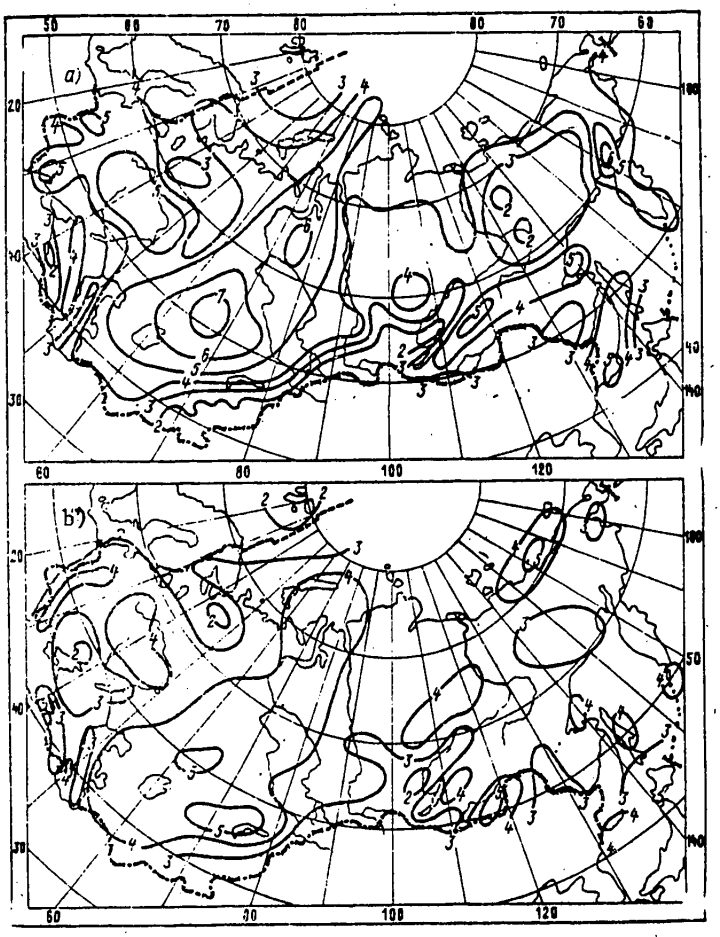

Figure 1. Climatic maps of the modulus of the vector wind shifts $\overline{\gamma}$ in the 0-100 meter layer (10^{-2} sec^{-1}).
a -- January, b -- July.

In the ground layer, near the underlying surface, the wind and shift characteristics have significant diurnal variation. It is known that over the plains the growth of the modulus of the wind velocity at the surface of the earth from night to day and some righthand rotation of the wind vector predominate. At the 100 meter level, that is, on the upper boundary of the layer, inside which a study is made of the vertical shifts, on the contrary, there is a decrease in the velocity modulus in the afternoon hours. Here inversion of the diurnal behavior is characteristic [10, 12, 15]. The diurnal variation of the wind shifts is formed accordingly.

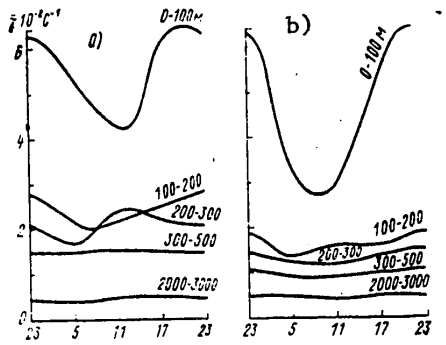

Figure 2. Diurnal variation of the modulus of the vector shift in various layers in January (a) and July (b). Kzyl-Orda.

Figure 2 shows an example of the manifestation of the diurnal behavior of the wind shifts. It is clearly expressed in the lower part of the boundary layer. The shifts decrease from night to day as a result of a decrease in the wind velocity at an altitude of 100 meters during the daylight hours. The author of reference [18] arrives at the same conclusion on the basis of using the observations at the Obninsk Tower. With an increase in altitude of the investigated layer the diurnal behavior damps, and at altitudes on the order of 500 meters and higher the shifts are insignificant.

In the table the July distribution is presented for the differences of the moduli of the wind vector shifts in the 0-100 meter layer between night and day observations. This distribution was obtained by analyzing the results of the observations of all 146 stations. The analysis demonstrated that in the 0-100 meter layer a decrease in the magnitude of the modulus of the wind vector shift from night to day predominates. On the average in July the shift decreases by $(0.8 \text{ to } 1.0)\cdot 10^{-2}$ sec^{-1}. The predominant number of cases (34.5%) fall in the gradation $(1.1\text{-}1.5)\cdot 10^{-2}$ sec^{-1}. As was already noted earlier, this takes place as a result of an increase in the wind velocity from night to day at the surface of the earth with a simultaneous decrease in it at the 100 meter altitude. However, the table data indicate that at some of the stations, a different diurnal behavior of the vector shift modulus is observed. A detailed analysis shows that this diurnal behavior is characteristic of stations over which local circulations are imposed on the air currents such as mountain-valley, breeze, foehn, and so on (Nagayev Bay, Ayan, Chita, Yuzhno-Kuril'sk, Dzhalal-Abad, Ust'-Barguzin).

For estimates of the degree of flight safety in practice frequently the probability characteristics that the shifts will exceed a given value are used. The authors constructed maps of the probabilities of the moduli of the vector shifts exceeding values of $8\cdot 10^{-2}$ sec^{-1} and $12\cdot 10^{-2}$ sec^{-1}. The shifts of the values of $12\cdot 10^{-2}$ sec^{-1} by the KAM-IV VMO scale [16] are considered strong. They can be recognized as still stronger if we consider that in the ground layer the wind gradients decrease rapidly with altitude, and for aviation the most sensitive is the shift in the lower 60-meter layer. The corresponding maps are not presented in the given paper.

Distribution of the Differences of the Wind Vector Shift Moduli Between Night and Day Observations

	Gradation, 10^{-2} sec^{-1}									
	<−1,1	−1,0 −0,6	−0,5 −0,1	0,0 0,5	0,6 1,0	1,1 1,5	1,6 2,0	2,1 2,5	2,6 3,0	3,1 3,5
Recurrence, %	1,4	5,0	8,5	17,0	19,5	34,5	9,2	3,5	0,7	0,7

It must be noted that these maps are to a great extent analogous to the maps presented in Figure 1. For the majority of stations in the USSR the recurrence of the shifts greater than $12 \cdot 10^{-2}$ sec^{-1} can be estimated in 2-3% of the cases in January and in 0.5-1% of the cases in July. In the regions of the largest vertical shifts, shifts larger than $12 \cdot 10^{-2}$ sec^{-1} can be observed in January over Kazakhstan with a probability of 7% and in July over Central Asia with probability of 2% and more. The fact of the appearance of strong wind shifts over Central Asia is confirmed in reference [9] on the basis of the analysis of balloon observations.

In Figure 3 the envelopes of the profiles of the maximum moduli of the vector shifts for 10 years are presented for the Kzyl-Orda station. As is obvious in this figure, shifts on the order of $20 \cdot 10^{-2}$ sec^{-1} and more can be observed in the lower layers. The probabilities of such shifts are small -- less than 0.5%; however, such shifts present serious danger on takeoff and landing of aircraft and by the KAM-IV VMO scale belong to the category of very strong shifts.

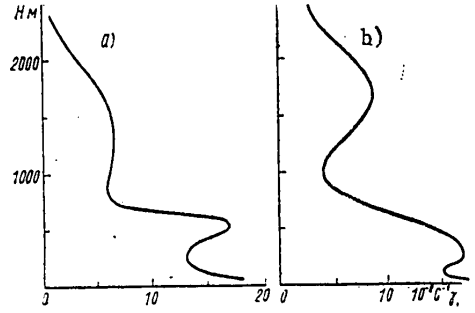

Figure 3. Envelopes of the profiles of the maximum vector shift moduli in January (a) and July (b).

The calculation of the probability characteristics of the wind shifts (recurrence, quantiles, and so on) directly from the observation series is very labor-consuming; therefore indirect calculation of them beginning with the use of hypothetical distribution laws and their parameters is of obvious interest.

Let us assume that the vector of the vertical wind shift is distributed by a normal law

$$f(\gamma_x, \gamma_y) = \frac{1}{2\pi\sigma_x\sigma_y\sqrt{1-r^2}} \times$$
$$\times \exp\left\{-\frac{1}{2(1-r^2)}\left[\frac{(\gamma_x-\bar{\gamma}_x)^2}{\sigma_x^2} - \frac{2r(\gamma_x-\bar{\gamma}_x)(\gamma_y-\bar{\gamma}_y)}{\sigma_x\sigma_y} + \right.\right.$$
$$\left.\left. + \frac{(\gamma_y-\bar{\gamma}_y)^2}{\sigma_y^2}\right]\right\}, \quad (1)$$

where γ_x, γ_y are the random shift components in the zonal and meridional directions;

$\bar{\gamma}_x$, $\bar{\gamma}_y$ are the components of the mean resultant shift;

σ_x, σ_y are the mean deviations of the component;

r is the correlation coefficient between them.

Let us further assume that $\sigma_x=\sigma_y$ and r=0. Then the shift vector is scattered by a circular law. In this case the joint density of the modulus γ and the direction of the random shift β in polar coordinates assumes the form

$$f(\gamma, \beta) = \frac{1}{\pi\sigma^2}\exp\left[-\frac{\gamma_r^2 - 2\gamma_r\gamma\cos(\beta-\beta_r)+\gamma^2}{\sigma^2}\right], \quad (2)$$

where $\sigma = \sqrt{\sigma_x^2+\sigma_y^2} = \sigma_x\sqrt{2} = \sigma_y\sqrt{2}$ is the vector mean square deviation.

By corresponding integration of (2) it is easy to obtain the distribution densities of the direction and modulus of the shifts:

$$F(\beta) = \frac{e^{-\lambda^2}}{2\pi}\{1+\sqrt{\pi}ze^{z^2}[1+\Phi(z)]\}, \quad (3)$$

$$G(\gamma) = \frac{2\gamma}{\sigma^2}\exp\left(-\lambda^2 - \frac{\gamma^2}{\sigma^2}\right)\cdot I_0\left(\frac{2\lambda\gamma}{\sigma}\right). \quad (4)$$

Here $\lambda = \gamma_r/\sigma$, $z = \lambda\cos(\beta-\beta_r)$,
$\gamma_r = \sqrt{\bar{\gamma}_x^2+\bar{\gamma}_y^2}$, $\beta_r = \operatorname{arctg}(\bar{\gamma}_x/\bar{\gamma}_y)$,

γ_r and β_r are the modulus and direction of the mean resultant shift. The angles β and β_r are reckoned from the north clockwise.

Distributions of the type of (3) and (4) are known from the literature on the wind statistics [7, 11]. The distribution of (4) is known as the generalized Rayleigh law.

In order to use the distributions (2)-(4), in addition to the resultant shift vector it is also necessary to know its dispersion. The mean square deviations of the shifts usually are not calculated, and they are presented extremely rarely in the literature. Therefore it is necessary to use another distribution parameter

analogous to the parameter of the climatic wind stability. It is determined by the ratio of the modulus of the mean resultant shift vector to the mean value of the vector shift modulus:

$$s = \frac{\gamma_r}{\gamma}. \tag{5}$$

This parameter proposed by G. Ya. Narovlyanskiy, N. V. Kobysheva and M. Ye. Kaulina [13] characterizes the degree of variability of the wind shifts with respect to direction. For recalculation of s to λ (this permits determination of σ), it is possible to use the functions relating the analogous wind parameters [11]. Then it is possible to use relations (2)-(4). Thus, in order to know the distribution function of the shift vector, parameters γ, γ_r, β_r must be known. For calculations of the probabilities and quantiles of the vector shift moduli, it is sufficient to know two parameters: γ and γ_r.

The calculations made by the authors in the example of the stations of the USSR demonstrated that, as a rule, the hypothesis of Rayleigh distribution of the vector shift modulus does not contradict the observation data for the 5% level of significance of the Pearson number.

BIBLIOGRAPHY

1. Abramovich, K. G.; Glazunov, V. G.; Stepina, M. P. "Vertical Wind Shifts in the Lower Layer of the Atmosphere," TRUDY GIDROMETTSENTRA SSSR [Works of the USSR Hydrometerological Center], No 70, 1970.

2. Borisenko, M. M. "Peculiarities of the Vertical High Wind Profile According to Measurement Data on High Towers," TRUDY GGO [Works of the Main Geophysical Observatory], No 241, 1969.

3. Gavrilova, Z. I.; Guterman, I. G.; Krylova, L. M.; Popkova, L. F.; Khanevskaya, I. V. "Basic Steps in the Development of Aerological Data Under the Program for the New Aeroclimatic Reference of the USSR," TRUDY VNIIGMI-MTsD [Works of the All-Union Scientific Research Institute of Hydrometeorological Information -- World Data Center], No 50, 1978.

4. Glazunov, V. G. "Vertical Wind Shift with Different Layer Thickness in the Ground Part of the Atmosphere," TRUDY GIDROMETTSENTRA SSSR, No 70, 1970.

5. Glazunov, V. G. "Vertical Wind Shifts for Different Temperature Stratification in the Lower 300-Meter Layer of the Atmosphere," TRUDY GIDROMETTSENTRA SSSR, No 60, 1972.

6. Glazunov, V. G. "Conditions of Occurrence of a Strong Vertical Shift in the Lower Part of the Ground Layer of the Atmosphere," TRUDY GIDROMETTSENTRA SSSR, No 62, 1975.

7. Guterman, I. G. RASPREDELENIYE VETRA NAD SEVERNYM POLUSHARIYEM [Wind Distribution over the Northern Hemisphere], Leningrad, Gidromegeoizdat, 1965.

8. Guterman, I. G. "Vertical Wind Shifts," TRUDY NIIAK [Works of the Scientific Research Institute of Aeroclimatology], No 56, 1969.

9. Isamukhamedova, U. "Powerful Vertical Wind Shifts in the Aircraft Takeoff and Landing Zone at the Airports of Uzbekistan," TRUDY SANIGMI [Works of the Central Asian Scientific Research Hydrometeorological Institute], No 25(40), 1966.

10. "Climate of the Free Atmosphere and Boundary Layer Over the Territory of the USSR," edited by I. G. Guterman, TRUDY VNIIGMI-MTsD, No 60, 1979.

11. Marchenko, A. S. "Circular and Elliptic Forms of the Two-Dimensional Normal Law in the Aeroclimatology of the Wind," TRUDY NIIAK, No 25, 1964.

12. Mashkova, G. B. "Problem of the Gradient Wind Velocity in the Boundary Layer," METEOROLOGIYA I GIDROLOGIYA [Meteorology and Hydrology], No 12, 1971.

13. Narovlyanskiy, G. Ya.; Kobysheva, N. V.; Kaulina, M. Ye. "One of the Possible Methods of Calculating the Maximum Vertical Wind Shifts," TRUDY NIIAK, No 38, 1967.

14. Orlenko, L. R. "Procedure for Processing the Temperature-Wind Sounding Data in the Boundary Layer," TRUDY GGO, No 257, 1970.

15. Orlenko, L. R.; Shklyarevich, O. B. "Vertical Wind Shifts in the Boundary Layer of the Atmosphere (According to the Experimental Data)," METEOROLOGIYA I GIDROLOGIYA, No 10, 1974.

16. Petrenko, N. V. "Resolutions of the Fourth Meeting of the Commission on Aviation Meteorology of the World Meteorological Organization," METEOROLOGIYA I GIDROLOGIYA, No 6, 1968.

17. Smit, K. OSNOVY PRIKLADNOY METEOROLOGII [Fundamentals of Applied Meteorology], Leningrad, Gidrometeoizdat, 1978.

18. Tsverava, V. G. "Studies of the Vertical Wind Vector Shift by Observations on a 300-Meter Meteorological Tower," METEOROLOGIYA I GIDROLOGIYA, No 2, 1967.

UDC 551.(558.1+509.6)

SIMULATION OF THERMALS

Moscow METEOROLOGIYA I GIDROLOGIYA in Russian No 5, May 81 pp 24-32

[Article by N. K. Didenko, V. N. Ivanov, Candidates of Physical and Mathematical Sciences V. Ya. Korovin and V. V. Smirnov, Institute of Experimental Meteorology, manuscript received 26 Aug 80]

[Text] The results of studying the evolution of thermals obtained during volumetric combustion of aerosuspensions in a pure atmosphere and under conditions of a model cloud environment are presented. The proposed model of a thermal takes into account the efficiency of the conversion of the chemical energy of the suspension to buoyancy energy and also the conversion of a spherical thermal to a turbulent vortex ring.

Examples of the practical application of the results are presented.

Thermals on the order of a meter in size and with a height of rise on the order of tens of meters were simulated by creating local sources of volumetric heat release in the atmosphere.

The study of the ordered vertical movements of air in the form of thermals and plumes is of interest from the point of view of constructing quantitative models of the development of convection [1], and it has a number of important practical applications in aviation and atmospheric process modification technology [13]. It is also important for the removal of impurities from atmospheric air [16], and so on. Some of the laws of the evolution of the structure of thermals with different initial parameters have been investigated theoretically [1-3, 14, 15] and experimentally (see, for example [1, 12] and the bibliography referenced in them). Nevertheless, there is no strict quantitative theory of the evolution of thermals with high initial buoyancy energy. Such thermals (hereafter called intense) are characterized by conversion to a spherical vortex during movement and then to a vortex ring [2, 12, 14]. The laws of the temperature distribution and variation of the rate of ascent of intense thermals with altitude under turbulent atmospheric conditions also require further study.

The purpose of this paper was an experimental study of the dynamics of the development of intense thermals created both under laboratory conditions and in a real atmosphere on igniting an aerosuspension based on a metal aerosol.

Experimental Procedure and Results

Analysis shows that for the simulation of artificial thermals with comparatively large initial volumes the use of the reaction of volumetric high-temperature oxidation of fuel, in particular, based on metals of the aluminum and magnesium type with high heat of combustion and high (by comparison with gas and liquid-drop fuels) combustion rate of their aerosuspensions turns out to be effective.

An air-atomizing burner with an output capacity of about 100 g of powder per pulse was used to spray the powder. Spark and remote laser techniques were used to ignite the aerosuspensions [6]. In order to insure continuous flame propagation in the aerosuspension, a concentration by mass of the fuel particles was created no less than some limiting value, the so-called lower concentration limit which for metallic aluminum is 45 g/m^3, but no more than a maximum value defined by the stoichiometry of the oxidation reaction (for aluminum, 300-310 g/m^3). In the experiments the concentration by mass of the reagent was 100-200 g/m^3, and the mean square particle diameter was 10 microns.

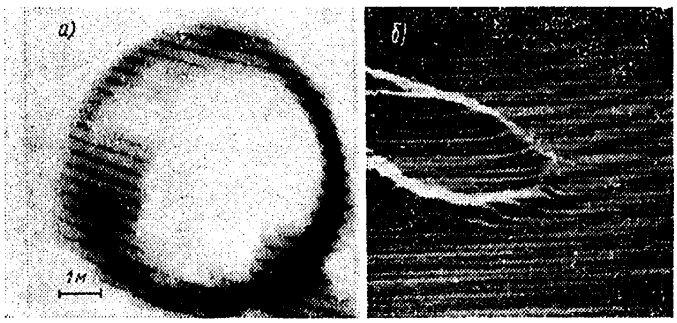

Figure 1. Television (a) and infrared (b) images of a thermal inhomogeneity for the 10-second time mark

The experiments were run under the conditions of indifferent and stable stratification at an air temperature of 290-300K and relative humidity of 60-100%. Using temperature gauges [4], television and infrared imager, the variations with time of the temperature, geometric dimensions and speed of the thermal were recorded. In order to obtain the infrared images (heat profiles of the thermal) on wave lengths of 2-5.6 microns, the AGA-680 model IR imager was used. On conversion of the IR-imager readings to the temperature of the thermal it was assumed that the radiation coefficient of the target is equal to one as a result of the large optical thickness of the cloud of combustion products. The value of the initial temperature of the thermal obtained in this way was 1300K. After completion of the combustion process (0.1-0.12 sec), a spherical cloud of heated air with a radius of $R_0 \sim 1$ meter with admixture of finely-disperse particles of combustion products was formed, which rose quickly.

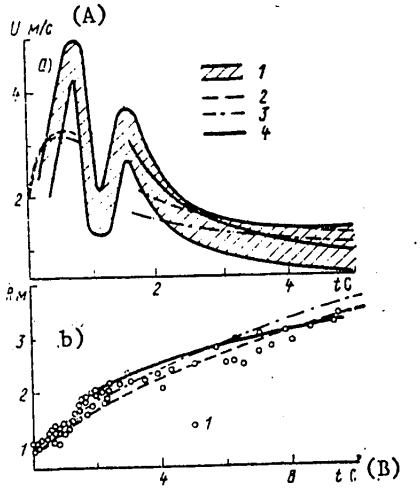

Figure 2. Time variation of the rate of ascent (a) and radius (b) of a thermal inhomogeneity:
1 -- experiment; 2 -- calculation by a model of a spherical thermal [15];
3 -- calculation by formulas of [3];
4 -- by the vortex ring model
Key:
A. U, m/sec
B. t, sec

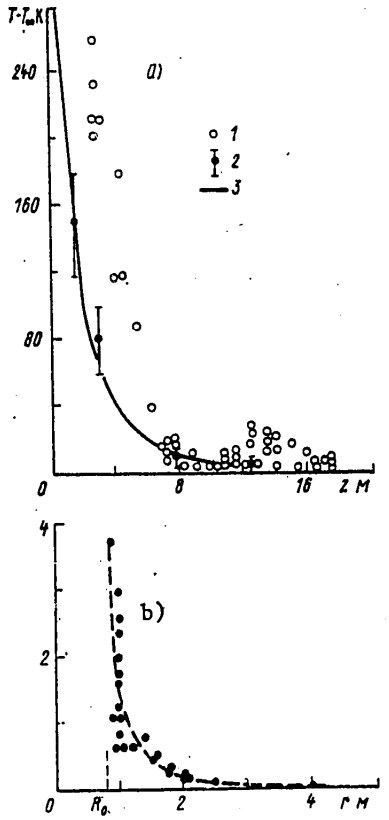

Figure 3. Variation of the mean temperature of a rising artificial thermal (a) and the temperature in the vicinity of the thermal for t=1 sec, z=0 (b):
1 -- infrared imaging; 2 -- contact measurements; 3 -- calculation by (2)

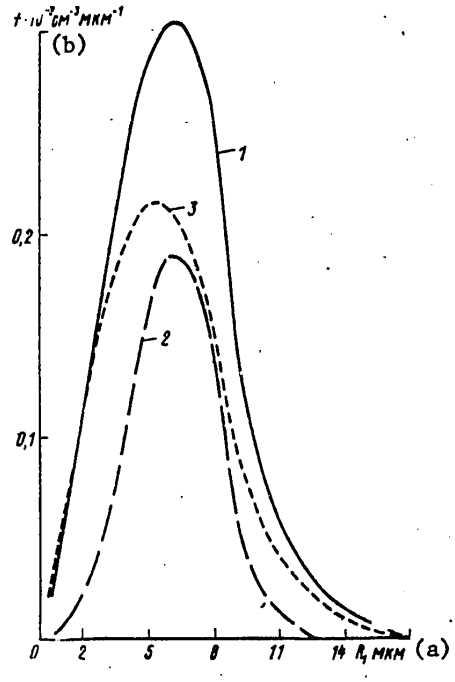

Figure 4. Effect of a radiation source on the spectrum of fog drops.
1 -- spectrum before modification; 2 -- after modification;
3 -- calculation by (6) for t=3 sec, $\Delta T=0.5K$

Key:
a. microns
b. $f \cdot 10^{-3}$ cm^{-3} $micron^{-1}$

An analysis of the television and IR images of a thermal inhomogeneity similar to those presented in Figure 1 demonstrated that in the initial phase of ascent for $t \leq 0.8$ sec, its shape is close to spherical. For 0.8 sec$<t<$1.6 sec, the spherical thermal is transformed to a vortex ring.

The variation of the basic parameters of the thermal with time is illustrated by Figure 2. The presence of two peaks previously not noted in the literature on the curve of the variation of the rate of ascent in Figure 2a is of special interest. The first peak is reached at the 0.8 second time mark. At that time conversion of the spherical thermal to a torus begins. The second peak (t=1.6 sec) coincides with the time of completion of the formation of the vortex ring. In Figure 2b, by the radius R for $t<0.8$ seconds we mean the radius of a sphere, and for $t>0.8$ sec, the outer radius of a torus. Figure 3 shows the results of measuring the temperature difference T (1 -- maximum, 2 -- average) of the inhomogeneity and the temperature of the medium T_∞ in different stages of ascent of the inhomogeneity (a) and also maximum superheating of the medium beyond the limits of the thermal in the z=0 plane. The altitude z is reckoned from the center of the thermal at the time t=0. The maximum values of the air temperature outside the thermal are reached a time on the order of 1 second after the time of its formation, and in the absence of wind they decrease to the initial temperature in the time 10-15 sec.

As follows from what has been discussed above, the simulated inhomogeneity is an intense source of thermal radiation. Accordingly, it was of interest to study the evaporation of fog under the effect of such sources. Experiments in the simulation of thermals in a cloud chamber 3200 m^3 in size were performed for this purpose. The experiments demonstrated that under the effect of a local radiation source such as a hot cloud of metal powder aerosuspension, in the vicinity of the combustion zone the liquid drop fog evaporates. Using the "Mars" aerosol particle television counter [9], the variation of the microstructure of the fog was recorded at a distance of 1 meter from the combustion zone. The differential spectra of the sizes of the fog drops before and after modification averaged after 3 seconds are presented as an example in Figure 4. As a result of modification by radiation of the combustion zone, the water content of the fog during the first 3-5 seconds decreases by 2-3 times by comparison with the initial content (amounting to about 1 g/m^3). During the subsequent 10-15 seconds, however, the drop spectrum acquires a form close to the initial form, which is connected with the mixing of air in the chamber caused by rise of the heated air.

Discussion of the Results

As is obvious from the presented results, an intense spherical thermal is converted to a torus already in the initial phase of ascent. The known models of a spherical thermal [1, 3, 12, 15] describing its evolution in terms of the temperature T_0, radius R_0, velocity U_0 and entrainment coefficient α thus become unacceptable.

Qualitatively, the mechanism of conversion of a spherical thermal to a torus can be characterized as follows. In the initial phase of ascent a vortex circulation current similar to the Hill vortex arises in the thermal under the effect of frictional forces. As the rate of ascent increases, the pressure and density gradients at the boundaries of the thermal lead to the fact that the thermal begins to flatten out, acquiring the shape of a torus, the air inside which rotates around a horizontal annular axial line, and a circulation current is formed outside the torus. As a result of the existence of a velocity circulation around an element of the vortex ring, it is affected by the Zhukov force directed perpendicularly to the direction of the velocity of the ring element. The horizontal component of this force stretches the ring to the sides, and the vertical component brakes the rise of the ring somewhat. Obviously, the effect of this force explains the decrease in the rate of ascent of the inhomogeneity observed in Figure 2a for 0.8 second$<t<$1.2 seconds.

On the whole, during movement of the obtained thermal inhomogeneities, we observe three phases of development: Ascent of the spherical thermal, transformation of the thermal to a torus, ascent of the formed vortex ring. Let us consider the evolution of the thermal parameters in more detail.

From the experimental data that we obtained it follows that the dimensions of the nonuniformities of sufficiently large initial volume (on the order of 1 m^3 or more) increase linearly with height: $R=R_0+\alpha z$. It is important to emphasize that in the initial section of the territory of motion (before conversion of the thermal to a torus) the entrainment coefficient α turns out to be less than in the phase of movement of the nonuniformity in the form of a vortex ring. The

corresponding values of α were 0.1 ± 0.03 for $t\leq0.8$ sec and 0.19 ± 0.03 for $t\geq1.6$ sec. The fact that in the vortex ring phase the value of α is close to values usually recorded for thermals obviously is a consequence of the generation of the vorticity in it as a result of buoyancy [12].

Using the known models of the spherical thermal [3, 15] and also the vortex ring [11], the functions R(t) and the rates of ascent U(t) of the thermal inhomogeneity with initial parameters $R_0=0.9$ m, $T_0\approx1300$K, $U_0=2$ m/sec were calculated numerically. The results of the calculation by a model of a spherical thermal [15] rising in a uniform medium and by formulas of [3] for the ascent of a cloud of light gas in the air are presented in Figure 2 in the form of curves 2 and 3, respectively. The variation of the dimensions of the thermal for times of more than 1.6 seconds is described satisfactorily by the semiempirical formula obtained in [11] for floating vortex rings

$$R(t)=R_0'\left[\frac{2(\rho_\infty-\rho_0')gV_0'^{\alpha}}{\rho_\infty\pi nR_0'^4}t'^2+\frac{4\pi U_0'}{R_0'}(t'+1)\right]^{1/4}, \qquad (1)$$

where $t'=t-1.6$ sec;

R_0', V_0', U_0', ρ_0' are the radius, volume, speed and density of the torus for $t'=0$;

ρ_∞ is the density of the medium at an infinite distance from the thermal.

The rate of ascent of the ring is found from (1) by the formula

$$U(t)=\frac{1}{\alpha}\frac{dR}{dt}.$$

In formula (1), $n=5.5$ is the proportionality coefficient in the expresssion for circulation $\Gamma=nUR$. As follows from Figure 2 (curves 4), formula (1) satisfactorily describes the process of ascent of the thermal inhomogeneity, although not all of the assumptions made when deriving it are completely justified in our experiments.

Thus, in the initial phase of ascent, the evolution of an intense thermal is described well by the model of a spherical thermal; hereafter, the model of a floating vortex ring. The laws of ascent in the phase of transformation of a spherical thermal to a torus require more detailed investigation.

The mean density and temperature of the rising thermal can be calculated by the formulas derived from the quite simple expressions

$$\rho(t)=\rho_\infty\left[1-\frac{(\rho_\infty-\rho_0)R_0^3}{\rho_\infty R_e(t)^3}\right];\quad T\simeq T_\infty\frac{\rho_\infty}{\rho}, \qquad (2)$$

where $R_e(t)$ is the radius of a sphere of equivalent volume;

T_∞ is the temperature of the medium at an infinite distance from the inhomogeneity.

Inasmuch as the value of $R_e(t)$ is determined from experimentation with large error, $\rho(t)$ is calculated under the assumption that a spherical thermal with R_0=0.9 m and α=0.19 rises. The results of the calculation are presented in Figure 3a (curve 3). The dispersion of the experimental points 2 (averaging with respect to 30 experiments) is caused by the nonuniform temperature distribution in the thermal and the random position of the measurement point in the coordinate system connected with the moving target. On the whole, it is possible to note satisfactory agreement of the calculated and measured temperatures.

The heating of the medium in the vicinity of the thermal observed experimentally (see Figure 3b), as analysis shows, cannot be explained either by the processes of thermal conductivity or by evaporation of the drops directly under the effect of the radiation of the flames and the combustion products. Obviously, the basic factor of the heating of the medium in the chamber is radiation heating of the aerosol particles contained in the air, in particular, particles with effective size on the order of 10 microns and concentration of 10 cm^{-3}. The evaporation of the fog in the cloud chamber (see Figure 4) takes place as a result of a rise in the temperature of the medium.

From a solution of the heat and mass transfer equations for an individual drop it follows that as a result of the rise in temperature of the aqueous aerosol by the amount $\Delta T=T-T_\infty$ the drop will evaporate by the law

$$\dot{R}_1 = -\frac{Dq}{\rho_1 R_1}\frac{\varkappa \Delta T}{\varkappa + LDq}, \quad q = \rho_H(T_\infty)\left(\frac{L\mu_1}{R_r T_\infty} - 1\right)\frac{1}{T_\infty},$$

where R_1 is the drop radius;

D is the diffusion coefficient of the water vapor in the air;

χ is the thermal conductivity of the air;

ρ_1, L, μ_1 are the density, the heat of vaporization and molecular weight of water;

$\rho_H(T_\infty)$ is the density of the saturated water vapor at a temperature T_∞.

Then the equation of the evolution of the spectrum of the drop sizes in the heated air can be represented in the form

$$\frac{\partial f}{\partial t} - f\frac{A}{R_1^2} + \frac{A}{R_1}\frac{\partial f}{\partial R_1} = 0; \quad A = -\frac{Dq}{\rho_1}\frac{\Delta T}{1 + LDq/\varkappa}. \tag{3}$$

Here $f(R_1, t)$ is the distribution function of the drops by sizes at the time t. Using the Laplace transformation with respect to the time variable, let us represent (3) in the form

$$s\bar{f} + A\frac{\partial}{\partial R_1}\left(\frac{\bar{f}}{R_1}\right) = f_0(R_1); \quad \bar{f}(s, R_1) = \int_0^\infty f(t, R_1)\, e^{-st}dt. \tag{4}$$

Here $f_0(R_1)$ is the distribution function of the drops by sizes in an undisturbed aerosol.

In general form the solution of equation (4) is written as follows:

$$\overline{f} = R_1 e^{-\frac{sR_1^2}{2A}} \frac{1}{A} \int_{c(S)}^{R_1} f_0(\xi) e^{\frac{S\xi^2}{2A}} d\xi, \tag{5}$$

where c(s) is an arbitrary function of the argument s.

From (5) in accordance with the theorem of inversion of the Laplace transformation we have

$$f(R_1, t) = \frac{1}{2\pi i} \int_{s-i\infty}^{s+i\infty} \frac{R_1}{A} e^{-\frac{sR_1^2}{2A}} \int_{c(S)}^{R_1} f_0(\xi) e^{\frac{S\xi^2}{2A}} d\xi e^{st} ds = R_1 F\left(R_1, t - \frac{R_1^2}{2A}\right).$$

where $F\left(R_1, t - \frac{R_1^2}{2A}\right)$ is an arbitrary function of the arguments R_1 and $t-(R_1^2/2A)$.

By direct substitution of the expression found for $f(R_1, t)$ in (3), we find that $F\left(R_1, t - \frac{R_1^2}{2A}\right) \equiv \Phi\left(t_1 - \frac{R_1^2}{2A}\right)$. Considering, in addition, that $f(R_1,0)=f_0(R_1)$, we obtain the solution of equation (3):

$$f(R_1, t) = R_1 \frac{f_0\left(\sqrt{R_1^2 - 2At}\right)}{\sqrt{R_1^2 - 2At}}. \tag{6}$$

Curve 3 in Figure 4 corresponds to expression (6) for t=3 sec and ΔT=0.5K (the value of ΔT for r=1.5 m, see Figure 3b). Considering the error in determining the characteristics of the microstructure of fog (about 30%), the correspondence of curves 2 and 3 must be recognized as quite satisfactory.

Practical Applications

Delivery of Reagents. One of the methods of delivering the reagent or impurity to the given region of the atmosphere is use of ascending movements of air (thermals, currents, vortex rings) [5, 7, 10, 13]. In real situations the maximum height of rise of the vortex rings is basically determined by the degree of turbulence. The vortex ring is destroyed when its energy becomes comparable to the energy of turbulent pulsations in the atmosphere on a scale on the order of the size of the vortex R. Then in order to estimate the maximum height of rise of the vortex ring under the conditions of local isotropic turbulence it is possible to use the equation

$$U_{z(\max)}^2 = c\,\varepsilon^{2/3} R_{(z_{\max})}^{2/3}, \tag{7}$$

where c is a constant on the order of one;

ε is the dissipation rate of the turbulent energy.

From (1), (7) we obtain

$$z_{max} \sim \frac{1}{\varepsilon^{1/4}} \left(\frac{Q_{пл}^{(1)} R_г g}{2 c_p p_\infty \mu \pi n a^{11/3} c} \right)^{3/8} - \frac{R_0'}{a}, \qquad (8)$$

Key: 1. buoyancy

where $Q_{пл}^{(1)} = c_p (T_0 - T_\infty) \frac{4}{3} \pi R_0^3 \rho_0$ is the energy of buoyancy of the thermal inhomogeneities;

Key: 1. buoyancy

$R_г$ is the universal gas constant;

p_∞ is the atmospheric pressure;

μ is the molecular weight of the air;

c_p is the specific heat capacity of the air for constant pressure. Then R'_0=1.75 m; R_0=0.9 m; T_0=1300K; T_∞=293K; $\varepsilon=10^{-2}$ to 10^{-4} m^2/sec^3; z_{max}=30 to 80 m.

According to the experimental data, $z_{max} \sim$ 30 to 50 meters. The estimates obtained using the equation of motion of the thermal indicate that the presence of a reagent in the thermal leads to variation of z_{max} by no more than 10% if the reagent concentration does not exceed 50 g/m^3.

Penetration of Blocking Layers (Inversions). One of the problems of dynamic modification of atmospheric processes is penetration of inversion layers. It is known, in particular, that under the conditions of large industrial cities inversions lead to the occurrence of smogs and vapor trails over the cities, and the lifted inversions can prevent the occurrence of convective clouds. For the penetration of such layers intense thermals and currents can be used [8, 6]. The minimum energy release in a thermal inhomogeneity required to penetrate the inversion layer by it, can be estimated using the approach of [12] for determining the height of rise of the floating element in a stably stratified atmosphere:

$$Q = kmq = \frac{1}{k_1} \left[\frac{z_и}{c(\alpha)} \right]^4 (\gamma_a - \gamma) c_p \rho_\infty,$$

where k and k_1 are coefficients taking into account the incompleteness of combustion of the fuel and combustion energy losses to radiation;

q and m are the heat of combustion and mass of the aerosuspension;

z_i is the thickness of the inversion;

$c(\alpha)$ is the coefficient taking into account the effect of entrainment and structure of the thermal, equal to one with respect to order;

γ_a and γ are the dry adiabatic and true vertical temperature gradients in the atmosphere.

For z_i=150 meters; $\gamma_a - \gamma = 2.5 \cdot 10^{-2}$ K/m; T_∞=273K; k=0.3; k_1=0.75; $c(\alpha)$=2.66 (a spherical thermal), energy expenditures $Q \approx 4.6 \cdot 10^8$ joules and fuel consumption m=50 kg for $q=3.1 \cdot 10^6$ joules/kg are necessary. Here the initial size of the thermal R_0 will be close to $R_0 \simeq \sqrt[3]{\frac{k_1 Q R_г}{4/3 \pi c_p p_\infty \mu}} \approx 6{,}5$ м.

Creation of a Clearing Zone in Fogs and Clouds. From the results of experimentation (Figure 4) and theoretical investigation it follows that the effect of a source of volumetric heat release on a cloud medium is manifested in the creation of a cleared zone in its vicinity. Using formulas (3) and (6) and also the experimental data it is possible to make estimates of the corresponding variation of the integral coefficient of attenuation of the radiation in the medium. The attenuation factor of visible radiation in fog is defined by the expression

$$\alpha_0(r,\ t) = \int_0^\infty \pi R^2 K_0 f(R,\ t,\ \Delta T(r))\, dR;\ \left(\frac{2\pi R}{\lambda_m} \gg 1\right), \tag{9}$$

where $K_0 \approx 2$ is the efficiency factor of the attenuation for one drop;

$\lambda_m \approx 0.8$ microns is the wavelength corresponding to the maximum spectral distribution of the flame radiation.

For fogs with initial attenuation factor $\alpha_{0H} \approx 0.226\ m^{-1}$ ($\bar{R}$=6 microns, $N \approx 10^3\ cm^{-3}$) the calculation by (6) and (9) for t=5 seconds; r=1.5 meter; ΔT=0.5K gives a value of $\alpha_0 \approx 0.5\alpha_{0H}$. This agrees satisfactorily with the data obtained from measurements of the fog microstructure during the modification process. The time of existence of the clearing zone, as has been pointed out, is on the order of 10-15 seconds, which is sufficient for a number of practical applications, for example, for observation of astronomical targets. It can be increased by periodically repeated "launching" of the thermals.

BIBLIOGRAPHY

1. Andreyev, V.; Panchev, S. DINAMIKA ATMOSFERNYKH TERMIKOV [Dynamics of Atmospheric Thermals], Leningrad, Gidrometeoizdat, 1975.

2. Andrushchenko, V. A. "Formation of a Vortex Ring During Rise of a Heated Mass of Air in a Stratified Atmosphere," MEKHANIKA ZHIDKOSTI I GAZA [Fluid and Gas Mechanics], No 2, 1978.

3. Gorev, V. A.; Gusev, P. A.; Troshin, Ya. K. "Ascent and Combustion of a Hydrogen Cloud in the Air," DOKLADY AN SSSR [Reports of the USSR Academy of Sciences], Vol 222, No 4, 1975.

4. Didenko, N. K.; Smirnov, V. V. "Equipment for Measuring the Parameters of Weak Air Currents," TRUDY IEM [Works of the Institute of Experimental Meteorology], No 9, 1970.

5. Didenko, N. K.; Ivanov, V. N.; Korovin, V. Ya.; Rusakov, Yu. S.; Smirnov, V. V. "Possibility of Transporting a Reagent Using Vortex Rings," MATERIALY VSESOYUZNOY KONFERENTSII PO FIZIKE OBLAKOV I AKTIVNYM VOZDEYSTVIYAM NA NIKH [Materials of the All-Union Conference on Cloud Physics and Modification of Them], Obninsk, 1979.

6. Ivanov, V. N.; Korovin, V. Ya.; Petrushin, A. G.; Smirnov, V. V. "Energy Threshold of Nonlinear Attenuation of Laser Radiation in an Aerosol," MATERIALY VSESOYUZNOGO SOVESHCHANIYA PO RASPROSTRANENIYU OPTICHESKOGO IZLUCHENIYA V DISPERSNOY SREDE [Materials of the All-Union Conference on Spatial Optical Radiation in a Disperse Medium], Moscow, Gidrometeoizdat, 1978.

7. Lavrent'yev, M. A.; Shabat, Ye. V. PROBLEMY GIDRODINAMIKI I IKH MATEMATICHESKIYE MODELI [Problems of Hydrodynamics and Their Mathematical Models], Moscow, Nauka, 1973.

8. Pshenay-Severin, S. V.; Rudneva, I. A. "Conditions of Penetration of the Blocking Layer by a Thermal with Large Condensation Centers," TRUDY IEM, No 6, 1969.

9. Smirnov, V. V.; Yaskevich, G. F. "Application of Imaging Equipment for Studying the Microstructure of Clouds," METEOROLOGIYA I GIDROLOGIYA [Meteorology and Hydrology], No 5, 1979.

10. Struchayev, A. I.; Yershov, V. A.; Salov, V. A. "Simulation of the Delivery of Hygroscopic Reagents into the Atmosphere Using a Turbulent Vortex Ring," FIZIKA AERODISPERSNYKH SISTEM [Physics of Aerodisperse Systems], Kiev-Odessa, Vishcha shkola, No 18, 1978.

11. Tarasov, V. F. "Movement of an Ascending Vortex Ring," DINAMIKA SPLOSHNOY SREDY [Dynamics of a Continuous Medium], Novosibirsk, Nauka, No 23, 1975.

12. Terner, J. EFFEKTY PLAVUCHESTI V ZHIDKOSTYAKH [Buoyancy Effects in Liquids], Moscow, Mir, 1977.

13. Lane, G. A. FOG ABATEMENT, USA patent No 3804328, 1972.

14. Simons, G. A.; Larson, R. S. "Formation of Vortex Rings in a Stratified Atmosphere," PHYS. FLUIDS, Vol 17, No 1, 1974.

15. Shui, V. H.; Weyl, G. M. "Motion of a Rising Thermal," PHYS. FLUIDS, Vol 18, No 1, 1975.

16. Spurr, G. "The Penetration of Atmospheric Inversions by Hot Plumes," J. METEOROL., Vol 16, No 1, 1959.

UDC 551.(521.3:593.52)(575.4)

PECULIARITIES OF VARIATIONS OF THE MICROSTRUCTURE OF ARID AEROSOLS

Moscow METEOROLOGIYA I GIDROLOGIYA in Russian No 5, May 81 pp 33-38

[Article by V. P. Ivanov, P. A. Maslennikov, V. I. Sidorenko, Candidate of Physical and Mathematical Sciences V. L. Filippov, Kazan', manuscript received on 1 Sep 80]

[Text] This paper contains the results of studying the variability of the disperse composition of aerosols in the ground layer of air in an arid zone (Karakumy). The data from the indicated experiments are generalized on the level of studying seasonal differences in the particle size spectra.

The results of the studies indicate strong variability of the concentration field of an atmospheric aerosol. On the other hand, the disperse phase of the air is one of the primary factors defining the variations of the heat exchange conditions in the atmosphere. These facts are defined as one of the basic problems of the complex GAREX Program [3], the performance of regular observations of the variations of the aerosol particle size spectral during the GAREX-77 and GAREX-79 expeditions. The data from the indicated observations are presented in this paper, the generalization of which is carried out on the level of studying seasonal differences in the size spectra N_r in the ground layer of the air of an arid zone (Karakumy) by the results obtained on the two indicated expeditions: in September-October 1977 and February-March 1979, that is, the fall (the number of spectra investigated further m_1=221) and winter (m_2=107).

The measurements of N_r were made by the procedure of [2] with the application of the "Kvant-902M" aerosol classifier [7]. Here we only note that in the interests of obtaining more reliable information and in a wide range of particle sizes with respect to radius r two instruments were used in the experiment simultaneously tuned to different (but overlapping) ranges of Δr in accordance with Table 1. Here the conditions of taking the aerosol samples of different fractions and the number of gradations N_r in the resultant spectrum are defined in the table.

Table 1

Instrument No	Date	Range of particle sizes with respect to radius, microns	Volume of the investigated air sample, cm^3	Time of taking the samples, min	Range of "matching" of the spectra, microns	Range of particle sizes of the total spectrum, microns	No of gradations in the total spectrum
1	September-October 1977	0.1-4.4	5	5	1.8-2.7	0.1-64	25
2		1.8-64	200	2			
1	February-March 1979	0.1-5	5*	5	0.6-0.85	0.1-15	22
2		0.6-15	1500	2			

*The operating conditions of the instruments on the second expedition were changed without losses to subsequent analysis of the results considering the experience of the first measurements, and they permitted the reliability of the obtained data to be improved.

The qualitative analysis of sets of spectra (N_{rm}) obtained in the fall demonstrated that in the investigated region it is necessary to distinguish two aerosol conditions: "normal" for wind velocities $V_B \leq 7$ m/sec and "dust storm" conditions for $V_B > 7$ m/sec which is observed, as a rule on passage of atmospheric fronts.

The quantitative base supporting the indicated principle of separation of the aerosol conditions was the data from the subsequent statistical analysis of the interrelation between the particle concentration and wind velocity -- the wind erosion characteristic -- which under desert conditions is one of the basic mechanisms regulating the turbidity of the boundary layer of the atmosphere. During the winter the wind velocity did not exceed 6 m/sec, and here it is necessary to consider only the conditions which we provisionally called "normal."

In accordance with the adopted subdivision of aerosol conditions of the arid zone for autumn two sets of particle size spectra were formed, the first of which contained a sample ($V_B \leq 7$ m/sec) including 202 separate realizations; the second sample ($V_B >$ m/sec) included 18 realizations. The third sample combined m_2 particle size spectra recorded during the winter.

The isolated sets (N_r) were subjected to statistical analysis. The result of this analysis was to obtain average aerosol particle distribution profiles by sizes $\overline{n(r)} = \frac{1}{m}\sum_{l=1}^{m}\frac{dN_{rl}}{dr}$, which are illustrated in the figure. The particle distribution with respect to size for the fall period (curves 1 and 2) has the form of a descending curve with a decrease in concentration toward the region of large particles. On the particle size distribution curves $\bar{n}(r)$, independently of weather conditions, two inflections are observed which are centered in the regions r=0.3 to 1.5 microns and 5 to 15 microns. This nature of the spectrum can be

interpreted as a reflection of the superposition of three partial distributions -- Junge distribution [8] with the index $\beta=4$ (background distribution) and two gamma distributions with modal radii of 0.4 and 6-8 microns.

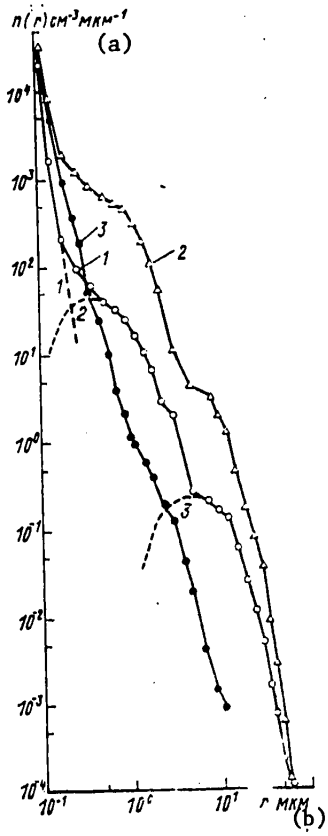

Mean particle size distribution spectra during autumn (curve 1 -- $V_B \leq 7$ m/sec; curve 2 -- $V_B > 7$ m/sec) and winter (curve 3)

Key:
a. cm^{-3} $micron^{-1}$
b. microns

The background distribution is the result of intraatmospheric nucleation and subsequent coagulation and heterogeneous condensation growth of the particles from low-volatile components of the gas phase.

For subsequent distributions, the coarsely disperse particle fraction of mechanical origin -- products of eolation from the soil surface -- is described. The first of them obviously describes the aerosol fraction which is made up of secondary products of fragmentation of the soil particles.

Table 2. Normalized Correlation

r_i, microns	r_k, microns										
	0,14	0,20	0,30	0,42	0,61	0,80	1,0	1,3	1,6	2,0	2,4
0,14	1,00	0,83	0,71	0,63	0,63	0,60	0,60	0,60	0,61	0,59	0,59
0,20		1,00	0,96	0,88	0,91	0,89	0,88	0,87	0,87	0,79	0,83
0,30			1,00	0,93	0,97	0,96	0,95	0,95	0,94	0,85	0,90
0,42				1,00	0,93	0,93	0,92	0,91	0,90	0,80	0,86
0,61					1,00	0,97	0,97	0,96	0,95	0,85	0,92
0,80						1,00	0,98	0,97	0,96	0,84	0,93
1,0							1,00	0,97	0,96	0,84	0,94
1,3								1,00	0,97	0,85	0,96
1,6									1,00	0,83	0,95
2,0										1,00	0,85
2,4											1,00
5,2											
7,7											
10											
14											
17											
22											
26											
32											
37											
43											
50											

Table 3. Normalized Correlation

r_i, microns	r_k, microns										
	0,11	0,21	0,26	0,31	0,38	0,49	0,65	0,78	0,92	1,1	1,3
0,11	1,00	0,93	0,88	0,86	0,80	0,72	0,80	0,71	0,39	0,21	0,15
0,21		1,00	0,98	0,96	0,86	0,65	0,75	0,69	0,34	0,16	0,09
0,26			1,00	0,98	0,89	0,63	0,74	0,70	0,35	0,17	0,10
0,31				1,00	0,94	0,68	0,79	0,75	0,43	0,26	0,20
0,38					1,00	0,73	0,82	0,81	0,56	0,43	0,41
0,49						1,00	0,84	0,90	0,79	0,67	0,62
0,65							1,00	0,91	0,72	0,57	0,49
0,78								1,00	0,89	0,74	0,63
0,92									1,00	0,93	0,84
1,1										1,00	0,95
1,3											1,00
1,6											
1,9											
2,4											
3,2											
4,0											
5,0											
6,0											
8,8											
11											
14											

Matrix $\rho_{r_i r_k}$

r_k, microns										
5,2	7,7	10	14	17	22	26	32	37	43	50
0,61	0,63	0,64	0,38	0,51	0,26	0,04	0,01	−0,02	−0,04	−0,05
0,83	0,82	0,81	0,51	0,70	0,38	0,11	0,06	0,01	−0,01	−0,02
0,89	0,87	0,85	0,53	0,74	0,41	0,15	0,10	0,05	0,01	0
0,85	0,83	0,81	0,50	0,70	0,36	0,13	0,08	0,03	0	0,01
0,91	0,88	0,86	0,55	0,76	0,43	0,18	0,13	0,07	0.04	0,06
0,90	0,87	0,85	0,55	0,74	0,42	0,16	0,11	0,07	0,05	0,05
0,92	0,89	0,87	0,56	0,78	0,45	0,20	0,14	0,09	0,06	0,05
0,94	0,92	0,90	0,57	0,78	0,45	0,20	0,14	0,10	0,07	0,06
0,93	0,92	0,90	0,57	0,78	0,44	0,20	0,13	0,09	0,07	0,05
0,81	0,79	0,78	0.50	0,72	0,46	0,22	0,18	0,12	0,08	0,05
0,95	0,94	0,92	0,59	0,85	0,55	0,31	0,26	0,21	0,15	0,11
1,00	0,98	0,97	0.60	0,83	0,50	0,25	0,20	0,17	0,13	0,15
	1,00	0,99	0,61	0,82	0,45	0,20	0,16	0,14	0,11	0,09
		1,00	0,62	0,84	0,45	0,20	0,15	0,13	0,10	0,09
			1,00	0,59	0,35	0,18	0,15	0,12	0,08	0,08
				1,00	0,79	0,51	0,51	0,43	0,34	0,23
					1,00	0,77	0,83	0,71	0,55	0,35
						1,00	0,83	0,76	0,61	0,39
							1,00	0,88	0,65	0,40
								1,00	0,77	0,53
									1,00	0,59
										1,00

Matrix $\rho_{r_i r_k}$

r_k, microns									
1,6	1,9	2,4	3.2	4,0	5,0	6,0	8,8	11	14
0,23	0,39	0,47	0,54	−0,23	−0,38	−0,34	−0,15	−0,18	−0,47
0,13	0,27	0,33	0,39	−0,19	−0,31	−0,27	−0,10	−0,13	−0,33
0,14	0,26	0,30	0,35	−0,18	−0,30	−0,27	−0,07	−0,12	−0,26
0,22	0,34	0,37	0,40	−0,20	−0,33	−0,29	−0,12	−0,14	−0,22
0,44	0,52	0,51	0,51	−0,25	−0,41	−0,36	−0,16	−0,19	−0,11
0,64	0,75	0,76	0,74	−0,19	−0,31	−0,27	−0,13	−0,16	−0,37
0,50	0,62	0,64	0,63	−0,18	−0,30	−0,25	−0,13	−0,19	−0,39
0,62	0,70	0,71	0,69	−0,16	−0,18	−0,12	−0,07	−0,20	−0,39
0,78	0,81	0,79	0,73	−0,16	−0,04	0,04	−0,01	−0,19	−0,28
0,91	0,87	0,80	0,71	−0,28	−0,09	0,01	0,11	−0,10	−0,11
0,98	0,93	0,85	0,72	−0,32	−0,29	−0,21	−0,10	−0,07	0,06
1,00	0,96	0,88	0,75	−0,33	−0,40	−0,33	0,05	−0,07	0,06
	1,00	0,96	0,87	−0,30	−0,44	−0,38	−0,01	−0,13	−0,09
		1,00	0,95	−0,25	−0,41	−0,35	−0,07	−0,18	−0,21
			1,00	−0,22	−0,34	−0,29	−0,07	−0,15	−0,32
				1,00	0,23	0,02	0	−0,04	−0,16
					1,00	0,96	0,10	−0,06	−0,25
						1,00	0,10	−0,05	−0,23
							1,00	0,08	−0,10
								1,00	0,24
									1,00

It must be noted that the profile that we obtained for a dust storm is distorted somewhat in the particle size range of r>10 microns, for usually a reduction in the concentration of particles of the indicated sizes as a result of a decrease in the aspiration factor with increasing wind velocities is observed in the opto-electronic spectrometers of the type described in [7] for a number of technical reasons. For the winter season the particle size distribution n(r) (curve 3) is described by the Junge distribution with index $\beta=3$ which corresponds to the conditions in temperate latitudes [8].

Seasonal differences in the investigated particle size spectra obviously have a stable nature and must be explained by two basic causes:

1. Karakumy belongs to the subtropical climatic zone: in the fall, tropical air predominates here, but in the winter the air from the temperate latitudes becomes predominant in the given region.

2. A no less important event for understanding the results is the condition of the underlying surface. In the fall, as a result of sharp heating of the soil in the presence of high winds, as a result of grinding and fragmentation of the coarse grains in the eolian sands characteristic of the region of investigation, soil particles are formed with sizes of less than 50 microns. In the presence of winds with velocity of $V_B>4$ m/sec, the latter are sucked off the earth's surface and carried by the ascending currents from a state of rest to motion in the suspended state [5]. In February-March 1979, the sand surface was wet, and above the wet surface the sand moved near the surface and did not rise into the air [5], that is, conditions were observed under which the transformation of the aerosol content of continental temperate air was not attenuated by the effect of a local particle source.

The aerosol particle size distribution spectra obtained during the fall period were compared with the results of measurements under the CENEX-70 program [1] and also with the data of I. Blifford [9]. It is possible to confirm good correspondence of the compared materials, which, first of all, indicates representativeness of the presented materials and, secondly, indicates the usefulness of the hypothesis of similarity of processes regulating the state of the dispersed material in the atmosphere within the limits of like geographic regions.

The normalized correlation matrix of $\rho_{r_i r_k}$ defining the spectrum sample $\{n(r)\}$ for "normal" conditions in the fall is presented in Table 2, and for the winter, in Table 3. The correlation matrix $\rho r_i r_k$ characterizing the spectrum sample $\{n(r)\}$ for a dust storm was not calculated in view of its statistical uncertainty. During the fall a quite strong correlation ($\rho_{r_i r_k}$~0.9 to 0.7) was noted between the particle fractions in the range of $0.2<r<20$ microns, which, according to the authors of [10], is primarily responsible for the visibility under arid zone conditions. According to our data some decrease in the coefficient ρ_{14, r_k} is observed, the interpretation of which is complicated at the present time. In the range of $r\geq 20$-60 microns the coefficients decrease sharply, approaching zero. The attenuation of the correlation between the variations of the number of particles with dimensions of r<10 microns and r>20 microns arises from the important fact that particles smaller than 10 micronsform the aerosol fraction, the variations of which in the region of observation are regulated by the relative humidity of the air and advective factors, for the aerosol can exist for a long time in the suspended state. At the same time the particles with dimensions of

more than 20 microns settle out quickly, and generation of them from the soil surface is determined by the fluctuations of the thermal and wind conditions of the layer of the atmosphere next to the earth.

For the winter season the correlation between the variations of the number of particles of different size was appreciably weaker with the exception of the narrow range of particle sizes $r \in 0.11\text{-}0.78$ micron, where $\rho_{r_i r_k} > 0.7$. In the range of $r > 3.2$ microns the correlation coefficients $\rho_{r_i r_k}$ pass through zero and become negative. The correlation matrix of the winter season is similar with respect to its structure to the corresponding correlation matrix for haze in the spring in temperate latitudes (see, for example [4]).

Thus, the seasonal variability of the aerosol size spectra in the arid zone is determined by the condition of the underlying surface and the circulation conditions in the given geographic region.

In conclusion the authors express their appreciation to G. Maksimov for help in performing the calculations on a computer and also the members of the GAREX-77 and GAREX-79 expeditions and K. Ya. Kondrat'yev for making it possible to participate in joint work.

BIBLIOGRAPHY

1. Dmokhovskiy, V. I.; Ivlev, L. S.; Semova, L. Yu. "Aerosol Measurements in the Layer of the Atmosphere Next to the Earth in Karakumy," TRUDY GGO [Works of the Main Geophysics Observatory], No 276, 1972.

2. Ivanov, V. P.; Filippov, V. L.; Sidorenko, V. I.; Maslennikov, P. A. "Statistical Characteristics of the Aerosol Particle Size Spectrum Variations in the Arid Zone," IZV. AN SSSR. FIZIKA ATMOSFERY I OKEANA [News of the USSR Academy of Sciences, Physics of the Atmosphere and Ocean], 1980, in press.

3. Kondrat'yev, K. Ya.; Vasil'yev, O. B.; Ivlev, L. S. GLOBAL'NYY AEROZOL'NO-RADIATSIONNYY EKSPERIMENT (GAREKS) [Global Aerosol-Radiation Experiment (GAREX)], Obninsk, VNIIGMI-MTSD, 1976.

4. Laktionov, A. G.; Lyubovtseva, Yu. S.; Malkevich, M. S. "Some Statistical Characteristics of the Aerosol Microstructure in the Layer of the Atmosphere Next to the Earth," IZV. AN SSSR. FIZIKA ATMOSFERY I OKEANS, Vol 9, No 2, 1973.

5. Petrov, M. P. PUSTYNI ZEMNOGO SHARA [Deserts of the Earth], Leningrad, Nauka, 1973.

6. Filippov, V. L. "Atmospheric Aerosol Formations. Morphology and Seasonal Gradations," IZVESTIYA VUZOV. FIZIKA [News of the Institutions of Higher Learning. Physics], No 5, 1976.

7. Filippov, V. L.; Kazakov, V. N.; Mirumyants, S. O. "Kvant-902M Aerosol Classifier," I VSESOYUZNOYE SOVESHCHANIYE PO ATMOSFERNOY OPTIKE [All-Union Conference on Atmospheric Optics], Part II, Tomsk, IOA SO AN SSSR, 1976.

8. Junge, H. KHIMICHESKIY SOSTAV I RADIOAKTIVNOST' ATMOSFERY [Chemical Composition and Radioactivity of the Atmosphere], Moscow, Mir, 1965.

9. Blifford, I. H.; Ringer, L. D. "The Size and Number Distribution of Aerosols in the Continental Troposphere," J. ATMOS. SCI., Vol 26, No 4, 1969.

10. Patterson, E. M.; Gillete, D. A.; Grams, G. W. "The Relation Between Visibility and Size-Number Distribution Soil Particle," J. APPL. METEOROL., Vol 15, No 5, 1976.

UDC 551.509.314

EFFECT OF STATION NETWORK DENSITY ON INTERPOLATED VALUE VARIABILITY CHARACTERISTICS

Moscow METEOROLOGIYA I GIDROLOGIYA in Russian No 5, May 81 pp 39-47

[Article by Doctor of Physical and Mathematical Sciences R. L. Kagan and Candidate of Physical and Mathematical Sciences Ye. I. Khlebnikova, Main Geophysics Observatory, manuscript received 2 Sep 80]

[Text] Abstract: A study is made of the problem of distortion of meteorological field variability characteristics during spatial interpolation of them. Evaluations are made of the underestimation of the dispersion and overestimation of correlation for fields of different statistical structure. The distortions of nongaussian value distribution are also considered (in the example of logarithmic-normal distribution). It is demonstrated that different station network density in different parts of the earth can lead to significant nonuniformity of the interpolated value field even in cases where the investigated field itself is uniform. Increasing the station network density during instrument observations can lead to a fictitious secular behavior of the variability characteristics of meteorological fields.

When investigating climate variations values of the meteorological elements interpolated to the nodes of a regular (for example, latitudinal-longitudinal) grid are often used instead of values actually measured at the stations. Naturally the variability characteristics of the investigated values must be distorted. The distortion can be different depending on different factors, including the station network density. For a comparatively sparse network used when studying climate variations, underestimation of the dispersion and overestimation of the spatial correlation of the interpolated values by comparison with the corresponding characteristics of the initial field, underestimation of the gradients and overestimation of the precision of the interpolation, and distortion of the nongaussian value distribution must occur.

The possibility of such effects has been pointed out many times (see, for example, [4, 6]), but the majority of specialists use the data at the grid nodes under the assumption that in quantitative respects the variability distortion is

comparatively low. In this article we shall try to illustrate how significant this distortion can be and how important it is to consider this distortion when investigating climate variability.

Numerical experiments were performed for this purpose in which the following were given: the statistical structure of the investigated meteorological field, mutual arrangement of the interpolation nodes and stations at which observation data are available for the value of f, and also the method of interpolation of the values from the stations to the grid nodes. Such field characteristics as the dispersion ($\sigma 2$) and spatial correlation (r) were determined by these data, evaluation of which with an interpolation of the type of

$$\tilde{f}_i = \sum_{k=1}^{n} p_k^i f_k, \tag{1}$$

where f_k are the values at the stations,

$\tilde{f}_i$ is the result of the interpolation at the i-th node of the grid,

p_k^i is the weight of the interpolation,

can be performed by the following simple formulas:

$$\tilde{r}_{ij} = \frac{1}{\alpha_i \alpha_j}\left(\sum_{k=1}^{n}\sum_{l=1}^{n} p_k^i p_l^j r_{kl} + \gamma_i^2 \sum_{k=1}^{n} p_k^i p_k^j\right), \tag{2}$$

$$\alpha_i^2 = \frac{\tilde{\sigma}_i^2}{\sigma_i^2} = \sum_{k=1}^{n}\sum_{l=1}^{n} p_k^i p_l^i r_{kl} + \gamma_i^2 \sum_{k=1}^{n} (p_k^i)^2. \tag{3}$$

Here η^2 is the measure of the errors in the initial data (see, for example [3]),

$r_{k\ell}$ is the correlation coefficient between the actual observation data at stations k and ℓ,

$\tilde{r}_{ij}$ is the correlation coefficient between the interpolated values at the nodes i and j,

$\tilde{\sigma}^2$ is the dispersion of the interpolated values.

These formulas pertain to the case of a uniform, isotropic field which, generally speaking, only roughly corresponds to reality, especially for large-scale areas. However, this is not basic; the indicated estimates can be performed also for a nonuniform field, but in the given step it is more significant to show that in the case where the actual initial field is uniform, the field of the interpolated values turns out to be nonuniform.

An estimate was also made of the distortion resulting from interpolation of the nature of the distribution of nongaussian meteorological fields. A statistical simulation of the values of the meteorological field at the stations and at the nodes of the given grid was performed for this purpose with subsequent estimation of the distribution of the interpolated values and its moments and comparison of these characteristics with the characteristics of the initial meteorological field.

In the described experiments, station networks of different density were simulated. Here, along with the reference station network, for which a regular square network was given with grid spacing H, a study was also made of irregular networks characterized by the same average station density with respect to area for which the coordinates of the stations were simulated by introducing random shifts in the reference network coordinates. Inasmuch as the characteristics of the interpolated values depend on how close the interpolation node is to the reference station, and in this sense, the interpolated value field obviously is nonuniform, in order to discover the regular differences of this field from the initial field we performed estimates for a group of dense interpolation nodes with subsequent determination of the average characteristics. The calculations were performed as applied to correlation functions characterizing the fields of different meteorological elements. Two procedures were used as the interpolation algorithms: optimal interpolation, for the application of which data are needed on the statistical structure of the initial field, and bilinear interpolation not requiring that information be supplied, for which the field is formally approximated in the vicinity of the node by a first-degree polynomial with respect to each of the coordinates. Interpolation to the grid nodes was carried out by the data from four stations, for the selection of which the newest station was found in each of the quadrants.

Let us present some results obtained for the case of an exponential correlation function of the type

$$r(\rho) = \exp(-\rho/\rho_0), \tag{4}$$

where ρ is the distance between points,

ρ_0 is the field correlation scale.

The estimates show that the interpolated value field dispersion is significantly underestimated by comparison with the initial field dispersion. In the case of optimal interpolation for distances between stations not exceeding $2\rho_0$, this underestimation is approximated well by a function of the type

$$\tilde{\sigma} = \sigma(1 - \gamma^2/8)(1 - 0{,}23\, H/\rho_0). \tag{5}$$

Thus, for $H=2\rho_0$ the mean square deviation of the interpolated values $\tilde{\sigma}$ turns out to be half the true values of σ. Comparison of the two interpolation methods shows that for bilinear interpolation when $H \leq \rho_0$ underestimation turns out to be approximately the same as for optimal interpolation. For a sparser network ($H>\rho_0$) bilinear interpolation understimates the field dispersion less than optimal interpolation, which in some sense compensates for its lower accuracy.

Table 1. Correlation $\tilde{r}(\rho)$ of Interpolated Values for Different Methods of Interpolation and Values of the Measure of the Observation Errors η^2

$(r(\rho) = \exp(-\rho/\rho_0);\ H = 0{,}25\,\rho_0)$

η^2	Способ интерполяции (2)	ρ (в долях от H) (1)							
		0,125	0,250	0,375	0,50	0,75	1,00	1,25	1,50
0	Оптимальный (3)	0,997	0,989	0,977	0,961	0,925	0,887	0,847	0,800
	Билинейный (4)	0,997	0,989	0,976	0,960	0,923	0,885	0,844	0,793
0,05	Оптимальный (3)	0,995	0,986	0,973	0,956	0,922	0,888	0,854	0,812
	Билинейный (4)	0,994	0,982	0,967	0,949	0,914	0,883	0,844	0,791
	$r(\rho)$	0,969	0,939	0,911	0,883	0,829	0,779	0,732	0,687

Key:
1. (in fractions of H)
2. Interpolation method
3. Optimal
4. Bilinear

Values of the correlation functions of the variables obtained by optimal and bilinear interpolation of the initial field are presented in Table 1 for the given grid size of a regular station network H, for presence and absence of observation errors. From these data it can easily be seen how much the interpolated value correlation is overestimated by comparison with the initial field correlation, where the optimal interpolation distorts the correlation function more than the bilinear interpolation. However, the difference of the correlation functions of the values obtained by different methods of interpolation, is small by comparison with the deviation from the true correlation function. The structural characteristics of the interpolated values also depend comparatively little on the measure of the initial data errors. Along with overestimation of the correlation as a result of interpolation, the nature of the correlation function changes significantly for small spacings: in contrast to the initial function, the correlation function of the interpolated values is characterized by differentiability at zero, which can lead to high distortion of the estimates of the field difference characteristics.

As has already been noted, the estimates of the distortions of the statistical structural characteristics of the field as a result of interpolation were made also for nonuniform arrangement of the stations. It was discovered that with averaging over large territories the statistical structural characteristics of the interpolated values calculated by the data from nonuniformly arranged stations turn out to be more distorted than the same characteristics obtained by a regular station network.

The calculations performed for the correlation functions of the type differing from (4) lead to conclusions analogous to those presented above.

Table 2. Distortion as a Result of Interpolation of the Distribution of a Logarithmically-Normal Value (mean equal to 0; $r(\rho)=\exp(-\rho/\rho_0)$; $H=\rho_0$)

Интервал (1)		Дифференциальная (2) функция распределения	
		истинные значения (3)	после интерполяции (4)
−2,5	−2,0	0,001	0,000
−2,0	−1,5	0,025	0,003
−1,5	−1,0	0,114	0,047
−1,0	−0,5	0,204	0,187
−0,5	0	0,219	0,295
0	0,5	0,174	0,235
0,5	1,0	0,116	0,137
1,0	1,5	0,069	0,057
1,5	2,0	0,038	0,025
2,0	2,5	0,020	0,010
2,5	3,0	0,010	0,002
3,0	3,5	0,005	0,001
3,5	4,0	0,003	0,001
Стандарт (5)		1,00	0,73
Коэф. асим. (6)		1,00	0,77
Коэф. эксц. (7)		1,83	1,17

Key:
1. Interval
2. Differential distribution function
3. True values
4. After interpolation
5. Standard
6. Asymmetry coefficient
7. Excess coefficient

Some estimates of the distribution of the interpolated values are presented in Table 2 for a logarithmically normal value with exponentially decreasing correlation coefficient (let us note that this model in many cases satisfactorily describes the statistical structure of the precipitation totals). From a comparison of this distribution with the true distribution it is obvious that the spatial interpolation leads not only to underestimation of the dispersion, but also to sharp distortion of the nature of the investigated value itself, making it rapidly approach normal.

The estimates show that the optimal interpolation underestimates the field dispersion more than the bilinear interpolation, just as it does with other methods of interpolation. Accordingly, the question arises of to what degree it is expedient to use it for various purposes. However, it turns out that it has a number of advantages by comparison with other methods of interpolation. Let us only point out that there is a unique relation between α and the mean square relative interpolation error ε_0 described by the simple expression

$$\alpha=\sqrt{1-\varepsilon_0^2}. \qquad (6)$$

The value of ε_0 is calculated automatically during the process of optimal interpolation, and the singularities of its spatial distribution have been studied quite well for various meteorological fields [1, 3]. This permits estimation of the geographic distribution of the measure of underestimation of the standard in various parts of the earth for many meteorological elements, using the previously performed estimates of the accuracy of the optimal interpolation.

Quantitative estimates of the distortion of the variability characteristics for fields of specific meteorological elements depend both on the form of the correlation function and on the relation between the density of the station network and the correlation scale. For example, the spatial correlation function of exponential type (4) is characteristic for a number of meteorological elements, including the precipitation totals, radiation, total ozone content, for the monthly values of which the correlation scale is several hundreds of kilometers, about 1000 km and 1600 km, respectively. As applied to the precipitation field the estimates show that in more populous areas where the average distance H between precipitation gauging stations is about 50 km, the underestimation is within the limits of 10%. For sparsely populated areas of the USSR, for which a value of H≈150 km is characteristic, this underestimation is different for different areas and in dry regions, it reaches values of 20-30%. The total radiation has significantly greater connectedness; inasmuch as, however, the actinometric station network is much sparser than the precipitation measuring network, even in continental regions there are broad expanses for which the underestimation of σ exceeds 20%. The situation is still worse in the oceans in which the actinometric network is in practice nonexistent. For total monthly ozone contents in Western Europe where the distance between stations H is about 400 km, the underestimation of σ is also within the limits of 10%. For values of H=800 km, characteristic of the ozonometric network of the USSR, it is about 20%. For H=2000 km, which approximately corresponds to the station density in the North Atlantic, the underestimation of σ is about 40%. For such regions, of course, the overestimation of the correlation function is very large.

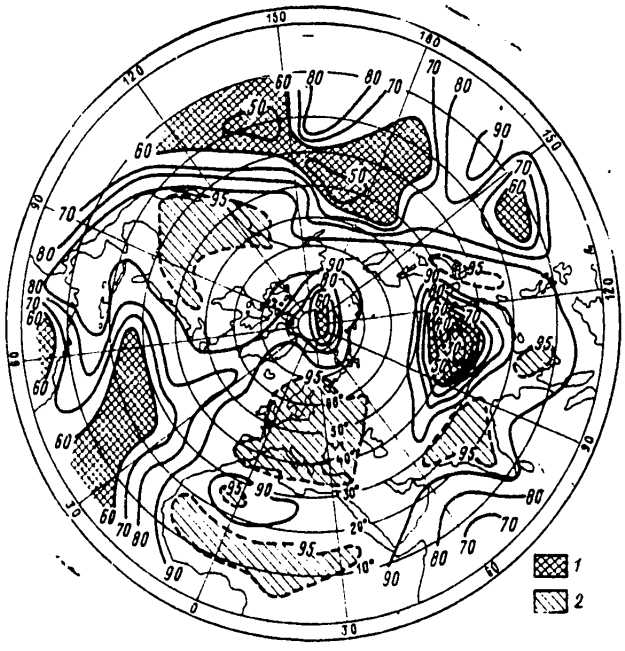

Figure 1. Measure of the underestimation of the standard (α) for the mean annual air temperature.
1) $\alpha<0.6$; 2) $\alpha>0.95$.

Estimates analogous to those presented can also be made for other correlation functions. In all cases significant dependence of the measure of underestimation of the mean square deviation α on the station network density is characteristic. Inasmuch as the general nature of the network distribution of stations that measure various meteorological elements on the earth is approximately identical, the geographic distribution of the measure of underestimation α for the interpolated values of different elements have analogous form: namely, regions of the largest values of α close to one are located in the populated areas of Western Europe, the European territory of the USSR, North America, and Japan. In addition, there are broad expanses in the polar and equatorial zones and in the oceans characterized by small values of α, 50% and less.

As an example, a distribution map of the value of α is presented in Figure 1 for the mean annual air temperature constructed on the basis of estimates performed by K. M. Lugina at the State Hydrological Institute of the accuracy of optimal interpolation by the data from a network of 776 stations in the northern hemisphere used to investigate climate variations [2]. On this map the differences can easily be seen between the values of α in the different regions of the earth. It is natural that for meteorological elements with less connectedness these differences are more expressed.

Thus, using the data at the grid nodes to estimate the variability of the meteorological parameters without the necessary consideration of the properties of the interpolated values and different station network density in the various regions, it is possible to arrive at a false conclusion regarding the spatial differences of the variability characteristics comparable with respect to order of magnitude to the actually observed values.

It is possible to expect to an equal degree that the variation of the station network density (and it increases monotonically during the instrument observation period) must lead to regular variation of the variability characteristics of the interpolated values with time. Let us present two examples giving a quantitative representation of how significant this effect can be.

Let the spatial structure of the field be described by an exponential correlation function (4). Then the measure of the underestimation of the variability α is described by an approximate formula (5). Knowing the average network density for different time periods, it is possible to estimate the behavior of α.

Let, for example, the number of stations be doubled in some region during the investigated time period. This appears to be quite realistic for regions with a sparse network. In this case, at the beginning of the observation period the average spacing between stations was $H_0=\sqrt{2}H$; correspondingly, the measure of the underestimation of the variability was

$$\alpha_0 = 1 - \sqrt{2}(1-\alpha). \qquad (7)$$

Hence, it is easy to see that for regions in which α=0.7 at the present time, doubling the number of stations led to an increase of 20% in this value; for α=0.6, the increase was 40%; for α=0.7, it was 70%. Of course, these estimates are quite rough inasmuch as formula (5) is insufficiently exact for such values of α, but the formula does permit estimation of the order of the corresponding anomaly variations.

Still greater variation of the station network density can be felt in the characteristics of the gradient of the interpolated value which in practice is estimated as the difference in the values of the element at different points. Specific values of the possible underestimation of the gradient characteristics depend on a number of conditions, including the method of interpolation. Let us consider, for example, a uniform linear interpolation

$$\tilde{f}(x) = f_0 + (f_1 - f_0)\frac{x}{H} \tag{8}$$

between values of f_0 and f_1 at the stations located a distance H from each other. When determining the gradient by the interpolated values at the nodes x_1 and x_2 located at a distance h in the interval between stations, the true value of the gradient $\Gamma(h)$ is replaced by the value of $\tilde{\Gamma}(h)=f(x_2)-\tilde{f}(x_1)=(h/H)\ (f_1-f_0)$. In this case the measure of the underestimation of the mean square deviation of the gradient can be estimated by the formula

$$\alpha_{\Gamma(h)} = \frac{\sigma_{\tilde{\Gamma}(h)}}{\sigma_{\Gamma(h)}} = \frac{h}{H}\sqrt{\frac{1-r(H)}{1-r(h)}}. \tag{9}$$

Some estimates made by formula (9) are presented in Table 3 as applied to the mean monthly and mean annual air temperature when using data on the spatial correlation of this element obtained by K. M. Lugina [7]. From the table it is obvious that for the regions where the distance between stations exceeds by several times the distance for which the gradient is estimated, its value even for this idealized interpolation scheme and with such a bound field as the air temperature field, can be underestimated by more than a factor of two. Nevertheless, for certain regions such large distances between stations are a reality.

Table 3. Measure of the Underestimation $\alpha_{\Gamma(1000)}$ of the Air Temperature Anomaly Gradient Calculated for 1000 km

H, km	1000	1500	2000	2500	3000	4000
Mean temperature for the month of January	1.00	0.87	0.78	0.70	0.64	0.54
Mean annual temperature	1.00	0.83	0.73	0.63	0.59	0.49

Let us note, for example, that for the zone north of 70° north latitude in this century it is possible to expect an increase in the interpolated value anomaly gradients by more than twofold if we consider that at the beginning of the century regular observations were performed in this area only by three stations, and they were located around the periphery of the polar basin, and at the present time there are almost 100 such stations. It is possible to expect a significant increase in the temperature gradients for the instrument observation period as a result of an increase in the station network density also in the equatorial zone. In temperate latitudes where the increase in station network density is noticeably less, the growth of the gradients as a result of this factor must be comparatively small.

In the light of these arguments, the data presented in [5] on the variations of the values of the air temperature anomaly gradient modulus in different latitudinal zones for the 1891-1976 period calculated by the data at the nodes of the latitude-longitude grid, are of interest. From Figure 2, in which the graphs of the gradient standards of the mean monthly temperature anomalies (averaged for the year) taken from [5] are reproduced, it is obvious that an increase in the gradients with time is characteristic of all zones, but it is most significant (by several times) for the Arctic Basin (the vicinity of 80° north latitude) and near the equator (20° north latitude).

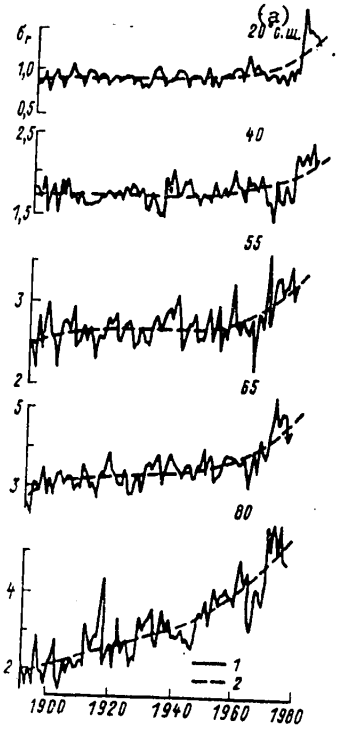

Figure 2. Standard (°C/10° meridian) of the anomaly gradient modulus of the mean monthly air temperature averaged for the year (according to the data of [5]).
1 -- initial time series; 2 -- result of approximation by a third-degree polynomial

Key:
a. 20° north latitude

Without rejecting the possibility of the existence of a trend, let us note that the discovered behavior of the gradients, generally speaking, can be explained by variation of the station network density over the course of the investigated period. It is obvious that to draw a conclusion about the actual increase in climate variability (or, let us say, about intensification of the meridional

transport) based on such secular behavior of the anomaly gradients, a careful estimate and exclusion of that part of the secular behavior which is determined by causes of a procedural nature, are required.

In conclusion, let us note that the authors are far from stating that the presented estimates are accurate and can be used for direct correction of the characteristics obtained at the grid nodes. The variety of interpolation schemes used in practice is too great, and the structural peculiarities of different meteorological fields are too complex for it to be possible to fit them in the very simple schemes that we have used. If, however, even the order of the obtained values corresponds to reality, it is necessary to consider the investigated factor in climate studies.

BIBLIOGRAPHY

1. Belousov, S. L., et al. OBRABOTKA OPERATIVNOY METEOROLOGICHESKOY INFORMATSII S POMOSHCH'YU ELEKTRONNYKH VYCHISLITEL'NYKH MASHIN [Computer Processing of Meteorological Data], Leningrad, Gidrometeoizdat, 1969.

2. Borzenkova, I. I.; Vinnikov, K. Ya.; Spirina, L. P.; Stekhnovskiy, D. I. "Air Temperature Variation in the Northern Hemisphere from 1881 to 1975," METEOROLOGIYA I GIDROLOGIYA [Meteorology and Hydrology], No 9, 1977.

3. Borisenkov, Ye. P. "Physical-Statistical Methods of Analysis and Overestimation of the Meteorological Fields," TRUDY AANII [Works of the Arctic and Antarctic Scientific Research Institute], Vol 263, 1963.

4. Gruza, G. V.; Polyak, I. I.; Shakhmeyster, V. A. "Time-Space Statistical Structure of the Mean Monthly Geopotential of the 500 millibar Surface," METEOROLOGIA I GIDROLOGIYA, No 4, 1979.

5. Gruza, G. V.; Ran'kova, E. Ya. DANNYYE O STRUKTURE I IZMENCHIVOSTI KLIMATA [Data on the Structure and Variability of Climate], Obninsk, VNIIGMI-MTSD, 1979.

6. Polyak, I. I. METODY ANALIZA SLUCHAYNYKH PROTSESSOV I POLEY V KLIMATOLOGII [Methods of Analyzing Random Processes and Fields in Climatology], Leningrad, Gidrometeoizdat, 1979.

7. STATISTICHESKAYA STRUKTURA METEOROLOGICHESKIKH POLEY [Statistical Structure of Meteorological Fields], Budapest, 1976.

UDC 551.52+630:551.5

RELATION OF MEAN ANNUAL VALUES OF THE ALBEDO AND SHORTWAVE RADIATION BALANCE TO THE SAME INDICES IN EARLY SPRING

Moscow METEOROLOGIYA I GIDROLOGIYA in Russian No 5, May 81 pp 48-52

[Article by Doctor of Biological Sciences Kh. G. Tooming, Estonian Agrometeorological Laboratory of the All-Union Scientific Research Institute of Agricultural Microbiology, manuscript received 16 Sep 80]

[Text]

Abstract: A close relation was detected between the mean annual albedo and shortwave radiation balance and the albedo and shortwave balance in snow-covered areas in the early spring. The parameters of the regression equations of these relations are presented.

The annual behavior of the albedo of the underlying surface has been well investigated by Soviet scientists [2, 4, 5]. Albedo distribution maps have been compiled for the territory of the USSR in various seasons, and the mean annual albedo has been established as a function of the time of existence of the snow cover [1, 3, 4]. On the basis of data from Tartu station we found that the mean annual albedo depends on the albedo of the early spring months -- March and April [6].

At a number of points in the USSR the total and reflected radiation have been continuously recorded for a number of years, and at Tartu station these values have also been integrated. Thus, we have the possibility of a more detailed study of the albedo questions. In this article we have set as our goal the discovery of the dependence of the mean annual albedo on the albedo in the early spring season at certain points in the USSR and also the dependence of the mean annual shortwave radiation balance (SWRB), that is, the shortwave radiation absorbed by the underlying surface in a year, on the shortwave radiation absorbed in the early spring season.

In this paper the mean annual albedo and the albedo for the early spring season are defined as the ratio of the corresponding sums of the reflected radiation to the sum of the total radiation. The shortwave radiation balance is defined as the difference in the sums of the total and reflected radiation.

The relation we detected between the mean annual albedo and the spring albedo is expressed by the following regression equation:

$$A_r = \overline{A}_r + R_{y/r}(A_n - \overline{A}_n), \qquad (1)$$

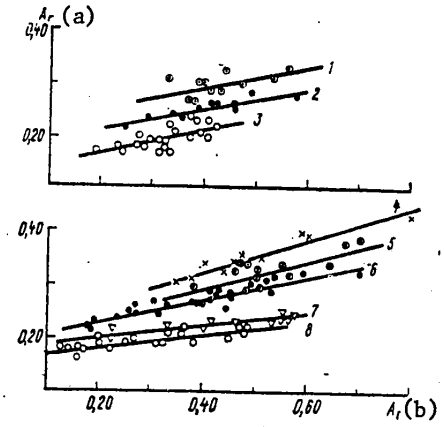

Figure 1. Mean annual albedo $A_Г$ as a function of the early spring albedo A_B.
1 -- Moscow (March-April), 2 -- Voyeykovo (March-April), 3 -- Irkutsk (February-March), 4 -- Verkhoyansk (April-May), 5 -- Petropavlovsk-na-Kamchatke (March-April), 6 -- Tartu (March-April), 7 -- Borispol' (Kiev) (February-March), 8 -- Kishinev (February-March).

Key:
a. $A_Г$
b. A_B

where $A_Г$ is the mean annual albedo,

$\overline{A}_Г$ is the mean perennial value of the mean annual albedo,

A_B is the albedo in the early spring season,

$\overline{A}_B$ is the mean perennial value of the early spring albedo,

$R_{y/x}$ is the regression coefficient.

The parameters of this equation for certain places are presented in Table 1.

By the data from the Verkhoyansk, Voyeykovo and Tartu stations (Figure 1, Table 1) it turns out that the relation of $A_Г$ to A_B is the closest, especially in northern regions. For these stations the dependence of the mean annual albedo on the March-April albedo is in practice functional (r=0.92 to 0.96, p=0.99). For Tartu station the mean annual albedo can be calculated by the equation

$$A_r = 0{,}27 + 0{,}21\ (A_{III+IV} - 0{,}39), \tag{2}$$

for Voyeykovo

$$A_r = 0{,}25 + 0{,}19\ (A_{III+IV} - 0{,}41), \tag{3}$$

for Verkhoyansk

$$A_r = 0{,}35 + 0{,}30\ (A_{IV+V} - 0{,}50). \qquad (4)$$

The relation of the mean annual albedo to the March-April albedo is also close by the data from the stations at Petropavlovsk-na-Kamchatke, Kuybyshev, Moscow and Arkhangel'sk (Table 1). Since beyond the Arctic Circle in Verkhoyansk and in Kamchatka, the snow goes off in May, a close relation is noted between the mean annual albedo and the April-May albedo. The relation is also comparatively good by the data from the stations at Kishinev, Borispol' (Kiev) and Omsk. A relation of $A_г$ to the February-March albedo is noted at these stations. The relation is weaker in Irkutsk, Vladivostok and Tashkent (Table 1), where the snow disappears in February at the last-mentioned station, and a relation is noted between $A_г$ and the January-February albedo.

Table 1. Parameters of the Regression Equation (1), the Correlation Coefficients r and their Probability Levels p for Certain Points in the USSR

Station	No of years of observation	$A_г$	Period	$\overline{A}_в$	$R_{y/x}$	r	p
Verkhoyansk	12	0.35	April-May	0.50	0.30	0.96	0.99
Arkhangel'sk	12	0.28	March-April	0.48	0.18	0.77	0.99
Yakutsk	11	0.31	The same	0.57	0.16	0.61	0.95
Voyeykovo	12	0.25	"	0.41	0.19	0.93	0.99
Tartu	26	0.27	"	0.39	0.21	0.92	0.99
Moscow	11	0.30	"	0.43	0.20	0.70	0.95
Petropavlovsk-na-Kamchatke	13	0.33	"	0.53	0.27	0.83	0.99
Petropavlovsk-na-Kamchatke	13	0.33	April-May	0.31	0.30	0.72	0.99
Kuybyshev	14	0.24	March-April	0.30	0.17	0.81	0.99
Vladivostok (Sad-gorod)	12	0.26	The same	0.25	0.23	0.50	0.90
Omsk	12	0.25	February-March	0.63	0.16	0.75	0.99
Irkutsk	23	0.20	The same	0.32	0.21	0.62	0.99
Borispol' (Kiev)	11	0.23	"	0.43	0.09	0.77	0.99
Kishinev	24	0.19	"	0.28	0.11	0.78	0.99
Tashkent	24	0.24	January-February	0.37	0.07	0.41	0.95

It is possible to see that the relation of the mean annual albedo to the early spring albedo in southern areas is weaker than in northern areas (Table 1, Figure 1). As a rule, in the northern regions the sensitivity of the mean annual albedo with respect to early spring albedo is higher than in the southern regions. This is indicated by the high slope of the straight lines and higher regression factor of the dependence of $A_г$ on $A_в$ in Verkhoyansk, Voyeykova, Tartu and in Petropavlovsk-na-Kamchatke by comparison with these indices for Kishinev, Borispol' (Kiev) and Tashkent (Figure 1, Table 1). It is also possible to note (Table 1) that the

regression factor of the relation $A_г=f(A_{II+III})$ is higher for Siberia (Irkutsk, Omsk) than for the European territory of the USSR (Borispol', Kishinev).

The main cause for the relation between the mean annual albedo and the early spring albedo consists in the fact that the total and reflected radiation sums in the early spring months are comparatively high. The total reflected radiation can vary within large limits depending on the duration of the snow cover and its reflectivity. The variations of the albedo in the winter and fall months do not have great significance in the formation of the annual albedo, for the total and reflected radiation sums are small in these months. In the summer and fall months the albedo of the grass cover varies comparatively little and has no significant influence on the variation of the annual albedo.

The shortwave radiation absorbed in a year, that is, the SWRB, is in a comparatively satisfactory correlation with the absorbed radiation for the early spring season. The regression equation of the mean annual SWRB with the early spring SWRB is the following:

$$B_{k_г}=\overline{B}_{k_г}+R_{y/x}(B_{k_в}-\overline{B}_{k_в}), \tag{5}$$

where $B_{k_г}$ is the mean annual SWRB,

$\overline{B}_{k_г}$ is the mean perennial value of the mean annual SWRB,

B_{k_B} is the SWRB for the early spring season,

$\overline{B}_{k_B}$ is the mean perennial value of the SWRB for the early spring season,

$R_{y/x}$ is the regression factor.

The correlation of the values of the SWRB is close in certain regions (Table 2). For example, in Verkhoyansk and Petropavlovsk-na-Kamchatke the relation of the mean annual SWRB to the SWRB for the early spring season is also closer and more significant ($r=0.68$ to 0.73, $p=0.95$ to 0.99) than the relation of the mean annual SWRB to the annual total radiation sums ($r=0.30$ to 0.40, $p<0.90$). The correlation between the values of the SWRB is also close in Borispol' ($r=0.72$, $p=0.99$) (Table 2). At the rest of the locations, the relation of the mean annual SWRB to the SWRB of the early spring season is somewhat weaker (Table 2). In Tartu, for example, the mean annual SWRB depends more on the arrival of the total radiation ($r=0.77$, $p=0.99$) than on the SWRB of the early spring season ($r=0.61$, $p=0.99$).

In the territory of the USSR in a number of regions (Voyeykovo, Tartu, Moscow, Petropavlovsk-na-Kamchatke), the relation of the mean annual SWRB to the SWRB of the early spring season (Figure 2) can be expressed by a common regression equation for all these points

$$B_{k_г}=60{,}0+1{,}2(B_{k_{III+IV}}-9{,}2). \tag{6}$$

Table 2. Parameters of the Regression Equation (2), Correlation Coefficients r and their Probability Levels p for Certain Points of the USSR

Station	No of years of observations	$\overline{B}_{k_\Gamma}$	Period	$\overline{B}_{k_B}$	$R_{y/x}$	r	p
Verkhoyansk	12	51.9	April-May	13.0	1.05	0.68	0.95
Arkhangel'sk	12	50.5	March-April	6.7	0.99	0.34	0.90
Yakutsk	11	61.8	The same	8.2	0.56	0.42	0.90
Voyeykovo	12	58.5	"	8.1	1.37	0.54	0.95
Tartu	26	60.4	"	9.8	1.34	0.61	0.99
Moscow	11	58.5	"	9.0	1.00	0.41	0.90
Petropavlovsk-na-Kamchatke	13	62.1	"	9.7	1.03	0.73	0.99
Kuybyshev	14	74.1	"	12.5	1.05	0.49	0.90
Omsk	12	70.5	February-March	4.3	1.77	0.40	0.90
Irkutsk	23	79.5	The same	8.9	2.63	0.54	0.99
Borispol' (Kiev)	11	72.2	"	6.0	1.72	0.72	0.99
Kishinev	24	83.6	"	7.8	1.52	0.58	0.99

The regression equations (Table 2) have some forecasting significance. They permit approximate prediction of the values of the mean annual SWRB in the early spring.

The variations of the mean annual albedo and the SWRB of the early spring season must have some climatological significance. A detailed role of the albedo and the SWRB of the early spring season during climate formation is difficult to establish as a result of the predominant significance of advective heat exchange in the majority of regions. We have been able to detect only a weak, but significant correlation of the sums of the effective temperatures before the end of June and July with the early spring albedo.

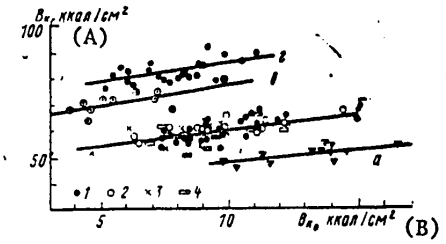

Figure 2. Mean annual SWRB B_{k_Γ} as a function of the SWRB in the early spring B_{k_B}.
a -- Verkhoyansk (April-May); b -- Tartu (1); Petropavlovsk-na-Kamchate (2), Voyeykovo (3), Moscow (4) (March-April); c -- Borispol' (Kiev) (February-March); d -- Kishinev (February-March)

Key:
A. B_{k_Γ}, kcal/cm^2
B. B_{k_B}, kcal/cm^2

Thus, for Tartu, the regression equation will be

$$\sum_{VI} t(>5^\circ C) = 520 - 290\,(A_{III+IV} - 0{,}39);\ r = 0{,}52,\ p = 0{,}99; \quad (7)$$

for Petropavlovsk-na-Kamchatke

$$\sum_{VII} t(>5^\circ C) = 335 - 260\,(A_{IV+V} - 0{,}31);\ r = 0{,}40,\ p = 0{,}90, \quad (8)$$

$$\sum_{vii} t(>10^\circ C) = 85 - 220\,(A_{IV+V} - 0{,}31);\ r = 0{,}45,\ p = 0{,}90. \quad (9)$$

At more southerly points, it was not possible to detect significant correlation of the early spring albedo with the thermal conditions of subsequent months.

Conclusions

1. A relation of the mean annual albedos and SWRB to the same indices in the early spring is noted in all snow-covered parts of the USSR, but it is more sharply noted in the northern regions.

2. Knowledge of the early spring albedo permits the mean annual albedo to be predicted well in the northern regions, and knowledge of the SWRB in the early spring makes it possible to judge the mean annual SWRB satisfactorily.

3. In some northern areas of the USSR, the early spring albedo has some influence on the thermal conditions of the subsequent spring and early summer months.

BIBLIOGRAPHY

1. Beriyand, T. G. "Radiation and Heat Balance of the European Territory of the USSR," TRUDY GGO [Works of the Main Geophysics Observatory], No 10(72), 1948.

2. Budyko, M. I. TEPLOVOY BALANS ZEMNOY POVERKHNOSTI [Heat Balance of the Earth's Surface], Leningrad, Gidrometeoizdat, 1953.

3. Yefimova, M. A. RADIATSIONNYYE FAKTORY PRODUKTIVNOSTI RASTITEL'NOGO POKROVA [Radiation Factors of Productivity of the Vegetation Cover], Leningrad, Gidrometeoizdat, 1977.

4. Kondrat'yev, K. Ya. AKTINOMETRIYA [Actinometry], Leningrad, Gidrometeoizdat, 1965.

5. Mukhenberg, V. V. "Albedo of the Underlying Surface of the Territory of the Soviet Union," TRUDY GGO, No 139, 1963.

6. Tooming, H. "Daily and Seasonal Variations of the Albedo of Some Natural Surfaces in the Estonian SSR," ISSLEDOVANIYA PO FIZIKE ATMOSFERY [Research in the Physics of the Atmosphere], No 2, 1960.

UDC 551.(521+576)

BRIGHTNESS VARIATIONS OF CLOUD FIELDS WHEN OBSERVED FROM DIFFERENT ALTITUDES

Moscow METEOROLOGIYA I GIDROLOGIYA in Russian No 5, May 81 pp 53-58

[Article by Candidate of Technical Sciences L. I. Chapurskiy, Leningrad, manuscript received 9 Oct 80]

[Text]

Abstract: The isophots of cloud fields are presented as applied to observation conditions from altitudes up to 9 and above 36,000 km. It is demonstrated that for observations from high altitudes the brightness of the global cloud fields varies within smaller limits than the sine of the solar angle at viewable points of the visible earth's disc as a result of nonuniform altitude of their upper boundaries and structural peculiarities.

When solving certain problems connected with remote sounding of the atmosphere, it is necessary to estimate the dynamic brightness range of clouds falling into the field of view of the equipment located at different distances from the earth's surface. The cloud brightness depends on the optical thickness of the clouds, the albedo of the underlying surface, the observation configuration, radiation absorption and scattering effects in the atmosphere above the clouds and other factors [7]. In this paper a study is made of the influence of indicatrix effects on the formation of the brightness fields of clouds observed from different altitudes with different values of the solar radiation scattering angle γ. The angle γ depends on the sun altitude angle at the observed point on the cloud surface $h_\odot$ (or the zenith distance at the sun $i=90°-h_\odot$), the azimuthal sun angle $\varphi_\odot$ included between the sun vertical and the viewing (scanning) plane and also on the angle of the zenith distance of the direction of the observer θ with apex at the viewed point of the cloud. In the case of a "flat" cloud, the angle θ is equal to the nadir scanning angle.

In reference [2] it is demonstrated that for solar angles of more than 30° the variations of the observed cloud brightness as a function of the solar angle angle for $\theta=0$ are well described by the theoretical brightness indicatrix of stratiformis presented in reference [7]. For $h_\odot<30°$ according to the experimental data the cloud brightnesses exceed the analogous values obtained when using the tabulated data from reference [7]. It must be noted that in [2] the results of integral measurements by a television unit based on the LI-408 tube and measurement data using the SPI-2M spectrometer installed on the I1-18 flying laboratory of the Main Geophysics Observatory were used to check the theoretical model of Ye. M. Feygel'son.

The spectral brightness indicatrices of cloud fields were measured in flights in the years of 1967-1972 [5, 6]. The flight data were used to construct brightness indicatrices for stratiformis. Figure 1 shows stratiformis isophots in the visible range of the spectrum for observations from altitudes up to 9 km. On the graphs in Figure 1 the brightnesses for different angles $\Theta, \varphi_{\odot}$ and three values of the solar angle $h_{\odot}$ are normalized with respect to the brightness in the nadir. From the figure it follows that for low solar and scattering angles close to mirror, the brightness coefficients of the clouds exceed a value of 6, for the brightness coefficients in the nadir for these sun altitudes are on the average from 0.6 to 0.7. In the near infrared region of the spectrum and also when observing crystalline clouds the brightness anisotropy of their upper boundary can be one and a half times more than in the visible range of the spectrum. The indicated indicatrix effects are one of the causes of the experimentally known increase in cloud albedo with a decrease in sun altitude above the horizon [10].

The relative variations of cloud brightness in the nadir are presented in reference [9] as a function of the solar angle in the visible and near IR regions of the spectrum. An analysis of the materials of this paper shows that in the spectral ranges of 0.4 to 0.75 micron and 1.35 to 2.55 microns the cloud brightness in the nadir is proportional to the cosine of the zenith distance of the sun, but for $h_{\odot}<10°$ deviations from the cosine function are observed in the direction of an increase in brightness.

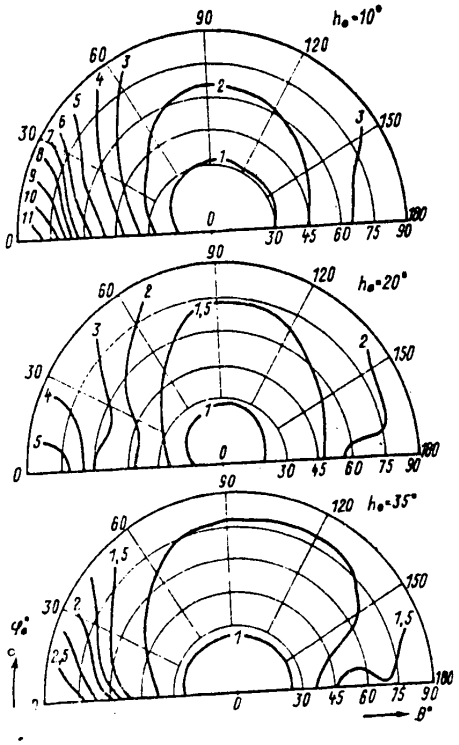

Figure 1. Isophots of the upper stratiformis boundary according to the SPI-2M data on a wavelength of 0.55 micron during observations from altitudes up to 9 km

The angular structure of the brightness distribution of cloud fields with vertical development differs from the brightness distribution of the upper boundary of stratiformis presented in Figure 1. Just as when observing vegetation cover [6], in the case of cumulus, the maximum brightnesses are observed for azimuthal angles of the sun close to 180°. As an example, the spectral brightness coefficients are presented in Table 1 for developed cumulus in the nadir and on different azimuths for a scanning angle θ=75° by measurements from an altitude of 7.2 km on 8 July 1971 during the CENEX-71 expedition [6].

Table 1. Spectral Brightness Coefficients of Cumulus by Measurements Using the SPI-2M for a Solar Angle of 59°

(1) Длины волн, мкм	θ=0°	θ=75°				
		(2) азимутальные углы Солнца, *град*				
		0	45	90	135	180
0,5	0,78	0,49	0,41	0,32	0,76	0,63
0,8	0,83	0,50	0,46	0,29	0,75	0,58
1,6	0,75	0,33	0,33	0,34	0,55	0,50
2,2	0,50	0,33	0,33	0,33	0,46	0,37

Key:
1. Wavelengths, microns
2. Azimuthal sun angles, deg

The presence of vertical components of the upper cloud boundary (altitude variations of the upper boundary) leads to the fact that the actually observed brightness of the cloud fields, as a rule, differs from the isophots presented in Figure 1. For calculations of the brightness of stratiformis more frequently observed in polar regions and in the winter over the continents, it is necessary first of all to consider the solar angle at the viewed point, and for calculations of the brightness of cumulus fields which are characteristic of tropical and temperate latitudes in the daytime, it is necessary to consider the scattering angles of the solar radiation from the surface of the cloud formations not arranged horizontally. The latter fact, as will be demonstrated below, is significant when calculating the brightness of cloud fields observed from great distances above the earth's surface.

Figure 2 shows the variations in brightness of the stratiformis uniformly covering the entire earth as applied to observation conditions from an altitude of 36,000 km above the earth's surface. The curves in Figure 2 are constructed using the results of aircraft measurements of cloud brightness indicatrices using the SPI-2M spectrometer, for three values of the phase angle Δ: 0, 45, 90°. The angle Δ corresponds to the angle with the apex at the center of the earth included between the directions of the sun and the vehicle from which the observation is made. From the above-described definitions it follows that for Δ=0° at all points of the visible disc of the earth $\phi \approx 180°$, and the equal solar angle lines (cosines of the zenith distance of the sun) are concentric circles. For Δ=90° the lines cos i=const appear to be straight lines. When constructing the isophots of Figure 2 attenuation of the reflected signals in the atmosphere above the clouds was not considered.

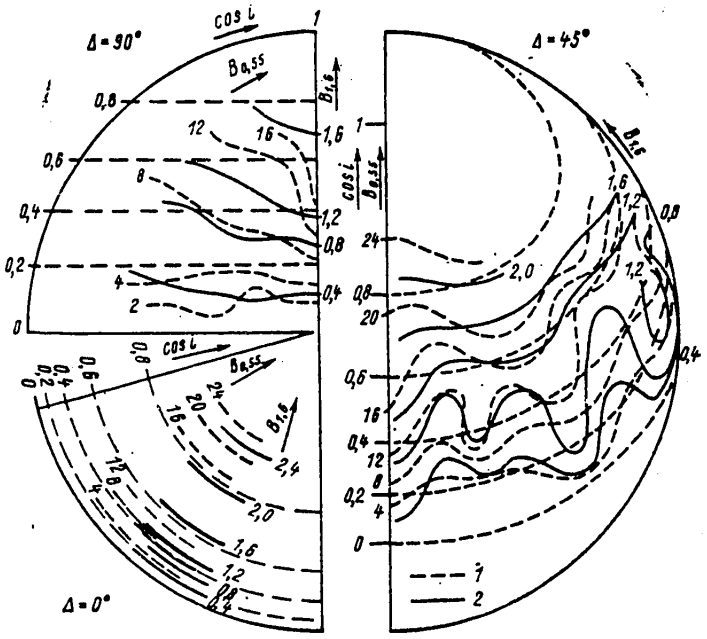

Figure 2. Stratiformis isophots on wavelengths of 0.55 micron (1) and 1.6 micron (2) according to aircraft measurement data using the SPI-2M as applied to observation conditions from an altitude of 36,000 km.

From Figure 2 it follows that the equal brightness lines of stratiformis constructed by the experimental data are located on the whole in accordance with the direction of the equal solar angle lines. For $\Delta=90°$, $\varphi_{\odot}\approx 0°$, the isophots are at an angle to the lines cos i=const as a result of the appearance of indicatrix effects at scattering angles close to mirror angles. For $\Delta=45°$ in the region of cosines of the zenith distance of the sun from 0.2 to 0.4 there are sharp bends in the isophots caused by altitude nonuniformities of the upper cloud boundary and errors in determining the scattering angles.

Analogous graphs were constructed using the brightness indicatrices of stratiformis presented in [7]; here the isophots lay strictly parallel to the cos i=const lines for all values of the phase angle Δ. However, for $0.2<\cos i<0.8$, the theoretical calculations gave a significantly larger range of variation of the brightness than the experimental data. The graphs for the variation of the mean values of the stratiformis as a function of the cosine of the sun's zenith angle at the viewed point according to experimental and theoretical data are presented in Figure 3 for three values of the angles Δ From the figure it follows that for phase angles of 45 and 90° and all values of cos i, and also for $\Delta=0°$, cos $i\leq 0.6$ the measured brightness is proportional to the cosine of the sun's zenith angle. The brightness variations, depending on the solar angle variations, obtained by the calculation results, are not subject to the cosine law. At the same time the calculated data coincide with the measurement results for $\Delta=0°$, $i>60°$.

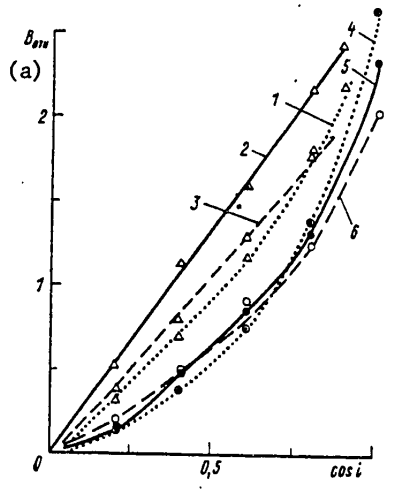

Figure 3. Brightness of the stratiformis upper boundary on a wavelength of 0.55 micron as a function of the cosine of the zenith distance of the sun according to the SPI-2M data (1-3) and the data from reference [7] (4-6) for different values of the phase angle of the sun as applied to observation conditions from an altitude of 36,000 km.
$\Delta=0°$ (1, 4), $\Delta=45°$ (2, 5) and $\Delta=90°$ (3, 6).

Key:

a. B_{rel}

It is obvious that if the results of aircraft measurements of cumulus, part of which are presented in Table 1, were used to construct the graphs of the isophots of the upper cloud boundaries, the range of variation of the cloud brightness with respect to the visible disc of the earth for all phase angles would be less than in the case of the stratiformis observation [8].

The latter thesis is confirmed by the results of photometric measurements of the earth obtained from on-board the "Zond-5" interplanetary station on 21 September 1968, for a phase angle of $\Delta=63°$ from a distance of about 90,000 km [3, 4]. In accordance with the measurements, the brightness of the part of the visible disc of the earth illuminated by the sun varied by sixfold, where the sea surface had minimum brightness, and the cloud fields, maximum. Analogous results were obtained during complex studies of this survey performed at Leningrad State University imeni A. A. Zhdanov [1]. Table 2 shows the results of photometric measurements of images of cloud fields located in equatorial latitudes. The maximum brightness was obtained from clouds located within the limits from 0 to 15° east longitude; for a mean value of cos i=0.84. The minimum values of the cloud brightness, amounting to 0.31 of the maximum value, were observed for three masses of clouds within the limits from 38° west to 15° east. For the same cloud masses, identical mean brightnesses were obtained amounting to 0.49 of the maximum brightness. It is characteristic that in scanning along the equator from the terminator to the edge of the visible disc of the earth, the range of brightness variations of individual cloud sections initially increases, reaching a maximum for cos i=0.84, and then it decreases. Near the edge of the disc the clouds have no brightness fluctuations.

Table 2. Relative Brightness Variations of Clouds Located in Equatorial Latitudes (by the Results of a Photometric Survey Obtained from the "Zond-5" Station)

	Longitude of the location on the photograph, deg				
	38-18 west	11-9 west	0-15 east	20-30 east	more than 60 east
Cos i	0.37	0.64	0.84	0.96	0.95
Angle γ, deg	122	116	115	110	113
Minimum brightness	0.31	0.31	0.31	0.35	0.54
Mean brightness	0.49	0.49	0.49	0.61	0.54
Maximum brightness	0.57	0.70	1.00	0.90	0.54

Analyzing Table 2, it is possible to see that if the values of cos i vary by 2.6 times, then the mean values of the cloud brightness vary by only 1.3 times, and the maximum, by 1.8 times, that is, the mean cloud brightness varies half as muchas the cosine of the angle with variation of the zenith distance of the sun. Thus, the results of the photometric survey confirm the thesis advanced above regarding the presence of equalization of the visible brightness of cloud fields when observed from high altitudes as a result of vertical nonuniformity of the altitude of their upper boundary. From Table 2 it also follows that within the investigated part of the visible disc of the earth, the angles at which the sun's rays are scattered by horizontal sections of the cloud fields varied from 110 to 122° in spite of the large variations of the zenith distance of the sun.

In conclusion, it is possible to note that when observing global cloud fields at great distances from the earth's surface as a result of the structural (vertical) nonuniformities of the upper cloud boundary, the dependence of their brightness on the cosine of the zenith distance of the sun at the viewed points is disturbed, that is, the effect of equalizing the brightness of the cloud cover within the visible disc of the earth is observed.

BIBLIOGRAPHY

1. Vinogradov, B. V.; Kondrat'yev, K. Ya. "KOSMICHESKIYE METODY ZEMLEVEDENIYA [Space Methods of Geography], Leningrad, Gidrometeoizdat, 1978.

2. Klemin, V. V.; Chapurskiy, L. I.; Fantikov, O. I. "Method of Experimental Testing of a Theoretical Calculation of the Brightness Characteristic of the Cloud-Atmosphere System," AKTINOMETRIYA I OPTIKA ATMOSFERY [Actinometry and Optics of the Atmosphere], Leningrad, Gidrometeoizdat, 1968.

3. Lavrova, N. P.; Sandomirskiy, A. B. "Photometry of the Planet Earth from the 'Zond' Space Station," IZVESTIYA VYSSHIKH UCHERNYKH ZAVEDENIY. GEODEZIYA I AEROFOTOS"YEMKA [News of the Higher Institutions of Learning. Geodesy and Aerial Photographic Surveying], No 4, 1972.

4. Lavrova, N. P.; Sandomirskiy, A. B. "Brightness Maps of the Earth Compiled by Photographic Data from the 'Zond' Automatic Interplanetary Station," IZVESTIYA VYSSHIKH UCHEBNYKH ZAVEDENIY. GEODEZIYA I AEROFOTOS"YEMKA, No 3, 1973.

5. Naydenova, K. A.; Chapurskiy, L. I. "Application of the Algebraic Approach for Automatic Classification of Natural Subjects," PROBLEMY FIZIKI ATMOSFERY [Problems of Atmospheric Physics], No 15, 1978.

6. POLNYY RADIATSIONNYY EKSPERIMENT [Total Radiation Experiment], edited by K. Ya. Kondrat'yev, Leningrad, Gidrometeoizdat, 1976.

7. Feygel'son, Ye. M. RADIATSIONNYYE PROTSESSY V SLOISTOOBRAZNYKH OBLAKAKH [Radiation Processes in Stratiformis], Moscow, Nauka, 1964.

8. Feygel'son, Ye. M.; Krasnokutskaya, L. D. POTOKI SOLNECHNOGO IZLUCHENIYA I OBLAKA [Solar Radiation Fluxes and Clouds], Leningrad, Gidrometeoizdat, 1978.

9. Chapurskiy, L. I.; Klemin, V. V. "Aircraft Studies of Spectral Brightness Characteristics of Clouds and Backgrounds in the Wavelength Range of 0.4 to 2.5 microns," AKTINOMETRIYA I OPTIKA ATMOSFERY [Actinometry and Optics of the Atmosphere], Leningrad, Gidrometeoizdat, 1969.

10. Chel'tsov, N. I. "Cloud Albedo," METEOROLOGIYA I GIDROLOGIYA [Meteorology and Hydrology], No 6, 1952.

UDC 551.509(329+314)(98)

FORECASTING THE NOVAYA ZEMLYA BORA BY THE METHOD OF CANONICAL CORRELATION

Moscow METEOROLOGIYA I GIDROLOGIYA in Russian No 5, May 81 pp 59- 64

[Article by Candidate of Geographic Sciences A. P. Polkhov, Murmansk Branch of the Arctic and Antarctic Scientific Research Institute, manuscript received 4 Aug 80]

[Text]

Abstract: A study is made of the possibility of asynchronous computerized mapping of a multi-dimensional space of meteorological signs (surface pressure, surface temperature, geopotential heights of the 850 and 500 mb surfaces, temperature at the 850 mb level) into values of the easterly and southeasterly storm winds (boras) at Novaya Zemlya. The canonical correlation method is used for this purpose. The performed study demonstrated the possibility of successful forecasting of the Novaya Zemlya bora 24 hours in advance.

It is known that in the presence of easterly and southeasterly storm winds on the west coast of Novaya Zemlya a dangerous meteorological phenomenon -- the bora -- occurs in the cold part of the year. According to [4, 8], the storm wind velocity during a bora often reaches 30 to 40 m/sec. Therefore successful forecasting of these storm winds from the indicated points of the compass is a highly urgent problem.

The procedure followed in forecasting the Novaya Zemlya bora is the subject of only one paper [8], according to which future values of the baric and thermal gradients at the 850 mb level and also the future position of the thermal frontal separation are used as the initial data. Naturally such initial data are the limiting condition of a successful forecast, for they automatically contain the forecasting error.

In the present article a different approach to forecasting the bora phenomenon at Novaya Zemlya is proposed. The new approach is based on using asynchronous relations between the wind field $\vec{V}$ at the earth's surface and the surface pressure field P, the surface temperature field T_{earth}, the geopotential heights of the 850 mb surface (H_{850}), the geopotential height of the 500 mb surface (H_{500}) and the temperature at the 850 mb level (T_{850}) characterizing the state of the atmosphere at a defined point in time and space.

Each field is described by a random vector, the components of which are values of the meteorological variable at q discrete points of two-dimensional space. On the time scale it is possible to characterize the field by a set of realizations of the vector X. Thus, a two-dimensional meteorological field can be represented by a vector function of the argument t

$$X(t) = [x_1(t), x_2(t), \ldots, x_q(t)]. \quad (1)$$

In accordance with the indicated interpretation let us express the wind field as a reaction of the state of the atmosphere in the form of a linear stochastic model

$$X_k(t+\tau) = \sum_{f=1}^{d=5} X_f(t) R_f + \varepsilon_k, \quad k = 1, 2; \quad f = 1, 2, \ldots, 5, \quad (2)$$

where $X_k(t+\tau)$ for k=1, 2 assumes the values of the fields of the components V_x, V_y of the vector field $\vec{V}$;

X_f for f=1, 2, ..., 5 has values of P, H_{850}, H_{500}, T_{earth}, T_{850};

τ is the given positive shift;

R_f is the vector of the parameters to be estimated;

ε_k is the model error.

The validity of expression (2) was investigated for the Malyye Karmakuly station located on the west coast of Novaya Zemlya (see the figure). The material of the investigation was the synoptic archive of the hydrometeorological library of Murmansk UGKS for the cold period (October-March) of 1960 to 1965 and 1975 to 1977 in the form of surface and high-altitude weather maps for the basic synoptic times of 0300 and 1500 hours.

The predictor fields of P, H_{850}, H_{500}, T_{earth}, T_{850} were given by the values of the corresponding variables at 30 nodes of a regular grid, the spatial discreteness of which was h=600 km (see the figure). The indicated grid is a fragment of the grid (h=300 km) of the two-parametric scheme of the Main Geophysics Observatory [31] used operatively at the Murmansk Weather Bureau. The values of the meteorological characteristic at the nodes were obtained as a result of synoptic (manual) interpolation. For this purpose observations by the coastal and marine stations for 0300 and 1500 hours were used. The predicted field $\vec{V}$ was presented by the value of the wind velocity $|\vec{V}|$ and wind direction d at one point (the Malyye Karmakuly station); the vector $\vec{V}$ was subsequently expanded in the components V_x, V_y. The wind data sample included values of $|\vec{V}| \geq 10$ m/sec for 0300 and 1500 hours in the easterly and southeasterly directions.

In order to reflect the climatic peculiarities of the bora phenomenon, the data sample for the wind was organized separately with respect to each of six investigated (October-March) months. The size of an individual sample was 150 values of $\vec{V}$. It is natural that this volume of realizations was provided for with respect to each predictor field.

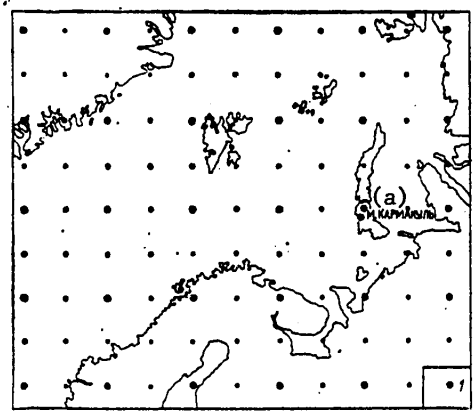

Fragment of the grid of the two-parametric system of the Main Geophysics Observatory.
1 -- grid nodes which the values of the meteorological fields were taken.

Key:
a. Malyye Karmakuly

According to the stated goal of finding asynchronous relations, provision was made for the diurnal positive shift τ of the predicted value with respect to the predictor.

When performing the investigation, information about the predicted value and the predictors of model (2) was involved in aligned and normalized form. This offered the possibility of obtaining the property of stationarity in the broad sense [7], which, in turn, permitted optimal application of the apparatus of the correlation theory of random functions for analysis

$$R_{kf} = X'_k(t)\, X_f(t), \quad k \equiv f, \tag{3}$$

$$R_{kf} = X'_k(t+\tau)\, X_f(t), \quad k \neq f, \tag{4}$$

where (3) is the matrix correlation function;

(4) is the mutual time-space correlation function.

The analysis (4) of the statistical structure of the interaction of the predicted parameters $X_k(t+\tau)$ with the predictors $X_f(t)$ revealed weak relations r=0.25 to 0.35. Consequently, for prediction of the vector $\vec{V}$ the necessity for maintaining the adopted dimensionality (q=30) of the predictor fields is obvious. Hence, as a consequence, model (2) becomes awkward and computationally unstable.

Accordingly, to eliminate the indicated deficiencies a search was made for analogs of the given predictor fields which would combine high asynchronous informativeness with respect to $X_k(t+\tau)$ with minimal dimensionality. The q-dimensional vectors $Y^k_f(t)$ of the new variables $y^k_{if}(t)$, (i=1, 2, ..., q) obtained as a result of conversion of the initial meteorological fields using the statistical apparatus of the canonical correlation [1, 5] became such analogs.

The generalized problem of eigenvalues Λ and eigenvectors L was solved for this purpose

$$(A-\Lambda B)L=0. \tag{5}$$

Here $A=R_{fk}R_{kk}^{-1}R_{kf}$, $B=R_{ff}$ (k=1, 2; f=1, 2, .., 5 with respect to the number of predicted values and predictors, respectively), where $R_{kk}=1$ as a result of $X'_k(t)X_k(t)$; R_{kf} is the mutual time-space correlation function (4) of the k-th predicted parameter with some f-th predictor field; R_{ff} is the matrix correlation function (3). It is easy to see that the matrix A is obtained as a result of the product of the column vector times the row vector, the elements of which were values of the mutual time-space correlation function (3).

When solving system (6), according to [2], it turned out that the relation between $X_k(t+\tau)$ and some $X_f(t)$ will become the most indicative in the direction of the first eigenvector ℓ^k_{1f} of the matrix L^k_f. The given fact follows from the value of the elements (analog of the square of the multiple correlation function) of the diagonal matrix Λ^k_f in which the first element λ^k_{1f} has a maximum value, and the remaining elements in practice do not differ from zero.

Then as a result of the linear transformation

$$Y^k_f(t)=X_f(t)L^k_f,\quad f=1,2,\ldots,5 \tag{6}$$

redistribution (compression) of the information of the f-th predictor field takes place for $X_k(t+\tau)$ such that it is concentrated in the first component $y^k_{1f}(t)$ of the vector of the new variables $Y_f(t)$.

From Table 1 where the informativeness of $y^k_{if}(t)$ for $X_1(t+\tau)$ (January) is presented in the form of eigenvalues λ^k_{1f} it follows that the f-th new variable $y^k_{1f}(t)$ describes a significant part of the dispersion $X_k(t)$. The given fact will become entirely explainable from a comparison of the time-space fields of the predicted parameter and the predictors. Consequently, the Novaya Zemlya bora is caused by atmospheric processes already on the eve of its occurrence. Therefore the time-space scale of the predictor fields was selected from the calculations such that it reflects the elementary synoptic process above the investigated region (see the figure).

Table 1

Компонент (1)	(2) Собственные числа				
	λ_{1p}	$\lambda_{1H_{850}}$	$\lambda_{1H_{500}}$	λ_{1T_3}	$\lambda_{1T_{850}}$
V_x	0,51	0,47	0,45	0,54	0,56
V_y	0,49	0,46	0,43	0,51	0,55

Key:
1. Component $\vec{V}$
2. Eigenvalues

An analysis of the statistical structure of the new variables $y^k_{1f}(t)$ and the structure of their interaction with $X_k(t+\tau)$ according to (3), (4) made it possible to arrive at the conclusion that the canonical values $y^k_{1f}(t)$ are analogs of the field gradients of P, H_{850}, H_{500}, T_{earth}, T_{850} characterizing the zonal and meridional components of atmospheric circulation in the near 5-kilometer layer of the atmosphere over Novaya Zemlya and the regions adjacent to it. Therefore instead of the awkward predictor fields it is possible to use a total of only five new variables characterizing the intensity of the atmospheric processes which offers the possibility of obtaining physical substantiation and statistical acceptability of the model (2).

As has already been noted above (Table 1), every new variable $y^k_{1f}(t)$ describes a significant part of the dispersion $X_k(t)$, but duplication is observed here (see Table 2), that is, the new variables are mutually related to one degree or another. In order to discover the contribution of each predictor $y^k_{1f}(t)$ to the dispersion $X_k(t)$, the partial correlation coefficients reflecting the estimate of the true relation of the predicted parameters and the predictors were calculated according to the expression from [7]

$$\rho_{kf\cdot d-1} = \frac{F_{kf}}{\sqrt{F_{(d+k)(d+k)}F_{ff}}}, \tag{7}$$

where k=1, 2; f=1, 2, ...; d=5 with respect to a number of new variables $y^k_{1f}(t)$; F_{kf}, $F_{(d+k)(d+k)}$, F_{ff} are the minors of the correlation matrix $R_{(d+k)(d+k)}$ of all variables $X_k(t+\tau)$, $y^k_{1f}(t)$ corresponding to the like-named elements of the indicated matrix. According to the data in Table 2, $y^k_{T_{earth}}(t)$, $y^k_{T_{850}}(t)$, that is, the thermal factors, have the greatest informativeness with respect to $X_k(t+\tau)$.

From the new variables $y^k_{1f}(t)$ it is possible to organize the predictor vector (Table 2)

$$Y_k(t) = [y^k_p(t),\ y^k_{H_{850}}(t),\ y^k_{H_{500}}(t),\ y^k_{T_3}(t);\ y^k_{T_{850}}(t)].$$

Accordingly, model (2) assumes the form

$$X_k(t+\tau) = Y_k(t)R_k + \varepsilon_k, \quad k = 1, 2, \tag{8}$$

where the vector of the parameters R_k is estimated by the least squares method using the pseudoinversion [6]

$$R_k = [Y'_k(t)\,Y_k(t)]^+ M_k, \tag{9}$$

where (+) is the sign of the pseudoinversion; M_k is the mutual correlation column vector of $X_k(t+\tau)$ with $Y_k(t)$. The operation (9) offers the possibility of avoiding the influence of the poor conditionality of the correlation matrix $Y'_k(t)Y_k(t)$ on R_k.

According to (9) and the data in Table 2, the numerical values of R_k are equal to R_1=(0.197771, 0.085369, 0.203391, -0.353029, 0.318305). The multiple correlation coefficient and the mean square error of the model (8) were in this case $\hat{R}_1$=0.93; $\hat{\sigma}_1$=2.4, respectively. Analogous results were also obtained for R_2, $\hat{R}_2$, $\hat{\sigma}_2$.

Table 2

Переменная (a)	(b) Корреляционная матрица $R_{(d+k)(d+k)}$, $k=1$						(c) Частный коэффициент корреляции $\rho_{kf \cdot d-1}$
	1	2	3	4	5	6	
1. $y^k_{1P}(t)$	1,00	0,70	0,51	—0,51	0,53	0,71	0,31
2. $y^k_{1H_{850}}(t)$		1,00	0,53	—0,50	0,54	0,68	—0,14
3. $y^k_{1H_{500}}(t)$			1,00	—0,43	0,53	0,67	0,36
4. $y^k_{1T_{земл}}(t)$ (d)				1,00	—0,49	—0,74	0,57
5. $y^k_{1T_{850}}(t)$					1,00	0,75	0,51
6. $x_k(t-\tau)$						1,00	—

Key:
a. Variable
b. Correlation matrix
c. Partial correlation coefficient $\rho_{kf.d-1}$
d. earth

Using expressions (3)-(7) and (9), high asynchronous relations (the results of training the model (8)) were obtained for each month of the cold part of the year, permitting use of the actual weather maps as the initial data for the forecast. The entire procedure of training the model (8) was implemented on the "Minsk-32" computer.

The above-described model (8) was tested (examined) on independent material for the cold period of 1978 to 1979. The results of an objective analysis of the fields P, H_{850}, H_{500}, $T_{земл}$, T_{850} for t_0=0.3 hours according to the system of the Main Geophysics Observatory [3] taken at 30 nodes of a regular grid (see the figure) were used as the initial data for forecasting the wind for the time $t_0+\tau$ (τ=24 hours).

The wind vector $\vec{V}$ was forecasted according to the expressions

$$\hat{X}_k(t_0+\tau) = \sum_{f=1}^{d=5} X_f(t_0)\, l^k_{1f}\, r^k_f, \quad k=1,2; \quad f=1,2,\ldots,5, \tag{10}$$

$$|\hat{\vec{V}}|(t_0+\tau) = \sqrt{\sum_{k=1}^{2} (\hat{X}_k(t_0+\tau)\,\hat{\sigma}_{X_k} + \overline{X}_k)^2}. \tag{11}$$

$$\hat{d}(t_0+\tau) = \begin{cases} \frac{\pi}{2} \pm \operatorname{arc}\left| \dfrac{(\hat{X}_2(t_0+\tau)\,\hat{\sigma}_{X_2} + \overline{X}_2)^2}{(\hat{X}_1(t_0+\tau)\,\hat{\sigma}_{X_1} + \overline{X}_1)^2} \right|, \end{cases} \tag{12}$$

where r^k_f is a component of the vector R_k of the estimates of the parameters of the model (8),

$\hat{\sigma}_{x_k}$ is an estimate of the mean square deviation of the variables $X_k(t)$,

$\overline{X}_k$ is their mean value,

ξ is a coefficient assuming the values of $\xi=1$ in squares I and II and $\xi=3$ in squares III and IV of the righthand cartesian coordinate system,

d is the estimate of the direction of the vector $\vec{V}$.

The sign of the second term of formula (12) is defined by the ratio of the signs of the estimates of the components $\hat{V}_x\hat{V}_y$ of the vector $\vec{V}$.

The entire forecasting procedure was implemented on the "Minsk-32" computer, and it takes several minutes.

When testing the proposed procedure, 75 cases of a storm bora were predicted with $|\vec{V}|\geq 15$ m/sec; in reality, 83 cases of easterly and southeasterly storm winds were observed. The success of the forecast with margins of $|\vec{V}|=5$ m/sec, d=20° was 91%.

BIBLIOGRAPHY

1. Bagrov, N. A.; Mertsalova, N. I. "Thermal Interaction of the Ocean and Atmosphere," TRUDY GIDROMETTSENTRA SSSR [Works of the USSR Hydrometeorological Center], No 64, 1970.

2. Bryleva, L. I.; Chernin, K. Ye. "Finding Proper Elements for the Generalized Problem with Symmetric Matrices," MATEMATICHESKOYE OBESPECHENIYE EVM "MINSK-32" [Software for the "Minsk-32" Computer], No 8, 1973.

3. Bushkova, T. A.; Il'in, B. M.; Kobyshev, G. A., et al. "Description of a Numerical Analysis and Operative Forecasting Scheme at the Northwestern UGMS," TRUDY GGO [Works of the Main Geophysics Observatory], No 353, 1975.

4. Vize, V. Yu. "Novaya Zemlya Bora," IZV. TSENTRAL'NOGO GIDROMETEOROLOGICHESKOGO BYURO [News of the Central Hydrometeorological Office], No 5, 1925.

5. Gandin, L. S. "Application of the Canonical Correlation Method in Meteorology," TRUDY GGO, No 208, 1967.

6. Gantmakher, F. R. TEORIYA MATRITS [Matrix Theory], Moscow, 1966.

7. Jenkins, G.; Watts, D. SPEKTRAL'NYY ANALIZ I YEGO PRILOZHENIYA [Spectral Analysis and Its Applications], Moscow, Mir, No 2, 1972.

8. Masterskikh, M. A. "Prediction of a Frontal Bora at Novaya Zemlya," TRUDY GIDROMETTSENTRA SSSR, No 199, 1978.

UDC 551.(322:53+578.46:53)(268)

HYDROCARBON DISTRIBUTION IN FRESHLY FALLEN SNOW AND ICE AT 'NORTH POLE-22' STATION (1977-1978 OBSERVATIONS)

Moscow METEOROLOGIYA I GIDROLOGIYA in Russian No 5, May 81 pp 65-68

[Article by F.A. Dmitriyev, S. V. Pivovarov, Arctic and Antarctic Scientific Research Institute, manuscript received 15 Sep 80]

[Text]

Abstract: Procedures are discussed for taking and analyzing ice samples, and a study is made of the hydrocarbon content and distribution in underlying surface objects in the vicinity of the "North Pole" drift stations.

Along with the fact that a larger and larger number of environmental subjects are being subjected to analysis for hydrocarbon content (water, soil, bottom sediments and representatives of the animal world), insufficient attention is being paid to the study of organic substances contained in snow and ice [5]. In individual papers on these forms of underlying surfaces, studies were made of the organic carbon content [2, 3]. The interest manifested in these subjects is entirely based on the fact that, first of all, we are dealing with a specific environment in which the hydrocarbon breakdown processes will be inhibited, which can lead to accumulation of hydrocarbons; secondly, the study of the hydrocarbon distribution both over a small territory and in a broad expanse can reveal a possible source of pollution; thirdly, in certain areas where ice and snow are to be found over a long period of time, it is important to consider the problem of hydrocarbon conversion in the atmosphere-snow-ice-water-bottom sediment system.

In the given paper a study was made of the hydrocarbon content and distribution in samples of freshly fallen snow and ice taken while the "SP-22" ["North Pole-22"] station was drifting out of the Arctic Basin into the northern regions of the Beaufort Sea. Observations were made from June 1977 to March 1978 which made it possible to characterize the hydrocarbon distribution as a function of seasonal behavior. Thaw water extracts were prepared at the location where the samples were taken, and an analysis was run at the Water Monitoring and Hydrochemistry Laboratory of the Arctic and Antarctic Scientific Research Institute. The purpose of the study was not to discover individual groups of hydrocarbons to use them as an example in demonstrating the possible influence of pollution sources. It is obvious that organic compounds of anthropogenic origin are part of the total substances released from subjects. The study was performed by the method of gas-liquid chromatography.

Sample Taking and Analysis Procedure

Considering the importance of the information on the pollutant content in snow and ice covers, the Water Monitoring and Hydrochemistry Laboratory of the Arctic and Antarctic Scientific Research Institute proposed a method of taking samples presupposing reliable protection of the samples taken from materials capable of distorting the actual hydrocarbon content. Special attention was given to the cleanness of the instruments and containers for taking samples.

The ice and snow samples were taken at a distance of 1-2 km from the station to avoid inclusion of the products of combustion of the diesel fuel used to heat the living quarters. A one or two-centimeter layer of freshly fallen snow was collected from an area of 5-10 m^2. Ice samples were drilled out by a 120-mm diameter circular bore. Cores 15-20 cm long were broken off and extracted from the hole. The upper layer of ice 5-10 mm thick was cleaned away. The samples were melted in a tightly covered enamel bucket over an electric stove in a facility not subject to contamination with fuel vapor or the products of its combustion.

The samples were extracted by distilled hexane in a 1-liter separating funnel, which was rinsed out twice with 25 ml of hexane and twice with 200-300 ml of thaw water before beginning work. One milliliter of chemically pure sulfuric acid and 15 ml of hexane were added to 1 liter of water in the separating funnel. The contents were mixed vigorouslyfor 15 minutes, then allowed to stand until complete separation of the layers. The extract was transferred to a container corresponding to the transport conditions. Extraction was performed four more times in the same manner. The extracts obtained were combined, adding 25 ml of hexane used to rinse out the separating funnel after extraction.

Chromatographic separation was performed on the "Tsvet-104" chromatograph with a 45-meter capillary column with 0.25 mm inside diameter; the dynamic phase was OV-17 silicon. The initial column temperature was 80°C with heating to 145°C after 4 minutes; thereafter heating took place at 5°C/min to 235°C. The carrier gas was helium at 3.0 atmospheres pressure. A flame-ionization detector was used with hydrogen pressure of 0.65 atm and air pressure of 0.75 atm. The evaporator and detector temperature was 300°C. The n-alkanes were identified by a standard $n\text{-}C_{13}$-$n\text{-}C_{35}$ hydrocarbon mixture by comparing the holding time; a quantitative estimate was made by comparison with a standard mixture of methane-naphthene hydrocarbons.

Discussion of Results

Chemical analysis made it possible to draw a number of conclusions with respect to hydrocarbon content in the underlying surface of the Arctic Basin.

All of the chromatograms of the samples have similar nature of hydrocarbon distribution: the presence of a sum of unsplit peaks -- "humps" -- and also n-alkanes and carbon isomers. The presence of peaks, the areas of which exceed the sum of the areas of the n-alkane peaks (Figure 1), is observed for all the chromatographic spectra in the C_{22}-C_{24} n-alkane region. These "predominant" components can be considered to be hydrocarbons of biogenic origin, for technogenic hydrocarbons are not characterized by the presence of individual compounds with concentrations differing significantly from all the rest. At the same time, the compounds of biological origin are not characterized by the formation of a series from a set of isomers -- "humps."

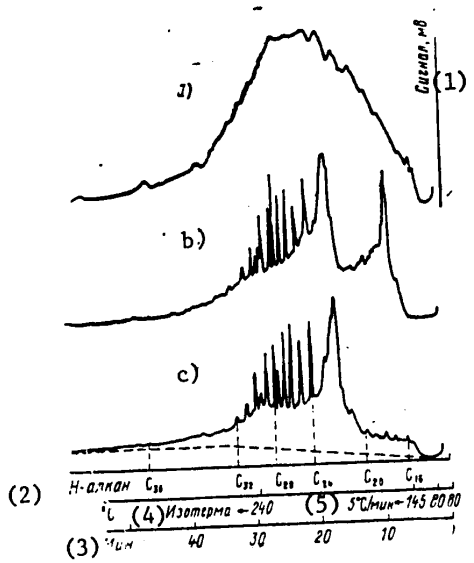

Figure 1. Chromatograms of snow samples No 6 (a), No 3 (b) and ice sample No 4, middle layer (c)

Key:
1. Signal, millivolts
2. n-alkane
3. minutes
4. Isotherm
5. 5°C/minute

The "humps" on the chromatograms begin with the n-alkanes from $n\text{-}C_{13}$-$n\text{-}C_{16}$ and end in the region of $n\text{-}C_{33}$-$n\text{-}C_{37}$. Individual representatives of normal alkanes clearly appear from $n\text{-}C_{16}$-$n\text{-}C_{18}$ and to $n\text{-}C_{33}$-$n\text{-}C_{35}$. In samples where $n\text{-}C_{17}$ and $n\text{-}C_{18}$ were discovered, isoprenoids, pristane and phytane are also present. For some snow samples taken during the winter, the presence of a "hump" on the chromatograms with the peak in the $n\text{-}C_{16}$-$n\text{-}C_{17}$ region is characteristic. The superposition of the spectrum of a mixture of relatively highly volatile hydrocarbons, for example, diesel fuel, on the general chromatogram is entirely probable.

Snow sample No 6 is an exception to the general nature of the hydrocarbon distribution. The chromatogram for snow sample No 6 does not give clearly expressed n-alkanes or components which we consider to be hydrocarbons of biogenic origin (Figure 1).

Now let us discuss the quantitative estimate of the hydrocarbons contained in the different ice layers (middle and lower) and in freshly fallen snow (see the table).

Comparing the ice data, it is possible to note that the hydrocarbon concentrations are close to each other both for individual samples and for different layers. The average hydrocarbon concentration for the ice samples is 0.038 mg/liter, and for snow samples, 0.017 mg/liter, that is, it differs from the similar characteristic for ice samples by more than twofold. The increase in the hydrocarbon content

Results of Determining the Hydrocarbon Concentrations in Samples of Freshly Fallen Snow and Ice

№ пробы (a)	Дата отбора (b)	(c) Координаты		Суммарная концентрация углеводородов, мг/л (f)	Относительное содержание биогенных углеводородов, % (g)	Относительное содержание н-алканов, % (h)
		с. ш. (d)	в. д. (e)			
		Лед (i)				
1 с. с.	13 VI 77	81°41′	232°50′	0,054	1,3	1,9
4 с. с.	06 IX 77	79 06	232 30	0,026	10,9	14,4
5 н. с.	06 IX 77	79 06	232 30	0,031	10,0	10,2
7 с. с.	03 X 77	79 06	234 00	0,035	10,5	9,6
8 н. с.	03 X 77	79 06	234 00	0,052	25,0	6,5
11 с. с.	24 XII 77	76 10	227 20	0,036	2,8	10,4
12 н. с.	24 XII 77	76 10	227 20	0,031	3,0	9,6
17 н. с.	12 III 78	75 13	223 27	0,021	1,8	20,4
		Снег (j)				
2	19 VI 77	81°41′	233°38′	0,012	13,5	4,4
3	04 IX 77	79 06	232 00	0,017	21,8	8,5
6	30 IX 77	79 04	233 26	0,163	—	0,3
9	01 XI 77	77 42	229 40	0,052	2,7	6,9
10	23 XII 77	76 11	227 27	0,020	2,2	5,7
13	02 I 78	76 12	226 47	0,020	—	10,0
14	28 I 78	75 49	227 18	0,019	1,6	7,8
15	13 II 78	75 29	226 44	0,014	—	9,0

Key:
a. Sample number
b. Date taken
c. Coordinates
d. north latitude
e. east longitude
f. Total hydrocarbon concentration, mg/liter
g. Relative biogenic hydrocarbon content, %
h. Relative n-alkane content, %
i. Ice
j. Snow

Note. c.c. -- middle layer of ice, H.c. -- lower ice layer.

in ice is connected with longer contact of the ice with organic matter which can be transferred to it from surface seawater and from melted snow. When calculating the average hydrocarbon concentration in snow the concentrations for samples No 6 and No 9 having "anomalous" characteristic by comparison with the other chromatograms, were thrown out in accordance with the methods of data evaluation used in [4]. The hydrocarbon concentration in snow sample No 6 taken at the end of September 1977 exceeds the concentrations in the other samples by an order. Sample No 9 taken a month after No 6 is also isolated; the hydrocarbon content in sample No 9 is two or three times higher than in the remaining samples.

Data are also presented in the table which reflect the predominance of the proportion of unsplit peaks -- "humps" -- over the sum of the n-alkanes, that is, S_{alk}/S_{total}. For snow samples the average value of S_{alk}/S_{total} is 7.5%, whereas for sample No 6 this value is 25 times less than average. This hydrocarbon distribution in sample No 6 is explained by the fact that the snow used for analysis was taken during a period of abundant snowfalls which, as the synoptic situation demonstrated, were connected with the inflow of warm, wet air masses from the southwest from the continent of North America, which carried a significant quantity of hydrocarbons by comparison with the average amount, the greater part of which are obviously of technogenic origin. One of the proposed products can be the sum of the substances formed during the combustion of fuel (motor vehicles, heating units, and so on). It is possible that this can explain the high hydrocarbon concentrations in sample No 9 which was taken under similar synoptic conditions. In these cases southerly atmospheric flows were observed which were caused by a cyclonic situation with its center in the vicinity of Northern Canada. The air flows reached the drift region of "SP-22" drift station in 2 days. Normal hydrocarbon content was noted under such synoptic conditions when the air masses came from the Eastern Siberian or Chukotskoye Seas or circulated for a long time in the Arctic Basin.

Hereafter, we shall consider such characteristics of the investigated samples as the relative content of hydrocarbons, the origin of which we consider to be biogenic. From the table it is obvious that this value has significant fluctuations. For certain extracts biogenic components are not isolated in general on the chromatograms, and for others, the areas of their peaks take up a quarter of the total amount of hydrocarbons. Assuming that the presence of biogenic hydrocarbons in the ice and snow samples is connected with the vital activity of marine organisms, we compared the values of the relative biogenic component content in the total mass of hydrocarbons S_b/S_{total} and the sample taking time.

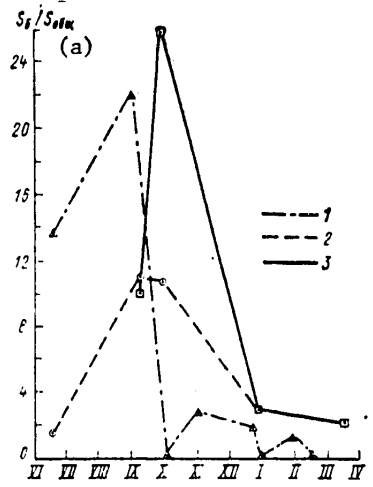

Figure 2. Distribution of the proportion of biogenic hydrocarbons with respect to total hydrocarbons S_b/S_{total} as a function of the analysis sample taking time.
1 -- snow, 2 -- middle ice layer, 3 -- lower ice layer

Key:
a. S_b/S_{total}

Figure 2 shows a relation which indicates that the maximum of S_b/S_{total} for all three types of investigated subjects (two ice layers and snow) comes in September -- the time of greatest productivity of the most widespread representative of the biota -- Arctic plankton [1]. It is obvious that ice takes on such components as a result of contact with water and, possibly, with snow. Biogenic hydrocarbons can get into freshly fallen snow from atmospheric air to which they are transferred when the air masses make contact with the water surface. The contribution of hydrocarbons of technogenic origin to the overall chromatographic picture offers the possibility of monitoring atmospheric pollution in the Arctic.

Conclusions

1. The average hydrocarbon concentrations in ice and snow amount to 0.038 mg/liter and 0.017 mg/liter, respectively. Smaller concentrations in freshly fallen snow samples obviously are explained by the formation of precipitation from local Arctic air masses and short-term contact of the precipitation with the environment.

2. The "hump" of unsplit peaks begins to form in the region of the C_{13}-C_{16} n-alkanes and ends in the n-C_{33}-n-C_{37} region. Normal alkanes are distinctly released from n-C_{16} to n-C_{35}, on the average accounting for 1/10 of the total hydrocarbon content.

3. On almost all of the chromatograms peaks were discovered for components considered to be of biogenic origin. The maximum relative content of these substances was analyzed in samples taken during an increase in Arctic plankton activity.

4. With comprehensive study of hydrocarbon synthesized biogenically (identification of the materials, distribution characteristic in a large body of water), they could become indicators providing information about the complex metabolic processes in the water surface-atmosphere-ice cover system.

BIBLIOGRAPHY

1. Bogorov, V. G. PLANKTON MIROVOGO OKEANA [Plankton in the World Ocean], Moscow, Nauka, 1974.

2. Volokitina, L. A.; Shuklin, V. S. "Effect of the Direction of Transfer of Air Masses on the Organic Microimpurity Content in Atmospheric Precipitation," METEOROLOGIYA I GIDROLOGIYA [Meteorology and Hydrology], No 2, 1980.

3. Mel'nikov, I. A.; Pavlov, G. L. "Peculiarities of the Distribution of Organic Carbon in Waters and Ice of the Arctic Basin," OKEANOLOGIYA [Oceanology], Vol XVIII, No 2, 1978.

4. Ford, R.; Gordon, A. SPUTNIK KHIMIKA [Chemistry Handbook], Moscow, Mir, 1976.

5. Herrmann, R. "Regional Patterns of Polycyclic Aromatic Hydrocarbons to Anthropogenic Influence and Air Flow," CATENA, Vol 5, No 2, 1978.

UDC 556.011

JOINT DETERMINATION AND REDUCTION OF STATISTICAL PARAMETERS TO A PERIOD OF MANY YEARS, EXTENSION AND MODELING OF TIME SERIES

Moscow METEOROLOGIYA I GIDROLOGIYA in Russian No 5, May 81 pp 70-81

[Article by Professor G. A. Alekseyev, State Hydrological Institute, manuscript received 8 Sep 80]

[Text]

Abstract: For the development of the known grapho-analytical method [1, 2, 10], a generalized analytical or graphoanalytical method is proposed for joint determination and reduction of statistical parameters (the mean, C_v, C_s) to a period of many years using several (2, 3 or more) paired straight lines or curves for the relationship of equally guaranteed values during joint observation periods at the reduction point and at adjacent point-analogs with longer observation periods (number of years).

Just as joint modeling [3], the time series are extended by the equations of the normalized conditional distribution curves using unconditional distribution curves reduced to a period of many years.

It is known that river runoff, precipitation and other hydrometeorological characteristics vary significantly with time and territory. This variation is most compactly described statistically in the form of unconditional and conditional distribution curves simultaneously reflecting the correlations between the investigated characteristics [6].

In order to improve the reliability (stability) of the statistical characteristics and consider all possible versions of time-space joint fluctuations of the investigated hydrometeorological characteristics during hydrological study and substantiation of water management projects it is necessary to solve four statistical problems: determination and reduction of parameters (the mean, C_v, C_s) to a period of many years, extension and modeling of time series. Scientific and technical progress in the methods of hydrology, climatology, and all-around water management planning depends on proper, scientifically substantiated, mathematically correct joint solution of these four interrelated problems.

With respect to the available time series of observations

$$x_{ji} \equiv x_{j1}, x_{j2}, \ldots, x_{jn_j} \tag{1}$$

at points with the numbers i=0, 1, 2,..., ℓ and with respect to the corresponding number of years of observations (in increasing order)

$$n_0 < n_1 < n_2 < \ldots < n_l \tag{2}$$

the paired interseries correlation coefficients between the eigenvalues (x_{0i}, x_{ji}) at the reduction point with the number j=0 and at adjacent points with the numbers j=1, 2, ..., ℓ are calculated for joint observation periods n_{0j}

$$r_{0j} = \frac{\sum_{i=1}^{n_{0j}} (x_{0i} - \bar{x}_0)(x_{ji} - \bar{x}_j)}{\sqrt{\sum_{i=1}^{n_{0j}} (x_{0i} - \bar{x}_0)^2 \cdot \sum_{i=1}^{n_{0j}} (x_{ji} - \bar{x}_j)^2}}, \quad j = 1, 2, \ldots, l. \tag{3}$$

The mean square errors of the correlation coefficients of (3) are calculated

$$\sigma_{r_{0j}} = \frac{1 - r_{0j}^2}{\sqrt{n_{0j} - 1}}, \quad j = 1, 2, \ldots, l. \tag{4}$$

Only the observation points for which the correlation coefficients of (3) are essentially significant are taken as point-analogs,

$$r_{0j} \geq 3\sigma_{r_{0j}}, \quad j = 1, 2, \ldots, l, \tag{5}$$

that is, for which the correlation coefficients exceed three-times the mean square errors of their determination (4). Hereafter we shall consider that the observation points with numbers j=0, 1, ..., ℓ satisfy condition (5).

Smoothed empirical overestimation probability distribution curves are constructed for all ℓ+1 observation points satisfying condition (5)

$$p = p(x_j) \quad \text{or} \quad x_{jp} = F_j(p), \quad j = 0, 1, 2, \ldots, l, \tag{6}$$

using the empirical overestimation probabilities [2, 4]

$$p_m = p(x'_{jm}) = \frac{m - 0{,}25}{n_j + 0{,}5}, \quad m = 1, 2, \ldots, n_j \tag{7}$$

of the ranked terms of the series in decreasing order x'_{fm}

$$x'_{j1} \geq x'_{j2} \geq \ldots \geq x'_{jn_j}, \quad j = 0, 1, 2, \ldots, l. \tag{8}$$

It is expedient to approximate the empirical distribution curves in the form of the Goodrich equations

$$p(x_j) = e^{-\left(\frac{x_j - a_j}{\alpha_j}\right)^{\frac{1}{\beta_j}}}, \quad x_{jp} = a_j + \alpha_j (-\ln p)^{\frac{1}{\beta_j}}, \quad j = 0, 1, \ldots, l, \tag{9}$$

the parameters of which a_j, α_j, β_j are related to three standard statistical parameters -- the mean value

$$\bar{x}_j \approx \tilde{x}_j = \frac{1}{n_j}\sum_{i=1}^{n_j} x_{ji}, \tag{10}$$

the standard deviation from the mean

$$\sigma_j \approx \tilde{\sigma}_j = \sqrt{\frac{\sum_{i=1}^{n_j}(x_{ji}-\bar{x}_j)^2}{n_j-1}}, \tag{11}$$

the asymmetry coefficient

$$C_{sj} \approx \tilde{C}_{sj} = \frac{\sum_{i=1}^{n_j}(x_{ji}-\bar{x}_j)^3}{\tilde{\sigma}_j^3}\cdot\frac{n_j}{(n_j-1)(n_j-2)} \tag{12}$$

-- by the following equalities [5]:

$$a_j = \bar{x}_j - \alpha_j\Gamma\left(1+\frac{1}{\beta_j}\right), \tag{13}$$

$$\sigma_j = \alpha_j\left[\Gamma\left(1+\frac{2}{\beta_j}\right)-\Gamma^2\left(1+\frac{1}{\beta_j}\right)\right]^{\frac{1}{2}}, \tag{14}$$

$$C_s = \frac{\Gamma\left(1+\frac{3}{\beta_j}\right)-3\Gamma\left(1+\frac{1}{\beta_j}\right)\Gamma\left(1+\frac{2}{\beta_j}\right)-2\Gamma^3\left(1+\frac{1}{\beta_j}\right)}{\left[\Gamma\left(1+\frac{2}{\beta_j}\right)-\Gamma^2\left(1+\frac{1}{\beta_j}\right)\right]^{3/2}} = \varphi(\beta_j). \tag{15}$$

From equation (15) the parameter β_j is defined as the inverse function of the asymmetry coefficient

$$\beta_j = \varphi^{-1}(C_{sj}) \approx \varphi^{-1}(\tilde{C}_{sj}), \quad j = 0, 1, \ldots, l. \tag{15'}$$

Two other parameters α_j and a_j are defined successively from formulas (14) and (13).

The empirical or analytical distribution curves (6) and (9) are used to determine the curves of the relationship of the values of equal guarantee (x_{op}, x_{jp}) of the investigated hydrologic characteristic x at the reduction point (j=0) and at the point-analogs (j=1, 2, ..., ℓ):

$$x_{0p} = F_0[p(x_{jp})], \quad j = 1, 2, \ldots, l; \tag{16}$$

in particular, according to the Goodrich equation (9)

$$x_{0p} = a_0 + \alpha_0\left(\frac{x_{jp}-a_j}{\alpha_j}\right)^{\frac{\beta_j}{\beta_0}}, \quad j = 1, 2, \ldots, l. \tag{17}$$

For identical asymmetry coefficients

$$C_{sj} = C_{s0}, \quad \beta_j = \beta_0, \quad j = 1, 2, \ldots, l, \tag{18}$$

the curves for the relationship of the values of equal guarantee (17) are straight lines

$$x_{0p} = a_0 + \frac{a_0}{\sigma_j}(x_{jp} - a_j), \tag{17'}$$

which, according to equalities (14) and (13), can be represented as follows:

$$x_{0p} = \bar{x}_0 + \frac{a_0}{\sigma_j}(x_{jp} - \bar{x}_j), \quad j = 1, 2, \ldots, l. \tag{19}$$

It must be kept in mind that when approximating the empirical distribution curves (6) by the Goodrich, type III Pearson and logarithmically normal distribution equations, the curves of the relationship of values of equal guarantee (16) can be expressed by the equation

$$x_{0p} = \bar{x}_0 + \frac{a_0}{\sigma_j}\frac{\Phi(p, C_{s0})}{\Phi(p, C_{sj})}(x_{jp} - \bar{x}_j), \quad j = 1, 2, \ldots, l, \tag{20}$$

where $\Phi(p, C_s) = (x_p - \bar{x})/\sigma$ are values of the normalized quantiles presented in the form of the tables in references [2, 5, 10].

It is important to note that under condition (18), equation (20) coincides with linear equation (19).

In reference [7] it was shown that for any given structure of the equation of the relation of values of equal guarantee (x_p, y_p)

$$y_p = f(x_p, a, b, \ldots), \quad x_p = f^{-1}(y_p, a, b, \ldots) \tag{21}$$

the parameters of the equation a, b, ... can be determined by the method of "least deviation rectangles" of the empirical points (x_i, y_i) from the curve of relationship (21), namely, from the condition of minimum of the function

$$S(a, b, \ldots) = \frac{1}{n}\sum_{i=1}^{n}[y_i - f(x_i, a, b, \ldots)] \times$$
$$\times [f^{-1}(y_i, a, b, \ldots) - x_i] = \min, \tag{22}$$

where $x = f^{-1}(y, a, b, \ldots)$ is the inverse function. The problem reduces to solving the system of equations

$$\frac{\partial S(a, b, \ldots)}{\partial a} = 0, \quad \frac{\partial S(a, b, \ldots)}{\partial b} = 0, \ldots \tag{23}$$

with respect to the parameters a, b, ...

Let us note that the "least rectangles" method gives a unique curve of the relationship (21) between the values of equal guarantee (x_p, y_p) at the same time as two regression curves y with respect to x and x with respect to y are obtained by the "least squares" method:

$$\tilde{y}=f_1(x, a, b, \ldots), \tag{24$_1$}$$

$$\tilde{x}=f_2(y, a, b, \ldots), \tag{24$_2$}$$

which coincide only for a single-valued functional relation between x and y.

The statistical parameters (mean, C_v, C_s) are jointly reduced to a period of many years by the following method. Using the curves (or straight lines) of the relationship of values of equal guarantee (16), (17), (19), (20) with respect to three reference quantiles at the point-analogs x_{jp}, for example, with guarantee of p=5, 50, 95%

$$x_{jp}=x_{j,5},\ x_{j,50},\ x_{j,95},\ j=1, 2, \ldots, l, \tag{25}$$

the corresponding 3ℓ partial reference quantiles $x_{0p}^{(j)}$ at the reduction point j=0 reduced to a period of many years are defined

$$x_{0p}^{(j)}=x_{0;5}^{(j)},\quad x_{0;50}^{(j)},\quad x_{0;95}^{(j)},\quad j=1, 2, \ldots, l \tag{26}$$

and by these quantiles, three calculated weighted mean quantiles $\bar{x}_{0p}$ at the reduction point are calculated:

$$\bar{x}_{0p}=\sum_{j=1}^{l}\gamma_j x_{0p}^{(j)},\quad p=5, 50, 95\%. \tag{27}$$

The weight coefficients γ_1, γ_2, ..., γ_ℓ, which add up to one, are calculated by the formula

$$\gamma_j=\frac{r_{0j}^2\sqrt{(n_{0j}-1)n_j}}{\sum_{j=1}^{l}r_{0j}^2\sqrt{(n_{0j}-1)n_j}},\quad j=1, 2, \ldots, l, \tag{28}$$

where r_{0j} are the pair interseries correlation coefficients calculated by formula (3) for joint observation periods n_{0j} at the reduction point (j=0) and the point-analogs (j=1, 2, ..., ℓ).

Formulas (27) and (28) are central in the method of joint determination and reduction of the statistical parameters to a period of many years. The inverse dependence of the weight coefficients of the point-analog γ_j on the mean square errors (4) of the paired interseries correlation coefficients r_{0j} and on the mean square errors of the partial reference quantiles (25), which decrease inversely proportionally to the square root of the lengths n_j of the observed time series (1) at the point analogs j=1, 2, ..., ℓ, is considered in formulas (27) and (28).

The desired statistical parameters reduced to a period of many years are calculated by three weighted mean quantiles (27) for the reduction point j=0 (see [1, 2, 10]): the distribution bias coefficient

$$S_0 = \frac{\bar{x}_{0;5} + \bar{x}_{0;95} - 2\bar{x}_{0;50}}{\bar{x}_{0;5} - \bar{x}_{0;95}} = \frac{\Phi(5\%, C_{s0}) + \Phi(95\%, C_{s0}) - 2\Phi(50\%, C_{s0})}{\Phi(5\%, C_{s0}) - \Phi(95\%, C_{s0})} = \psi(C_{s0}), \tag{29}$$

the distribution asymmetry coefficient

$$C_{s0} = \psi^{-1}(S_0) = f(S_0), \tag{30}$$

mean square deviation

$$\sigma_0 = \frac{\bar{x}_{0;5} - \bar{x}_{0;95}}{\Phi(5\%, C_{s0}) - \Phi(95\%, C_{s0})}, \tag{31}$$

mean value

$$\bar{x}_0 = \bar{x}_{0;50} - \sigma_0 \Phi(50\%, C_{s0}), \tag{32}$$

variation coefficient

$$C_{v0} = \frac{\sigma_0}{\bar{x}_0}. \tag{33}$$

The statistical parameters (mean, C_V, C_S) are successively reduced to a period of many years at the points j=1, 2, ..., ℓ-1 in an analogous manner, taking the points with longer observation periods as the analogs, that is, successively, with the numbers

$j=l,$
$j=l, l-1,$
$j=l, l-1, l-2$

and so on.

By the statistical parameters reduced to a unique period of many years (n_ℓ years) at ℓ+1 observation points

$$\bar{x}_j, \sigma_j, C_{sj}, j = 0, 1, \ldots, l, \tag{34}$$

using the Goodrich equation (9) or the existing tables of normalized quantiles [2, 5, 10], the analytical cellular probability guarantee curves are constructed

$$p = p(x_j), x_j = F_j[p], j = 0, 1, \ldots, l, \tag{35}$$

and the observed time series (1) are normalized according to these curves by double functional transformation (see [2, 3])

$$u_{jl} = \varphi^{-1}[p(x_{ji})] \equiv u(x_{ji}),\ i = 1, 2, \ldots, n_j;\ j = 0, 1, \ldots, l, \tag{36}$$

where $\varphi^{-1}[p(x)] = u_p$ is the inverse function (quantile) of the normalized normal overestimation probability distribution

$$p(x) = \frac{1}{\sqrt{2\pi}} \int_{u(x)}^{\infty} e^{-\frac{t^2}{2}} dt \equiv \varphi[u(x)] \tag{37}$$

(see [2], pp 284 and 287).

The normalized pair interseries (spatial) correlation coefficients are calculated by the normalized observed time series (36) for joint observation periods n_{jk} at the j-th and k-th points

$$r_{jk} = \frac{\sum_{i=1}^{n_{jk}} u_{ji} u_{ki}}{\sum_{i=1}^{n_{jk}} u_i^2} \approx \sum_{i=1}^{n_{jk}} u_{ji} u_{ki},\quad k \neq j = 0, 1, \ldots, l; \tag{38}$$

the number of these coefficients

$$C_{l+1}^{2} = \frac{l(l+1)}{2},$$

for $r_{jk} \equiv r_{kj}$.

The intraseries (time) normalized autocorrelation coefficients for adjacent terms of each normalized time series are also calculated,

$$r_j = \frac{\sum_{i=2}^{n_j} u_{ji} u_{j,i-1}}{\sqrt{\sum_{i=2}^{n_j} u_{ji}^2 \cdot \sum_{i=1}^{n_j - 1} u_{ji}^2}} \approx \sum_{i=2}^{n_j} u_{ji} u_{j,i-1},\quad j = 0, 1, \ldots, l. \tag{39}$$

In the case of significant inequalities of the observation periods (number of years) at four points j=0, 1, 2, 3

$$n_0 < n_1 < n_2 < n_3 \tag{2*}$$

we shall consider three versions of extension of the normalized observation series (36) at point j=0 successively

$$u_{0i} = u_{01}, u_{02}, \ldots, u_{0n_0} \tag{36_0}$$

with respect to longer normalized observed series (36) at the points j=1, 2, 3 using the normalized conditional distribution equations or, in brief, according to the reduction equations:

1) by the observations at one point j=3

$$u_{0i} = r_{03} u_{3i} + \sqrt{1 - r_{03}^2}\, u_{p_i}, \quad i = n_0 + 1, n_0 + 2, \ldots, n_3, \tag{40}$$

where r_{03} is the pair correlation coefficient between normalized observed series at the points j=0, j=3 calculated by formula (38),

$u_{p_i} = \varphi^{-1}(p_i)$ are the quantiles of the normalized normal distribution defined by a special table (see [2], p 287) or determined directly by computer as inverse functions from equation (37) for random values of the conditional overestimation probabilities p_i defined by a random number table (see [2], p 334) or generated by computer;

2) by observations at two points j=2, 3

$$u_{0i} = k_{02} u_{2i} + k_{03} u_{3i} + \sqrt{1 - R_{023}^2}\, u_{p_i}, \quad i = n_0 + 1, n_0 + 2, \ldots, n_3; \tag{41}$$

3) by observations at three points j=1, 2, 3

$$u_{0i} = k'_{01} u_{1i} + k'_{02} u_{2i} + k'_{03} u_{3i} + \tag{42}$$

$$+ \sqrt{1 - R_{0123}^2}\, u_{p_i}, \quad i = n_0 + 1, n_0 + 2, \ldots, n_1,$$

where k_{02}, k_{03} are the coefficients in the regression equation u_{0i} with respect to u_{2i}, u_{3i}

$$\tilde{u}_{0i} = k_{02} u_{2i} + k_{03} u_{3i}, \tag{43}$$

which is the determinant term in equation (41), k'_{01}, k'_{02}, k'_{03} are the coefficients in the regression equation u_{0i} with respect to u_{1i}, u_{2i}, u_{3i}

$$\tilde{u}_{0i} = k'_{01} u_{1i} + k'_{02} u_{2i} + k'_{03} u_{3i}, \tag{44}$$

which is the determinant term in equation (42).

The regression coefficients k_{02}, k_{03} and k'_{01}, k'_{02}, k'_{03} are defined by solving the systems of linear normal equations (see [2, 3])

$$\left.\begin{aligned} k_{02} + r_{23} k_{03} &= r_{02} \\ r_{32} k_{02} + k_{03} &= r_{03} \end{aligned}\right\}, \tag{45}$$

$$\left.\begin{aligned} k'_{01} + r_{12} k'_{02} + r_{13} k'_{03} &= r_{01} \\ r_{21} k'_{01} + k'_{02} + r_{23} k'_{03} &= r_{02} \\ r_{31} k'_{01} + r_{32} k'_{02} + k'_{03} &= r_{03} \end{aligned}\right\}. \tag{46}$$

The summary set correlation coefficients R_{023} and R_{0123} for joint observation periods at the points j=0, 2, 3 and j=0, 1, 2, 3 entering into the reduction equations (41) and (42), are calculated by the formulas (see the righthand sides in equations (45) and (46))

$$R^2_{023} = r_{02}\,k_{02} + r_{03}\,k_{03}, \tag{47}$$

$$R^2_{0123} = r_{01}\,k'_{01} + r_{02}\,k'_{02} + r_{03}\,k'_{03}. \tag{48}$$

The transition from the normalized terms of the series u_{0i} reproduced by equations (40)-(42) to the initial values $x_{0i}=f(u_{0i})$ is made by using the distribution curves (35) reduced to a period of many years by double functional transformation

$$x_{0i} = F_0[\varphi(u_{0i})],\ i = n_0+1,\ n_0+2,\ \ldots,\ n_j,\ n_j = n_3,\ n_2,\ n_1, \tag{49}$$

where $\phi(u)$ is a normalized normal distribution function (37) (for the values of which see [2], p 284). Let us note that the transformations (36) and (49) are reversible with respect to each other.

Joining the observed series (1) and the corresponding reduced series (49) together, we obtain extended time series

$$x_{0i} = x_{01},\ x_{02},\ \ldots,\ x_{0n_0},\ x_0,\ n_0+1,\ \ldots,\ x_{0n_j},\ n_j = n_3, n_2, n_1. \tag{50}$$

Analogously, according to equations of the type of (40)-(49) it is possible to extend the time series at the points j=1, 2 with respect to longer observed series at the points j=2, 3.

The extension of the proposed method for joint extension of four or more time series does not encounter any theoretical difficulties.

The reduction equation (40) represents the normalized conditional distribution of all possible values of u_{0i} at the reduction point j=0 for any fixed observed value of u_{3i} at the point analog j=3 and permits quantitative estimation of the relation of the values of the regression (statistically determined) term

$$u_{0i} = r_{03}\,u_{3i} \tag{40_1}$$

and random term

$$u_{0i} - \tilde{u}_{0i} = \sqrt{1-r^2_{03}}\,u_{p_i} \tag{40_2}$$

with respect to the corresponding weight (unnormalized) coefficients r_{03} and $\sqrt{1-r^2_{03}}$:

r_{03}	0	0,2	0,3	0,4	0,6	0,8	0,9	0,95	0,98	0,99	1,0
$\sqrt{1-r^2_{03}}$	1,0	0,98	0,96	0,92	0,80	0,60	0,44	0,31	0,20	0,14	0

Hence, it is obvious that even for very high interseries correlation coefficients (r_{03}=0.95-0.99), the addition of the random term to the regression line still remains highly significant. This important fact can be detected only for normalization of the time series. It falls out of consideration when extending (and modeling) the time series without proper consideration of the random term and

without application of normalization [8, 9]. The method of reduction of time series to a period of many years used in references [8, 9] leads to a distorted structure of the extended series and high or low mean value, depending on the relation of the mean values of the terms of the series at the point analog for long and short (joint) time periods. These deficiencies of the methods of [8, 9] disappear only for a single valued linear relation between the corresponding terms of the investigated time series.

It is expedient to generalize the spatial regression equations of the type of (43)-(44) by introducing one more time argument $u_{0,i-1}$, that is, the observed (for $i \leqslant n_0$) or reduced (for $i > n_0$) normalized values at the point j=0 for the preceding i-1 years (or another calculated time interval):

$$\tilde{u}_{0i} = k_0 u_{0,\,i-1} + \sum_{j=m}^{l} k_{0j} u_{ji}, \quad i = n_0 + 1,\ n_0 + 2,\ \ldots,\ n_m, \tag{51}$$

where the regression coefficients k_0, k_{0m}, k_{0m+1}, ... $k_{0\ell}$ are defined by solving a system of $\ell-m+2$ linear normal equations

$$\left.\begin{aligned}
&k_0 + r_0 r_{0m} k_{0m} + r_0 r_{0,\,m+1} k_{0,\,m+1} + \ldots + r_0 r_{0l} k_{0l} = r_0 \\
&r_0 r_{m0} k_0 + k_{0m} + r_{m,\,m+1} k_{0,\,m+1} + \ldots + r_{ml} k_{0l} = r_{0m} \\
&r_0 r_{m+1,\,0} k_0 + r_{m+1,\,m} k_{0m} + k_{0,\,m+1} + \ldots + r_{m+1,\,l} k_{0l} = r_{0,\,m+1} \\
&\ldots\ldots\ldots\ldots\ldots\ldots\ldots\ldots \\
&\ldots\ldots\ldots\ldots\ldots\ldots\ldots\ldots \\
&r_{l0} r_{l0} k_0 + r_{lm} k_{0m} + r_{l,\,m+1} k_{0,\,m+1} + \ldots + k_{0l} = r_{0l}
\end{aligned}\right\}. \tag{52}$$

Here r_0 is the intraseries (time) normalized autocorrelation coefficient calculated by formula (39) for the point j=0; the interseries (spatial) correlation coefficients r_{0j}, r_{jk} are calculated by formula (38).

For the generalized time-space normalized regression equation (51), the square of the set correlation coefficient $R^2_{0m,\ldots\ell}$ is calculated by a formula of the type of (48):

$$R^2_{0m\ldots l} = r_0 k_0 + \sum_{l=m}^{l} r_{0j} k_{0j}, \quad m = 1, 2, \ldots, l-1. \tag{53}$$

The mean square errors of the regression coefficients k_{0j} are calculated by the formula from [2]

$$\sigma_{k_{0j}} = \sqrt{\frac{1 - R^2_{0m\ldots l}}{n_c - (l - m + 2)} \frac{\Delta_{jj}}{D_{00}}}, \quad j = m,\ m+1,\ \ldots\ l, \tag{54}$$

where n_c is the joint observation period at the points with the numbers 0, m, ... ℓ,

D_{00} is the determinant of the system of equations (52),

$$D_{00}=\begin{vmatrix} 1 & r_0r_m & r_0r_{0,m+1} & \cdots & r_0r_{0l} \\ r_0r_m & 1 & r_{m,m+1} & \cdots & r_{ml} \\ r_0r_{0,m+1} & r_{m+1,m} & 1 & \cdots & r_{m+1,l} \\ \cdots & \cdots & \cdots & \cdots & \cdots \\ \cdots & \cdots & \cdots & \cdots & \cdots \\ r_0r_{0l} & r_{lm} & r_{l,m+1} & \cdots & 1 \end{vmatrix}. \tag{55}$$

Δ_{jj} is the minor obtained by plotting the j-th row and the j-th column in the determinant D_{00}.

Regression values of $\tilde{u}_{0i}$ are calculated by the generalized space-time regression equation (51) for values of $i=n_0+1, n_0+2, \ldots, n_m$. Then the reduced terms of the normalized series are determined by the equation

$$u_{0i}=\tilde{u}_{0i}+\sqrt{1-R^2_{0m\ldots l}}\,u_{p_i},\quad i=n_0+1, n_0+2, \ldots, n_m \tag{56}$$

and the reduced terms x_{0i} for extension of the observed short series at the point j=0 corresponding to them with respect to expression (49)

$$x_{0,n_0+1},\ x_{0,n_0+2},\ \ldots,\ x_{0n_m}. \tag{57}$$

In the absence of analogs (ℓ=0), equation (56) has the form

$$u_{0l}=r_0u_{0,l-1}+\sqrt{1-r_0^2}\,u_{p_l},\quad i=n_0+1, n_0+2, \ldots, N. \tag{58}$$

This recurrent equation makes it possible to model a normalized time series of any length N of interest to us at the investigated observation point j=0 and any other point with the number j taken individually:

$$u_{jl}=r_ju_{j,l-1}+\sqrt{1-r_j^2}\,u_{p_l},\quad i=n_j+1, n_j+2, \ldots, N. \tag{58'}$$

Joint modeling of the time series is carried out by the procedure discussed in reference [3]. All possible pair normalized correlation coefficients are considered here -- space (38), time (39) and space-time $r^{(1)}_{jk}$ between the terms shifted by one number of every two (j-th and k-th) normalized time series defined in [2, 3] as the product

$$r^{(1)}_{jk}\equiv r_{u_{ji}u_{k,i-1}}=r_jr_{jk},\quad k\neq j=0, 1, \ldots, l \tag{59}$$

of the time (r_j) and space (r_{jk}) correlation coefficients. It is necessary to consider that

$$r^{(1)}_{jk}\neq r^{(1)}_{kj}=r_kr_{kj},\quad r_{kj}\equiv r_{jk}. \tag{59'}$$

The total number of space-time correlation coefficients $r^{(1)}_{jk}$ and $r^{(1)}_{kj}$ is equal to $\ell(\ell+1)$.

Let us remember that for total symmetry purposes joint modeling of $\ell+1$ time series at points with numbers $j=0, 1, \ldots, \ell$ must be carried out by the rule of cyclic permutation of points using $(\ell+1)^2$ recurrent equations of normalized distribution conditions for $\ell+1$ adjacent modeling steps $i, i+1, \ldots, i+\ell$ (see [3]).

For the case of joint modeling of three time series in reference [3], nine (3^2) normalized conditional distribution equations (21_1)-(21_9) are presented in which the first terms represent the regression values calculated by the equations (22_1)-(22_9) as a function of the last observed or modeled terms in each time series.

Considering the last terms u_{jn_j} in the observed normalized series (36), the following normalized time series are modeled according to the procedure of [3]

$$u_{ji} = u_{j,n_j+1}, \quad u_{j,n_j+2}, \ldots, u_{jN}, \quad j=0, 1, \ldots, l, \tag{60}$$

supplementing the observed normalized series (36) to the length N of interest to us.

The transition from normalized modeled series (60) to the series of the investigated variable (x_{ji}) is realized using the distribution curves (35) reduced to a period of many years by double functional transformation of the type of (49)

$$x_{ji} = F_j[\varphi(u_{ji})], \quad i=n_j+1, n_j+2, \ldots, N; \quad j=0, 1, \ldots, l. \tag{61}$$

Joining the observed series (1) in the corresponding modeled series (61) together, we obtain long, jointly modeled time series at $\ell+1$ points:

$$x_{jl} = x_{j1}, x_{j2}, \ldots, x_{jn_j}, x_{j,n_j+1}, \ldots, x_{jN}, \; j=0, 1, \ldots, l. \tag{62}$$

In conclusion, let us emphasize that the proposed method of joint reduction of the statistical parameters to a single period of many years is applicable on satisfaction of conditions (5) for pair correlation coefficients (3) and the errors in determining them (4).

On extension or joint modeling of time series, conditions of the type of (5) must be satisfied for the normalized pair correlation coefficients (38), and analogous conditions must be satisfied for normalized set correlation coefficients of the types of (47), (48):

$$R > 3\sigma_R, \quad \sigma_R = \frac{1-R^2}{\sqrt{n_c-(l-m+2)}}, \tag{63}$$

where n_c is the joint observation period (number of years) at the investigated points ($j=0, 1, 2, \ldots, \ell$; $m=0, 1, 2, \ldots$).

The effectiveness of joint reduction of statistical parameters to a period of many years, extension and modeling of time series increases with an increase in the pair and set correlation coefficients and with a decrease in their mean square determination errors for joint observation periods.

Based on the observed time series (1), it is possible to perform all of the calculations and graphical constructions both manually and (more expediently) with the help of a computer.

It must be noted that as a result of the interseries correlations, the random "recoilling" points at the ends of the empirical distribution curves (6) corresponding to rare extremal phenomena are not, as a rule, the recoilling points on the empirical curves of the relationship of values of equal guarantee (16). Therefore the latter are more stable and are subject to more reliable extrapolation beyond the observation limits than the empirical distribution curves (6).

Actually, in the equations of the relationship of the values of equal guarantee (16), as a result of the interseries correlations, the empirical parameters of the distribution curves x_0, σ_0, C_{s0} and x_j, σ_j, C_{sj} calculated for joint short observation periods n_{0j}, are, as a rule, deflected to one side of the general values of the parameters corresponding to long joint observation periods ($n_{0j}=\infty$). Accordingly, the empirical estimates of the ratios

$$\frac{\sigma_0}{\sigma_j}, \quad \frac{\Phi(p, C_{s0})}{\Phi(p, C_{sj})}, \quad j = 1, 2, \ldots, l, \tag{64}$$

entering into equations (16) are, as a rule, close to the true values of the ratio (64) corresponding to long, joint observation periods ($n_{0j}=\infty$).

It is necessary also to consider that statistical parameters (29)-(33) reduced to a period of many years do not have systematic bias and do not require correction for short observation periods at the reduction points (see [2], pp 49-50, 149).

BIBLIOGRAPHY

1. Alekseyev, G. A. "Graphoanalytical Methods of Determination and Reduction of the Observations of the Distribution Curve Parameters to a Long Period," TRUDY GGI [Works of the State Hydrological Institute], No 73, 1969.

2. Alekseyev, G. A. OB"YEKTIVNYYE METODY VYRAVNIVANIYA I NORMALIZATSII KORRELYATSIONNYKH SVYAZEY [Objective Methods of Equalizing and Normalizing Correlations], Leningrad, Gidrometeoizdat, 1971.

3. Alekseyev, G. A. "Joint Modeling of Time Series Based on Normalization of Distribution Laws," VODNYYE RESURSY [Water Resources], No 1, 1979.

4. Alekseyev, G. A. "Problem of Determining Empirical Quantiles and the Correlation Coefficient," METEOROLOGIYA I GIDROLOGIYA [Meteorology and Hydrology], No 4, 1963.

5. Alekseyev, G. A. "Application of the Goodrich Distribution Curve to Hydrologic Calculations," TRUDY NIU GMS [Works of the Scientific Research Administration of the Hydrometeorological Service], series IV, No 29, 1946.

6. Alekseyev, G. A. "Proper Statistical Description and Consideration of Time-Space Factors of River Runoff," MEZHDUNARODNYY SIMPOZIUM PO SPETSIFICHESKIM ASPEKTAM GIDROLOGICHESKIKH RASCHETOV DLYA VODOKHOZYAYSTVENNOGO PROYEKTIROVANIYA [International Symposium on Specific Aspects of Hydrologic Calculations for Water Management Planning], Moscow, Gidrometeoizdat, 1979.

7. Velikanov, M. A. OSHIBKI IZMERENIYA I EMPIRICHESKIYE ZAVISIMOSTI [Measurement Errors and Empirical Relations], Leningrad, Gidrometeoizdat, 1962. (see Appendix II, G. A. Alekseyev, Finding the Form of the Relationship Between Random Variables by the Quantile Method).

8. VODNYYE RESURSY REK ZONY BAM [Water Reserves of the Rivers in the BAM [Baykal-Amur Railroad] Region], Leningrad, Gidrometeoizdat, 1977.

9. Rozhdestvenskiy, A. V.; Lobanova, A. G. "Reduction of River Runoff Series to a Long Period by the Method of Set Linear Correlation," TRUDY GGI, No 163, 1968.

10. RUKOVODSTVO PO OPREDELENIYU RASCHETNYKH GIDROLOGICHESKIKH KHARAKTERISTIK [Handbook for Determining Calculated Hydrologic Characteristics], Leningrad, Gidrometeoizdat. 1973.

UDC 627.157

MECHANISM OF LIFTING SOLID PARTICLES OFF THE BOTTOM OF A TURBULENT STREAM

Moscow METEOROLOGIYA I GIDROLOGIYA in Russian No 5, May 81 pp 82-91

[Article by Candidate of Physical and Mathematical Sciences N. N. Grishin, Water Problems Institute, manuscript received 23 Sep 80]

[Text]

Abstract: A study is made of three basic hypotheses with respect to the mechanism of lifting solid particles off the bottom of a turbulent stream of water: the effect of gradient lift, the bottom[1] eddy effect, collision of particles with bottom roughness elements and with each other. Results are presented from an experimental investigation of saltation of bottom particles indicating the effect of the elasticity of the particles on the probability of their being lifted off the bottom. A qualitative comparison is made between the discussed hypotheses and experimental data, and a quantitative estimate is made of the probability of the realization of these hypotheses under specific hydrodynamic conditions. It has been established that in the investigated experiments collisions of the particles with bottom roughness elements play the predominant role in the mechanism of lifting the particles off the bottom.

In the opinion of many researchers, bed load migration plays a very important role in channel processes. Various probability schemes which differ insignificantly from each other from the mathematical point of view, are widely used at this time to describe this phenomenon. They can be considered either as repair processes within the framework of queueing theory [3] or as versions of the problem of random walk of a point on a segment [32]. One of the basic parameters of any stochastic system of movement of sediment particles is the probability of lifting the particles off the bottom. Accordingly, it is necessary to have a clear idea of the physical laws of this phenomenon.

---

[1] [Translator's note: the Russian text actually says "natural eddies," but the subsequent text indicates that this is a misprint.]

At the present time there is no united point of view regarding the cause of lifting the particles off the bottom. Therefore we shall consider the basic hypotheses of the mechanism of lifting bed load off the bottom, and we shall first perform a qualitative check of them using experimental data. Then we shall make a quantitative estimate of the probability of realization of the discussed hypotheses under specific hydrodynamic conditions.

As the experimental data confirming or refuting one hypothesis or another we shall use the results of a study of saltation of spherical particles in a turbulent stream of water [7]. Let us present some characteristics of these experiments with indication of the mean square error of the values: particle radius $R=(3.50\pm0.02)\cdot10^{-3}$ m; density $\rho_1=(1.40\pm0.01)\cdot10^3$ kg/m^3; steady-state free-fall speed in a liquid $W=0.28\pm0.01$ m/sec; size of the bottom roughness elements equal to $(1.00\pm0.02)\cdot10^3$ [sic][1]meters. The dimensionless index of the bed load transport stage (according to Francis [26])

$$V_{*F}=(V_*:V_{*0})=3{,}7 \text{ to } 4.5,$$

where V_* is the dynamic velocity,

V_{*0} is the value of this velocity for which the particles begin to move. The kinematic parameters of the experiments are presented below (see the table).

The particle trajectories were obtained by the movie photography method with a speed of 40 frames/sec. A computer was used to determine the velocity components of the particles at different distances from the bottom by the trajectories. The mean square error in determining the vertical coordinate of a particle was $\delta[z]=2.5\cdot10^{-4}$ meter. The relative error in determining unit values of the vertical velocity of particles lifted off the bottom corresponding to it was quite large: $(\delta[U_z]/U_z)=0.12$. We could not be satisfied with this accuracy; therefore in the numerical estimates we used values of the kinematic parameters of the particles averaged with respect to a set of trajectories. Hereafter, this averaging will be denoted by the symbol $\langle\ldots\rangle$, and a value averaged in this way will be designated by a circumflex $\hat{\ldots}$. For example, $\langle a\rangle=\hat{a}$; $\langle a^2\rangle=(\hat{a})^2+\sigma^2[a]$, where $\sigma[\ldots]$ is the symbol for the mean square deviation.

The average number of trajectories N in the described experiment was no less than 144; therefore the relative error of the average data was no more than a percentage [11]:

$$(\delta[\hat{U}_z]/\hat{U}_z)=(\delta[U_z]/U_z)/\sqrt{N})\leq0{,}01.$$

[1][Translator's note: probably 10^{-3} is meant.]

Experimental data on the movement of spherical particles ($R=(3.50\pm0.02)\cdot10^{-3}$ m, $\rho_1=(1.40\pm0.01)\cdot10^3$ kg/m^3) near the bottom of a turbulent stream and estimation of the probability of realizing the mechanisms of lifting particles off the bottom corresponding to hypotheses A and B

(a) Экспериментальные данные	(b) Опыты 1	2	3	(c) Оценка вероятности	(b) Опыты 1	2	3
V_{*F}	3,7	3,9	4,5	$\left\langle \frac{dU_z}{dt} \right\rangle_\Delta$	2,91	3,73	4,21
$\overline{V}_x$	1,53	1,62	1,85	$\langle V_x \rangle_\Delta$	3,85	4,38	4,71
$\sigma[V_x]$	0,24	0,22	0,29	$\langle V_z \rangle_\Delta$	1,82	2,07	2,18
$\sigma[V_z]$	0,13	0,13	0,14	$K_A >$	9	12	9
$\langle U_D \rangle$	1,06	1,25	1,48	$K_Б >$	13	16	15
$\langle U_x \rangle$	1,03	1,19	1,32	$P_A <$	10^{-19}	10^{-23}	10^{-19}
N	164	154	120	$P_Б <$	10^{-23}	10^{-23}	10^{-23}

Key:
a. Experimental data
b. Experiments
c. Probability estimate

Notes. 1. All of the dimensionless kinematic parameters of a liquid and particles (except acceleration $\langle dU_z/dt \rangle_\Delta$ normalized by the amount of gravitational acceleration 9.81 m/sec^2) are normalized by the amount of the steady-state free fall speed of the particles in the liquid W=0.28 m/sec.

2. The provisional notation: $\overline{V}_x$ is the mean longitudinal velocity of the liquid near the bottom; $\sigma[V_x]$, $\sigma[V_z]$ are the mean square deviations of the longitudinal and vertical components of the velocity of the liquid near the bottom; U_D is the speed of rolling of the particles along the bottom; U_x is the longitudinal velocity of the particles after lifting off the bottom (in the layer z/R=0 to 0.5); N is the number of particle trajectories processed in the experiment; the remaining notation is explained in the text of the article.

Basic Hypotheses and Some Experimental Data on Lifting Particles Off the Bottom

Hypothesis A: A particle lifts off the bottom as a result of large instantaneous values of the lift caused by asymmetry of the flow of liquid around the particle as a result of a significant longitudinal flow velocity gradient near the bottom.

Apparently this hypothesis is most widespread (see, for example, [1, 4, 12, 17, 29, 34]), which raises some doubt inasmuch as the experimental checking of it more than 40 years ago by Goncharov [2] gave negative results.

The experimental data on saltation of bed load particles moving along the bottom known to us contradict hypothesis A, for example, the fact of a decrease in longitudinal velocity of the particles averaged over a set of trajectories (Fig 1) when they are lifted off the bottom. It is obvious that the lifting of the particle under the effect of gradient lift must in the general case take place at instantaneous velocities of the liquid significantly exceeding the average value and no less than this amount [16, 17]. Consequently, in accordance with hypothesis A, for the liquid particles the longitudinal velocity on the average must increase and not decrease as was observed in the described experiments and also in the experiments of Francis [26].

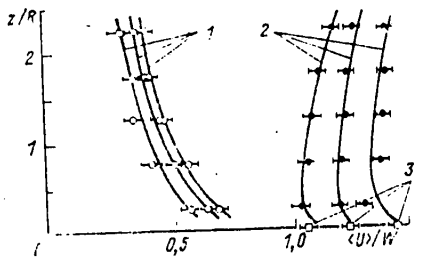

Figure 1. Velocities of lifted saltating particles at different distances from the bottom averaged over a set of trajectories. 1 -- vertical, 2 -- longitudinal, 3 -- speed of rolling along the bottom.

The vertical velocity of the particles averaged over a set of trajectories on lifting them from the bottom decreased monotonically (Figure 1). This result indicates absence of acceleration of the particles in the vertical direction at least outside a thin bottom layer (to the first experimental point from the bottom at the level z=0.5 R). There is little probability that the gradient lift, the average value of which usually is much less than the weight of the particle in the liquid, could not only lift the particle off the bottom, but accelerate it so significantly in the vertical direction in the time it takes to pass through this thin bottom layer. The numerical estimate of this probability presented below confirms the correctness of this argument.

Let us note that in the general case the asymmetry of the flow around the particle causing lift can arise not only from nonuniformity of the velocity field of the liquid, but also the peculiarities of the form of the particles (the Joukowsky force) or their rotation (the Magnus force). For spherical particles investigated in this paper, their form obviously cannot cause asymmetry of the streamlining flow. As for the Magnus force, numerical estimates [7, 8] demonstrated that under the investigated conditions for bed load, this force, although it promotes lift, is not its cause.

Hypothesis B: The separation and lift of particles from the bottom are caused by the effect of bottom eddies or, in other words, positive pulsations of the vertical component of the liquid velocity near the bottom.

According to this also quite widespread [2, 13, 23, 30] point of view, the particles can be lifted and undergo saltation only in turbulent flows. This is contradicted by the experimental results showing that saltation of particles occurred in the case of almost completely extinguished turbulence [25] and even in a laminar flow [26].

In the case of developed turbulence, the lifting of the particles off the bottom was observed both for positive and for negative vertical velocities of the liquid washing over these particles [6]. The results of experiments studying bed load saltation for different particle sizes but the same density [6, 17] demonstrated that under other equal conditions on the average the larger particles rose higher than the fine particles. These facts are also unexplainable within the framework of hypothesis B.

When processing one of the experiments we tried to consider the movement of particles with respect to the liquid surrounding them directly when they are lifted. This is not a simple problem, for it is necessary that an indicator particle of neutral density used for visual representation of the stream of liquid be located near the particle (at a distance not exceeding the diameter) when the particle lifts off the bottom. In the experiment 170 trajectories of saltating particles were obtained, and in only 14 cases was an indicator particle near the saltating particle when it lifted off the bottom. Let us note that it is impossible significantly to increase the concentration of the indicator particles inasmuch as this complicates their identification on adjacent processed frames.

Out of the described 14 cases of lifting, in only two did the vertical velocity of the liquid exceed the vertical velocity of the lifting particles, and in the remaining cases the particles rose more quickly than the liquid surrounding them (see Figure 2). It is obvious that in this situation it is hardly possible to consider vertical pulsations of the liquid velocity responsible for lifting the bed load. A numerical estimation of the probability of realizing hypothesis B will be presented below.

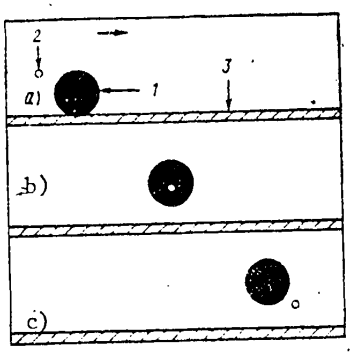

Figure 2. Example of lifting of a particle off the bottom for negative vertical velocities of the liquid.
1 -- saltating particle, 2 -- indicator particle with neutral buoyancy, 3 -- bottom.

Hypothesis C: Particles are lifted off the bottom as a result of collisions with bottom roughness elements or collisions with other particles.

The given hypothesis is not so widespread as the first two, but it also has its proponents (for example [7, 14, 26, 33]). All of the above-presented experimental results fail to contradict hypothesis C, and some confirm it. Thus, the decrease in longitudinal velocity of particles lifted off the bottom is easily explainable within the framework of this hypothesis: on lifting as a result of recoil, the vertical velocity component of the particles appears as a result of a corresponding decrease in the horizontal component.

Checking hypothesis C, we tried experimental determination of whether the elastic properties of the collisions of the particles with bottom roughness elements influence the mechanism of their lifting from the bottom. For this purpose a study was made of saltation of two types of spherical particles in a turbulent stream of water. They had the same size $R_1=R_2=(3.50\pm0.02)\cdot10^{-3}$ m and similar density $\rho_1=(1.40\pm0.01)\cdot10^3$ kg/m^3, $\rho_2=(1.35\pm0.01)\cdot10^3$ kg/m^3, but they differed significantly with respect to elastic properties -- magnitude of the relative velocity recovery coefficient after impact $e_1=0.65\pm0.07$, $e_2=0.32\pm0.06$.

For the experiment 100 particles of each type were selected. They were coated with nitro paint, which insured equality of the dynamic friction coefficients. Therefore the average speed at which the particles rolled along the bottom were similar for particles of both types ($U_{D1}=0.365\pm0.003$ m/sec; $U_{D2}=0.370\pm0.003$ m/sec).

By taking movies of the particle trajectories, the probability distributions that particles of both types would be at different distances from the bottom of the stream, including the zero distance (the particle on the bottom) were obtained. It turned out that for the more elastic particles the probability of being on the bottom is lower, and the probability of being at greater height is higher than for the less elastic particles (Figure 3).

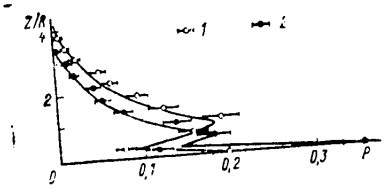

Figure 3. Probabilities that two particles of different elasticity will be at different distances from the bottom of the stream. 1 -- more elastic particles; 2 -- less elastic particles

Consequently, in spite of the greater density, the elastic particles lifted off the bottom more frequently and with greater vertical velocity than the less elastic particles, which confirms hypothesis C regarding the role of collisions in the mechanism of lifting bed load off the bottom. On the other hand, within the framework of hypotheses A and B, elasticity of the particles should have no defining influence on the probability of lifting.

Thus, the only hypothesis which qualitatively does not contradict the presented experimental data is hypothesis C. In all fairness, let us note that under other conditions, for example, in the case of bed movement of the sediments, not only particles moving along the bottom can saltate, but also particles that at first appear to be stationary. Consequently, hypothesis C does not appear to be absolutely valid, but only as applied to the conditions of the analyzed experiments. For greater substantiation of our conclusions regarding the laws of the mechanism of the lifting of particles off the bottom, let us perform a quantitative estimate of the probability of realization of the investigated hypotheses under the specific hydrodynamic conditions of our experiments.

Probability of Different Lifting Mechanisms

Let us estimate the probability of the realization of different lifting mechanisms as follows. Let us determine what instantaneous values the horizontal (or vertical) component of the liquid velocity must have near the bottom in order that particles lifting off the bottom be accelerated in the vertical direction within the framework of hypothesis A (or B), as was observed in the experiments. Then, knowing the values of the mathematical expectations and mean square deviations of the values of the components of the bottom velocity of the liquid from the experiments, let us determine the probabilities that the liquid velocity can assume values required by hypothesis A (or B). These probabilities will also be considered probabilities of realization of the indicated hypotheses.

It is possible to write the equation of motion of a single spherical particle in general form as follows [9, 19, 28]:

$$\frac{4}{3}\pi R^3\left[\rho_1\frac{d\vec{U}}{dt}+\varepsilon\rho\frac{d}{dt}(\vec{U}-\vec{V})\right]=\sum_{i=1}^{7}\vec{F}_i, \qquad (1)$$

where ρ is the density of the liquid;

ε is the added mass ratio;

U and V are the particle and liquid velocities, respectively;

F_i are the forces: F_1 is the hydrodynamic drag; F_2 is the gradient lift; F_3 are the effects of interaction of the flow with the solid boundary (displayed, for example, with an increase in the values of the drag factor and added mass ratio [15, 24]); F_4 is the force of the excess pressure gradient for accelerated movement of the liquid (the acceleration force, according to the terminology of reference [9]); F_5 is the force caused by rotation of the particle (the Magnus force); F_6 is the force considering deviation of the stream of liquid from the steady state (Basset force); F_7 is the external potential force (in our case the gravitational force considering the Archimedes force).

Analysis of equations of the type of (1), which is fruitful to a defined degree for Stokes particles which, as a rule, in the case of bed load interact nonlinearly with the liquid ($Re=2R|U-V|/\nu>1$), presents significant, if at the present time generally surmountable, difficulties [22, 27]. However, we have grounds for significant simplification of this equation when used for our purposes.

The previous qualitative comparison of hypotheses A and B with the experimental data indicates low reliability of them. Therefore it is sufficient for us to estimate only the upper values of the reliability of these hypotheses. Here, we can adopt a number of very significant simplifications of equation (1) under the condition that each of them clearly favors realizations of hypotheses A and B. If even with such simplifications the probabilities of the existence of the discussed lifting mechanisms turn out to be small (and this does occur), they can be taken as unreliable.

Hypothesis A: The following simplifications are assumed: a) the added mass ratio is equal to zero; b) the gradient lift does not decrease with distance of the particle from the bottom; c) the total effect of the forces directed toward the bottom does not exceed the Magnus lift. Then the equation of acceleration of the particle in some layer Λ by the gradient lift can be written as follows:

$$\frac{4}{3}\pi R^3 \rho_1 \frac{dU_z}{dt}\Big|_\Lambda = \frac{1}{2} C_L \pi R^2 \rho (V_x - U_x)^2\Big|_\Lambda. \tag{2}$$

Here C_L is the lift coefficient; the index Δ denotes averaging with respect to the hypothetical acceleration layer Λ.

Performing the averaging operation over a set of particles of equation (2)

$$\frac{4}{3}\pi R^3 \rho_1 \left\langle \frac{dU_z}{dt} \right\rangle_\Lambda = \frac{1}{2} C_L \pi R^2 \rho \{ \langle V_x \rangle_\Lambda^2 + \sigma^2[V_x] + \langle U_x \rangle_\Lambda^2 +$$

$$+ \sigma^2[U_x] - 2[\langle V_x U_x \rangle_\Lambda + \langle V_x \rangle_\Lambda \langle U_x \rangle_\Lambda] \}$$

and neglecting the terms in the righthand side of the averaged equation, the value of which is two orders less than the value of the lefthand side of this equation, after elementary transformations we obtain an estimate of the longitudinal velocity of the liquid in the vicinity of particles lifting off the bottom:

$$\langle V_x \rangle_\Lambda = \langle U_x \rangle_\Lambda + \sqrt{\frac{8 R \rho_1}{3 C_L \rho} \left\langle \frac{dU_z}{dt} \right\rangle_\Lambda}. \tag{3}$$

We took only a positive value of the radical as physically more realistic. Thus, if hypothesis A is valid, then when the particles are lifted the speed of the liquid must differ from its mean value $\overline{V}_x$ by $\overline{V}_x$ на $K_A = \frac{\langle V_x \rangle_\Lambda - \overline{V}_x}{\sigma[V_x]}$ of the mean square deviations $\sigma[V_x]$.

The probability of this event will be defined using the existing representations of the bottom velocity of a liquid as a variable, the components of which are distributed according to a normal law [1, 17]:

$$P_A = P\left(\frac{V_x - \overline{V}_x}{\sigma[V_x]} > K_A\right) = \frac{1}{\sqrt{2\pi}} \int_{K_A}^{\infty} \exp\left[-\frac{1}{2} t^2\right] dt. \tag{4}$$

For numerical estimation of the upper bound of the probability P_A it is necessary to estimate the known acceleration in the acceleration layer entering into the expression for the velocity $\langle V_x \rangle_\Delta$ (3). For this purpose let us consider the motion of particles in the bottom layer 0.5R thick -- from the time of lifting off the bottom (level z=0) to reaching a height of z=0.5R.

If inside this layer 0.5R thick there is a layer of acceleration of particles in the vertical direction Δ, it is obvious that the vertical acceleration of the particles averaged over the acceleration layer cannot be less than their acceleration averaged over the 0.5R layer, that is, $\langle dU_z/dt \rangle_\Delta \geq \langle dU_z/dt \rangle_{0.5R}$. In the case of constant acceleration which is favorable for realization of both hypotheses, its value is expressed trivially in terms of the average velocity and thickness of the layer: $\left\langle \frac{dU_z}{dt} \right\rangle_{0,5R} = \frac{4}{R} \langle U_z^2 \rangle_{0,5R}$.

As is known [5], the square of the mean value of a random variable is less than the mean value of the square of this variable; the final estimate of the hypothetical acceleration $\langle dU_z/dt \rangle_\Delta$ has the form

$$\left\langle \frac{dU_z}{dt} \right\rangle_\Delta \geq \frac{4}{R} \langle U_z^2 \rangle_{0,5R} > \frac{4}{R} \langle U_z \rangle_{0,5R}^2. \qquad (5)$$

For determination of the value of $\langle V_x \rangle_\Delta$ (3), in addition to estimation of (5), a triple value of C_L=0.6 favorable for realization of hypothesis A [18, 31] and a value less than $\langle U_x \rangle_\Delta \approx \langle U_x \rangle_{0.5R}$ determined experimentally were used. The values of $\langle V_x \rangle_\Delta$ calculated in this way and $\sigma[V_x]$ and $\overline{V}_x$ determined experimentally indicate that in accordance with (3) for realization of hypothesis A instantaneous values of the longitudinal velocity of the liquid near the bottom must deviate from their mean value by K_A=9 to 12 of the mean square deviations (see the table).

The probability of such events P_A (4) estimated with the help of [21] is negligibly small, less than 10^{-19} (see the table). Thus, under the investigated conditions hypothesis A appears to be unrealistic.

Hypothesis B: Simplifications of equation (1) favorable for realization of this hypothesis are similar to the ones assumed earlier: a) the added mass ratio is zero; b) the total effect of forces preventing lift does not exceed the effect of the lift forces (gradient and Magnus). The equation for the hypothetical acceleration of a particle in some layer Δ by ascending liquid flows simplified in this way has the form

$$\frac{4}{3} \pi R^3 \rho_1 \frac{dU_z}{dt}\Big|_\Delta = \frac{1}{2} C_D \pi R^2 \rho (V_z - U_z)^2 \Big|_\Delta,$$

where C_D is the frontal drag.

Just as when discussing hypothesis A, let us perform the averaging operation with respect to a set of rising particles and neglect the small terms in the averaged equation. Here we find that if hypothesis B is valid, then on lifting of the particles off the bottom the vertical velocity of the liquid volumes surrounding them must have values no less than

$$\langle V_z\rangle_\Delta = \langle U_z\rangle_\Delta + \sqrt{\frac{8R\rho_1}{3C_D\rho}\left\langle\frac{dU_z}{dt}\right\rangle_\Delta}, \qquad (6)$$

that is, it must deviate from its mean value of zero by $K_B=(\langle V_z\rangle_\Delta/\sigma[V_z])=13$ to 16 mean square deviations (see the table).

The probability of such events, that is, the probability of validity of hypothesis B is still less than the negligibly small probability of realization of hypothesis A, and it is equal to [11]

$$P_B = P\left(\frac{V_z}{\sigma[V_z]} > K_B\right) = \frac{1}{\sqrt{2\pi}}\int_{K_B}^{\infty}\exp\left[-\frac{1}{2}t^2\right]dt < 10^{-23}.$$

For numerical estimation of the vertical velocity (6), empirical values of $\langle U_z\rangle_\Delta \approx \langle U_z\rangle_{0.5R}$ (see the table), the acceleration estimate (5) and the high value of the frontal drag $C_D=3$ favorable to hypothesis B were used.

Let us note that if the instantaneous values of the bottom velocity components of the liquid are distributed not by a normal law [10, 20], then the validity of our conclusions is maintained. This is connected with the fact that the values of K and K_B are so high (see the table), that we can in general not make any assumption about the form of the distribution of the liquid velocity components, and for estimation of the probability of the discussed hypotheses, we can use the Chebyshev inequality

$$P\left(\frac{|x-\bar{x}|}{|x|} \geqslant K\right) \leqslant K^{-2},$$

which is valid for any distribution law of the random variable [5].

Even for such an estimate (using a very weak inequality) hypotheses A and B turn out in practice to be unrealistic inasmuch as the probability of their realization is on the order of 10^{-2}, which is an order lower than that observed experimentally.

A numerical estimate of the probability of realizing hypothesis C similar to the ones performed for hypotheses A and B is procedurally impossible. However, inasmuch as under the investigated condition hypotheses A and B are clearly unrealistic, we must adopt the third hypothesis -- that lifting of the particles from the bottom occurred as a result of their collisions with bottom roughness elements. Let us remember that even qualitatively only hypothesis C does not contradict all of the previously investigated experimental results.

Our conclusion, however, should not be understood as meaning that the factors of the dynamic effect of the flow on a particle (gradient lift, Magnus force, effect of the liquid velocity pulsations, and so on), not being the primary cause of lift under the investigated conditions, in general play an insignificant role in bed load dynamics. Lifting of the particles from the bottom is the result of the interaction of all of the enumerated factors, and possibly certain others which have not been sufficiently clearly revealed at the present time.

The degree of significance of each of these factors in the lifting phenomenon depends on specific hydrodynamic conditions.

In conclusion, let us note that the lifting mechanism in which the primary role is played by collisions of the particles with bottom roughness elements and with each other has as its corollary the possibility of greater turbulization of the flow transporting saltating bed load particles by comparison with a pure liquid flow.

BIBLIOGRAPHY

1. Velikanov, M. A. DINAMIKA RUSLOVYKH POTOKOV [Dynamics of Channel Flows], Vol 2, Moscow, GITTL, 1955.

2. Goncharov, V. N. DVIZHENIYE NANOSOV V RAVNOMERNOM POTOKE [Bed Load Motion in a Uniform Flow], Leningrad-Moscow, ONTI, 1938.

3. Grishanin, K. V. "Bed Load Motion as a Renoir Process," TRUDY GGI [Works of the State Hydrological Institute], No 190, 1972.

4. Grishanin, K. V. DINAMIKA RUSLOVYKH POTOKOV, Leningrad, Gidrometeoizdat, 1979.

5. Grishin, V. K. STATISTICHESKIYE METODY ANALIZA REZUL'TATOV IZMERENIY [Statistical Methods of Analyzing Measurement Results], Moscow, MGU, 1973.

6. Grishin, N. N. "Kinematics of Solid Particles in the Bottom Region of a Turbulent Flow and the Probability of Their Collisions," VINITI (DEP.), RZH MEKHANIKA [Mechanics Abstract Journal], No 8, 1977.

7. Grishin, N. N. "Some Physical Laws of Motion of Solid Particles in the Bottom Region of a Turbulent Flow," VINITI (DEP.), RZH MEKHANIKA, No 7, 1978.

8. Grishin, N. N. "Magnus Effect for a Spherical Particle Lifted Off a Solid Surface," METEOROLOGIYA I GIDROLOGIYA [Meteorology and Hydrology], No 11, 1979.

9. Kashcheyev, V. M.; Muranov, Yu. V. "Problem of the Effect of Magnus Pulsation Forces and Acceleration on the Motion of Particles in a Turbulent Gas Flow," TEPLOFIZIKA VYSOKIKH TEMPERATUR [High Temperature Thermal Physics], Vol 13, No 5, 1975.

10. Klein, S.; Reynolds, W.; Straub, F.; Ranstedler, P. "Structure of Turbulent Boundary Layers," MEKHANIKA [Mechanics], No 4, 1969.

11. Kramer, G. MATEMATICHESKIYE METODY STATISTIKI [Mathematical Methods of Statistics], Moscow, Mir, 1975.

12. Levi, I. I. INZHENERNAYA GIDROLOGIYA [Engineering Hydrology], Moscow, Vysshaya shkola, 1967.

13. Mikhaylova, N. A. PERENOS TVERDYKH CHASTITS TURBULENTNYMI POTOKAMI VODY [Solid Particle Transport by Turbulent Streams of Water], Leningrad, Gidrometeoizdat, 1966.

14. Olevinskaya, S. K. "Experimental Study of the Saltation of Gravel in a Turbulent Stream," author's review of dissertation for a scientific degree, Moscow, MGU, 1976.

15. Riman, I. S.; Kreps, R. L. "Additional Masses of Bodies of Different Shapes," TRUDY TSAGI [Works of the Central Institute of Aerohydrodynamics], No 635, 1947.

16. Romanovskiy, V. V. "Study of Bed Load Displacement Velocity," TRUDY GGI, No 242, 1977.

17. Rossinskiy, K. I.; Lyubomirova, K. S. "Basic Laws of Motion of River Bed Load " VODNYYE RESURSY [Water Resources], No 1, 1972.

18. Rossinskiy, K. I.; Arbudiyeva, K. M. "Flow Around Bodies in a Turbulent Stream Near a Solid Surface," VODNYYE RESURSY, No 6, 1977.

19. Sou, S. GIDRODINAMIKA MNOGOFAZNYKH SRED. [Hydrodynamics of Multiphase Media], Moscow, Mir, 1971.

20. Ibragimov, M. Kh.; Subbotin, V. I.; Bobkov, V. P.; Sabeyev, G. I.; Taranov, G. S. STRUKTURA TURBULENTNOGO POTOKA I MEKHANIZM TEPLOOBMENA V KANALAKH [Structure of a Turbulent Flow and Heat Exchange Mechanism in Channels], Moscow, Atomizdat, 1978.

21. TABLITSY VEROYATNOSTNYKH FUNKTSIY [Tables of Probability Functions], Moscow, VTS AN SSSR, Vol 2, 1970.

22. Fidman, B. A. "Theory of the Motion of Suspended Bed Load " DINAMIKA I TERMIKA RECHNYKH POTOKOV [Dynamics and Thermics of River Flows], Moscow, Nauka, 1972.

23. Fomenko, G. S. "Study of the Kinematic Structure of a Flow and the Motion of Particles in Its Bottom Zone," author's review of dissertation for scientific degree, Moscow, MGU, 1975.

24. Huppel, J.; Brenner, G. GIDRODINAMIKA PRI MALYKH CHISLAKH REYNOL'DSA [Hydrodynamics in the Presence of Small Reynolds Numbers], Moscow, Mir, 1976.

25. Bagnold, R. A. "Some Flume Experiment on Large Grains But Little Denser Than the Transporting Fluid and Their Application," PROC. INST. CIV. ENG, London, Vol 4, No 1, 1955.

26. Francis, J. R. D. "Experiments on the Motion of Solitary Grains Along the Bed of Water Stream," PROC. ROY. SOC., London, A332, No 1591, 1973.

27. Herring, R. A. "On the Motion of Small Spheres in Oscillating Liquids," CHEM. ENG. J., Lausanne, No 2, 1976.

28. Hinze, J. O. "Some Problem in the Study of Turbulent Transport," PROC. XV CONG. IAHR, Istambul, Vol 6, 1973.

29. Jeffreys, H. "On the Transport of Sediment by Streams," PROC. CAMB. PHIL. SOC., Vol 25, 1929.

30. Mitsuhire, S. "Ekhime Daygaku Nogakuby kie," MEM. COLL. AGR. EHIME UNIV., Vol 22, No 2, 1978 (referenced by RZh MEKHANIKA [Mechanics Abstract Journal], No 9, abstract B 1095, 1978).

31. Shen, H. W.; Hans, A. "Einstein's Contribution in Sedimentation," JHD ASCE, No 5, 1975.

32. Todorovic, P.; Nordin, K. "Evaluation of Stochastic Models Describing Movement of Sediment Particles on River Beds," J. RES. US GEOL. SURV., Vol 3, No 5, 1975.

33. Tsuchiya, Y. "On the Mechanics of Saltation of Spherical Sand Particle in a Turbulent Stream," PROC. XIII CONG. IAHR, Kyoto, Vol 2, 1969.

34. Yalin, M. S. "An Expression for Bed Load Transportation," JHD ASCE, Vol 89, No 3, 1963.

UDC 551.579

EFFECT OF TEMPERATURE ON SOIL MOISTURE POTENTIAL AND ITS AVAILABILITY TO PLANTS

Moscow METEOROLOGIYA I GIDROLOGIYA in Russian No 5, May 81 pp 92-98

[Article by Candidate of Biological Sciences N. A. Muromtsev, Soils Institute,
manuscript received 3 Sep 80]

[Text]

Abstract: A study is made of setting up experiments to study the effect of air temperature and soil on the capillary potential of soil moisture under controlled (laboratory) conditions.

The soil temperature distribution laws were established as a function of the soil water-physical properties and air temperature. The relation was established for the capillary potential of soil moisture as a function of temperature in two soils differing with respect to granulometric composition and water-physical properties. An interpretation of this function is presented. A theoretical explanation is offered for the laws of temperature impact on moisture potential in different soils.

The hysteresis phenomena of the soil moisture as a function of soil temperature consisting in disagreement of the values of the moisture potential for a decrease and increase in temperature were established.

The soil moisture potential characterizes the water-retentive forces of the soil and the availability of moisture to plants. In practical respects the potential is widely used to diagnose the irrigation of farm crops and evaluate their moisture utilization [1-3], when studying moisture and salt transport processes [3], when substantiating optimal drainage parameters, and so on.

Temperature as an environmental factor is the most important thermodynamic parameter functionally related to moisture potential. Hence, it is necessary to perform a careful study of the influence of temperature on the moisture potential and consider this influence when developing recommendations for hydrotechnical amelioration measures. However, the effect of temperature on soil moisture, especially in the optimal soil moisture range, has been studied very little. The scientific literature available on the given subject [2] is meager, and the

information contained in it is highly contradictory. Thus, Richter [6] performed studies on four soils differing with respect to clayey fraction (from 9.4 to 48.6%), and he established that the air temperature has the strongest influence on the capillary moisture potential (P_k) in argillaceous and sandy soils: with a rise in temperature from 15 to 45°C, P_k increased by 50 to 10 kPa in both soils. According to Gardner's data [4], an increase in temperature in the range from 0 to 50°C leads to an increase in P_k by 0.9 kPa for each degree in coarse-grained sand, fat sandy clay and mountain-meadow humus soil. In Taylor's opinion [7], the temperature effect in the high soil moisture range is low, and it increases as the moisture content decreases, reaching a maximum for moisture corresponding to the lower limit of moisture available to plants, that is, for maximum hygroscopicity. Kedziora [5] adheres to an analogous opinion, but he points out that the effect of temperature on P_k is felt more sharply in sandy soils than in argillaceous soils.

The primary deficiency of some of the referenced papers is the use of air temperature, but not the soil temperature, inasmuch as the dynamics of the air temperature cannot coincide in time with the dynamics of the soil temperature. On the other hand, a number of experiments have been performed under uncontrolled conditions, which complicates discovery of the effect of the temperature on P_k in pure form.

In this paper a study is made of the effect of the air and soil temperatures on the capillary moisture potential using information obtained under laboratory (controlled) conditions. The procedure followed in the studies is as follows. Soil weighing 10 kg was placed in metal pots, in the centers of which a tensiometer and thermometer were located. After establishment of the required moisture in the soil, its surface was mulched with a 2-centimeter layer of coarse-grained sand, and the entire pot was sealed with three layers of polyethylene film. An upper (0-25 cm) layer of alluvial loamy and dern-podsolic sandy-loam soils widespread in the floodplain of the Moscow River (the Odintsovskiy Rayon of Moscow Oblast) was used in the experiments.

The upper layer of alluvial loamy soil is light loam with respect to granulometric composition and is characterized by the following properties: density 1.3 g/cm^3, porosity 45%, specific weight 2.70 g/cm^3, least water capacity 22%, humus content 2.8%, granulometric composition sandy loam. Two moisture level were created for each soil: moisture on the HB level (25.0% for alluvial loamy soil and 22% for dern-podsolic sandy loam) and 0.7 HB. The studies were performed in the fall-winter period of 1978/79; the air and soil temperature variations were created by alternately placing the pots in heated and unheated rooms.

The nature of variation of the soil and air temperature, the temperature gradient (between the air and soil) and Pk can be determined by the data in Figure 1 (alluvial meadow soil, 0.7 HB). On the whole, during the study period, the air temperature varied from 31 to 0°C; the soil temperature also varied within the same limits. The maximum temperature gradient is observed in alluvial loamy soil up to HB moisture; for both soils with 0.7 HB moisture the temperature gradients are approximately the same. Analysis of the temperature dynamics indicates that all the soil temperature variations are synchronous with the air temperature variations. Here, some delay in the soil temperature variations with respect to air temperature variations is observed for entirely understandable reasons in all versions. In accordance with the temperature dynamics, the moisture potential gradient dynamics were found which, however, correlate more with the temperature gradients than with the temperatures themselves. This is explained by some "inertia" of P_k by

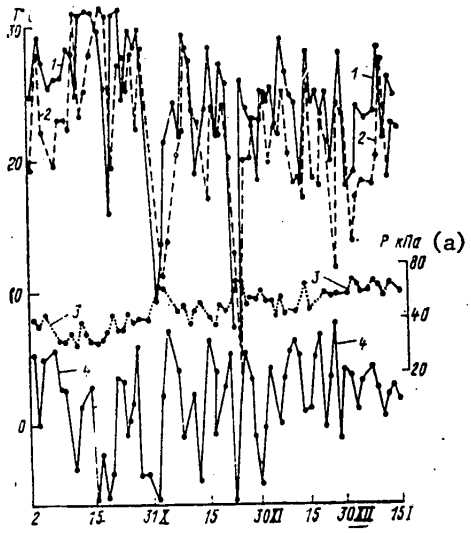

Figure 1. Behavior of the air temperature (1) and soil temperature (2), the temperature gradient between the air and soil (4) and the soil moisture potential gradient (3) in alluvial meadow loamy soil. 1978/79.

Key:
a. P, kPa

comparison with the soil temperature (the more so by comparison with the air temperature). Table 1 gives a visual representation of the nature of the soil temperature variation and P_k as a function of the air temperature variations.

Three cases of soil temperature distribution with time presented in Table 1 as a function of the air temperature variation were selected from a large data file, because the most frequent temperature determinations during the course of the experiment were made on these days, and they can be considered random rather than especially selected. Analysis of the data indicates that in each case on reduction of the air temperature from maximum values to minimum (4 October 1978 and 9 February 1979) and with a rise in air temperature from minimum to maximum (6 October 1978), the variation rate of the soil temperature is different and depends on the type of soil and its moisture. The temperature drops and rises most rapidly in version 4 (sandy loam, 0.7 HB) and most slowly, in version 3 (sandy loam, HB). With higher moisture (versions 1 and 3), although the rate at which the soil temperature drops is insignificant, it is still lower than for low moisture. This is explained by the high heat capacity of water by comparison with the heat capacity of the mineral skeleton of the soil.

With an increase in the soil temperature (and the air temperature) the moisture potential decreases, and with a decrease in temperature, it increases. This takes place because the surface tension (σ) of the water decreases; a rise in temperature from 0 to 50°C causes a decrease in surface tension by 7.73 dynes/cm [2]. Inasmuch as an increase in temperature causes a decrease in σ, the energy expenditures on extraction of a unit mass (volume) of water from the soil consequently decrease, that is, the water becomes more active. However, the degree of variation of the

Table 1. Soil temperature ($T_п$ °C) and capillary potential of the soil moisture ($P_к$, kPa) as functions of the air temperature ($T_в$ °C) in alluvial meadow loamy soil (for HB -- 1; for 0.7 HB -- 2) and in dern-podsolic sandy-loam (for HB -- 3; for 0.7 HB -- 4)

Time	$T_в$	Version 1		2		3		4	
		$T_п$	$P_к$	$T_п$	$P_к$	$T_п$	$P_к$	$T_п$	$P_к$
					4 October 1978				
	19,6	22	3,32	31,8	46,82	21,4	4,26	21,4	42,56
	27,0	22	3,32	23,0	44,02	22,4	4,52	22,0	38,30
	10,0	21,2	3,32	21,0	46,02	21,0	3,72	20,2	43,89
	8,2	19,0	3,32	20,0	47,88	21,0	3,72	18,0	45,88
	7,0	16,8	3,32	16,8	50,27	16,9	3,59	15,6	47,48
	6,8	14,8	3,32	14,5	52,00	14,8	3,46	13,4	48,15
	6,8	10,4	3,32	10,6	53,86	12,4	3,46	11,2	48,41
	6,4	10,4	3,32	10,3	53,60	10,8	3,46	10,4	48,41
	7,8	9,4	3,32	9,2	55,06	9,2	3,46	9,6	47,88
					6 October 1978				
8[30]	9,6	9,1	3,32	9,1	46,15	8,6	4,26	8,4	44,82
9[30]	20,5	10,0	3,72	10,4	46,95	9,6	5,72	10,0	41,10
10[30]	24,6	11,0	3,46	11,7	44,67	11,0	6,65	12,9	37,90
11[30]	25,7	14,4	3,46	15,2	42,43	14,8	6,92	15,6	36,31
12[30]	25,3	16,9	3,46	17,5	42,56	16,7	7,05	18,0	35,51
13[30]	25,3	18,7	3,46	19,4	38,70	18,4	7,05	19,6	35,24
14[30]	24,5	20,0	3,46	20,7	37,37	19,6	7,05	20,7	35,24
15[30]	25,8	20,8	3,32	21,8	36,31	20,6	7,05	21,6	35,24
16[30]	25,0	21,6	3,32	22,2	35,78	21,4	7,05	22,2	35,24
21[30]	26,2	24,0	3,32	23,8	35,24	23,4	7,45	24,0	35,51
23[30]	26,2	24,8	3,32	24,2	35,24	24,0	7,85	24,2	35,51
					19 February 1979				
9[00]	18,1	17,4	3,99	17,5	41,89	17,4	5,45	17,4	53,20
10[00]	0,2	16,7	4,65	17,2	46,15	16,6	5,32	16,1	51,74
11[00]	−1,2	13,9	4,65	15,0	50,01	14,0	5,05	12,9	54,53
12[00]	−1,8	11,1	4,65	19,8	53,73	11,3	5,19	9,9	55,46
13[00]	-1,0	8,8	4,65	9,8	55,39	9,2	5,32	7,6	55,73
16[00]	−0,3	4,6	4,65	5,8	57,99	4,9	5,45	3,6	55,86

capillary potential of the moisture with variation of the temperature differs and depends strongly both on the moisture content and on the type of soil and its water-physical properties. The data in Table 1 indicate the magnitudes of the moisture potential variations with variation of the soil temperature. It is obvious that the maximum influence of the soil temperature on the potential is observed in version 2 (alluvial loamy soil for 0.7 HB), and the minimum, in version 1 (the same soil, but for HB). In the first case the maximum decrease in P_k occurred on 19 October 1978 and amounted to 13.3 kPa (100 mm Hg) for 18°C; in the second case the temperature variation of the alluvial loamy soil (version 1, for HB) by 13°C (4 October 1978) did not cause potential variations (3.32 kPa). The data characterizing the variation of P_k per °C are presented in Table 2.

Table 2. Increase in P_k per °C on variation of the temperature in alluvial meadow loamy soil (HB -- 1, 0.7 HB -- 2) and dern-podsolic sandy loam (HB -- 3 and 0.7 HB -- 4)

Date	Version											
	1			2			3			4		
	ΔT	ΔP_k	$\frac{\Delta P_k}{\Delta T}$	ΔT	ΔP_k	$\frac{\Delta P_k}{\Delta T}$	ΔT	ΔP_k	$\frac{\Delta P_k}{\Delta T}$	ΔT	ΔP_k	$\frac{\Delta P_k}{\Delta T}$
4 X 1978	13	0	0	13	8,25	0,64	13	0,80	0,06	12	5,85	0,49
6 X	16	0,27	0,01	14	10,91	0,77	14	3,46	0,24	16	9,31	0,58
19 X	13	0,40	0,03	18	13,30	0,73	12	2.13	0,17	12	8,25	0,68
1 XI	14	0,93	0,07	13	9,44	0,72	12	2,39	0,20	12	6,92	0,57
14 XI	14	0.13	0,01	13	10,91	0,84	13	2,26	0,17	13	11,44	0,88
25 XII	8	0,27	0,03	8	10,91	0.60	8	1,33	0,16	8	7,45	0,93
19 II 1979	12	0,66	0,05	13	10,84	0,60	12	0,13	0	14	2,66	0,19

Note. ΔT is the soil temperature gradient, °C; ΔP_k is the moisture potential gradient , kPa; $\Delta P_k/\Delta T$ is the increase in moisture potential per °C, kPa/°C.

The data contained in Table 2 were calculated by twice-daily observations. They indicate that the temperature gradients in all versions are close to each other, but the potential gradients differ. In versions 1, ΔP_k are insignificant, and they are frequently in the measurement accuracy limits. The maximum value is 0.065 kPa, and the minimum is close to zero. In version 2, which is an analog with respect to moisture content (HB) of version 1, $\Delta P_k/\Delta T$ are also insignificant, but nevertheless, noticeably higher than in version 1 (from 0.01 to 0.24 kPa).

The values of ΔP_k in versions 2 and 4 (0.7 HB) are appreciably higher than in the investigated cases. In alluvial loamy soil (version 2), $\Delta P_k/\Delta T$ are in a narrower range of potential values by comparison with version 4 (0.60-0.84 kPa and 0.19-0.88 kPa per °C, respectively), and the absolute values of P_k for in practice identical temperature gradients are appreciably higher for alluvial loamy soil. Thus, for example, for T=18°C, P_k was 13.3 kPa and 8.25 kPa, respectively, in versions 2 and 4.

Consequently, the data in Table 2 indicate that the nature of the effect of the temperature on P_k is identical in soils that differ with respect to granulometric composition and with different moisture. However, the degree of the temperature effect differs and depends both on the granulometric composition of the soil and the moisture content in it. The strongest temperature effect with high moisture (HB) is observed in sandy loam dern-podsolic soil; in loamy alluvial soil this effect is very low, and it can be neglected for practical purposes. With a decrease in the moisture content to 0.7 HB the greatest reduction in P_k with an increase in temperature takes place in alluvial loamy soil.

The relations for the capillary moisture potential as a function of temperature are presented in Figure 2 (alluvial loamy soil, 0.7 HB) and Figure 3 (dern-podsolic sandy loam, 0.7 HB). It is obvious that in the first case (Figure 2) the relation constructed by observations on different days is expressed by a straight line and can be approximated by the empirical equation y=-Ax+B. In the second case (Figure 3) the function is expressed by a parabola type curve, and it is approximated by an empirical equation of the type y=-Ax+Bx+C. Here the experimental points corresponding to observations of T and P_k on different days, for alluvial meadow

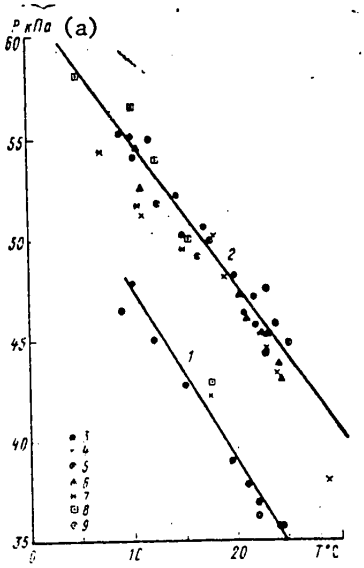

Figure 2. Soil moisture potential as a function of temperature in alluvial meadow loamy soil.
1 -- with an increase in soil temperature from 9.6 to 25°C; 2 -- with a decrease in soil temperature from 30 to 4°C according to observation dates: 3 -- 4 Oct 78, 4 -- 19 October, 5 -- 1 November, 6 -- 14 November, 7 -- 25 December, 8 -- 19 February 1979 and 9 -- 6 October 1979.
Key:
a. P, kPa

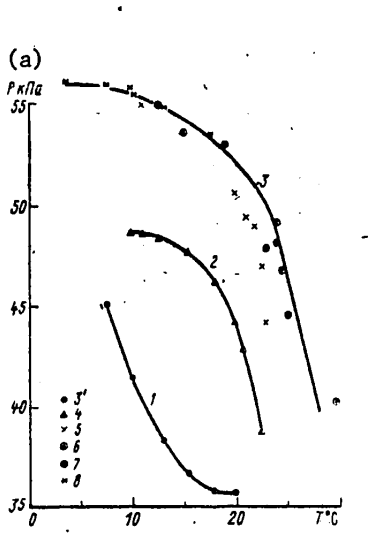

Figure 3. Soil moisture potential as a function of temperature in dern-podsolic sandy loam.
1 -- with an increase in soil temperature from 8 to 20°C; 2 -- with a decrease in soil temperature from 20 to 9°C; 3 -- with a decrease in soil temperature from 30 to 4°C by observation dates: 3' -- 4 October 1978, 4 -- 6 October, 5 -- 19 October, 6 -- 14 November, 7 -- 25 December, 8 -- 19 February 1979.
Key:
a. P, kPa

loamy soil are characterized by less dispersion than for sandy loam dern-podsolic soil.

The relations reflecting the effect of temperature on P_k with an increase in temperature (from minimum values to maximum occurring in the experiments) do not coincide with the relations (Figures 2 and 3, lines 1, 2) $P_k f(T)$ with a decrease in temperature, forming the "plane" P_k hereafter called hysteresis. The function $P_k f(T)$ for both soils with higher moisture content (moisture for HB) is characterized by very low closeness of the relation (a correlation coefficient of about 0.1).

Thus, the studies reveal the following interesting characteristic features. For the same range of temperature variations (increase or decrease) the variation of P_k is different and depends both on the moisture content in the soil and on the properties of its solid phase, primarily the granulometric composition. With a high moisture content the effect of the temperature on P_k in loamy meadow alluvial soil is in practice absent, and in sandy loam it is insignificant.

For moisture corresponding to 0.7 HB, the effect of temperature on P_k is significant; The function $P_k f(T)$ for loamy alluvial soil is expressed by a straight line, and for sandy loam, by a parabola type curve.

The function $P_k f(T)$ is characterized by hysteresis, that is, the dependence of the potential on temperature during a reduction of it from the provisional maximum to the provisional minimum does not coincide with the dependence of the potential on temperature when it increases.

The discovered laws of the effect of temperature on the capillary potential of soil moisture arise from the peculiarities of the water-retentive forces of the soil determined by the properties of its solid phase and the water content in it. For high moisture content in the soil (HB and higher) a significant part of the moisture is held by the soil as a result of capillary forces and it is characterized by comparatively high activity (the free energy of the soil moisture is relatively high). In this case the temperature effect leads to an insignificant increase in its activity; here the absolute magnitude of the increased activity depends on the temperature variation rate, as a result of which the potential variation per °C is different in time. In this soil moisture range the properties of the solid phase of the soil are poorly manifested.

With a decrease in moisture content to 0.7 HB the forces of its retention by the soil increase, the moisture becomes more bound (the thermodynamic potential of the moisture increases), its activity decreases, and viscosity increases. In this case a rise in temperature leads to a significantly higher degree of increase in activity of the soil moisture and its free energy.

With a decrease in temperature from 30 to 10°C in sandy loam dern-podsolic soil the potential increases progressively to 55.9 kPa; with a further decrease in temperature to 7°C, the rate of increase in the potential drops noticeably, and in the 7-4°C range the rise in P_k in practice stops. Here the rate of increase in the potential depends on from what maximum level the temperature begins to decrease, which causes significant fluctuation of $\Delta P_k/\Delta T$. In loamy alluvial soil the moisture (with the same moisture content) is bound by high matrix forces; its activity is lower than in sandy loam. The different rate of decrease in temperature has a lesser degree of effect on the potential variation, as a result of which the values of $\Delta P_k/\Delta T$ are in a narrower interval (Table 2). With a decrease in temperature from 30 to 4°C, the moisture potential increases progressively in the entire temperature range. As for the hysteresis phenomenon of the function $P_k f(T)$, its nature and mechanism are still not entirely clear. It is possible that this is connected with different variation of the surface tension and viscosity of the water with a rise and fall in temperature.

Thus, the data obtained indicate that the variation of the capillary potential of soil moisture in the temperature range from 0 to 30°C is highly significant. The decrease in potential connected with an increase in temperature in this range is different and depends on the soil properties and the water content in the soil.

Up to now all scientific research, design and production work (the latter includes the diagnosis of farm crop irrigation, estimation of availability of soil moisture to plants and prediction of their moisture utilization) has been done in practice without considering the potential variations. Ignoring this phenomenon leads to serious errors in all hydrophysical, hydrologic and land improvement calculations and in the plans and designs. Accordingly, it becomes obvious that it is necessary to introduce the corresponding corrections to the potential in all cases where a noticeable decrease or increase in the air and soil temperature occur.

BIBLIOGRAPHY

1. Muromtsev, N. A. "Diagnosing the Irrigation of Plants by Tensiometers," POCHVOVEDENIYE [Soil Science], No 1, 1974.

2. Muromtsev, N. A. ISPOL'ZOVANIYE TENZIOMETROV V GIDROFIZIKE POCHV. [Use of Tensiometers in Soil Hydrophysics], Leningrad, Gidrometeoizdat, 1979.

3. Sudnitsyn, I. I. DVIZHENIYE POCHVENNOY VLAGI I VLAGOPOTREBLENIYE RASTENIY [Movement of Soil Moisture and Moisture Consumption of Plants], Moscow, Izd-vo MGU, 1979.

4. Gardner, R. "Relation of Temperature to Moisture Tension of Soil," SOIL SCI., Vol 79, No 4, 1955.

5. Kedziora, A. "Wplyw Zmizn temperatury i wilgatnosci gleby na wartose potenejalu kapilarnego wody glebowei," PRZ. GLOXIZ, Vol 18, No 1-2, 1973.

6. Richter, J. "Zur Abhändingkeit des Bodenwassertessides von der Temperatur," Z. PFLANZENERNAHR UND BODONK, Vol 131, No 3, 1972.

7. Taylor, S. A. "Measurements Soil Water Potential," ARID ZONE RES., No 26, 1965.

UDC 551.509.313(-062.5)

ANALYSIS OF SYNOPTIC SCALE WAVE DISTURBANCES IN TROPEX-72 AND GATE

Moscow METEOROLOGIYA I GIDROLOGIYA in Russian No 5, May 81 pp 99-108

[Article by Professor Ye. M. Dobryshman, Candidate of Physical-Mathematical Sciences I. G. Sitnikov, Atmospheric Physics Institute, USSR Hydrometeorological Scientific Research Center, manuscript received 11 Nov 80]

[Text]

Abstract: An analysis is made of the characteristic features of the wave processes in the tropics by Soviet research data gathered on the TROPEX-72 and GATE expeditions. The methods of determining the wave disturbances are discussed, and a brief description of the results of their application is presented. Waves with previously known period (a day, half-day) are determined directly. Otherwise the periods are determined by the spectral density. Examples of long-period oscillations detected in GATE are indicated. An analysis of the quasibiannual zonal wind cycle is presented. Some characteristics of the tradewinds circulation are discussed.

One of the knotty problems of GATE was the problem of establishing the interrelation of processes at low latitudes with processes in the rest of the atmosphere. Therefore from the very beginning of the preparations for GATE in a number of the national programs, in particular, in the national program of the USSR, the problems of studying the large-scale processes in the tropics were considered as separate items. In addition to the general problematics, individual aspects of studying various circulation mechanisms were specified. Thus, one of the goals of the TROPEX-72 expedition was "... determination of the phase of the quasibiannual cyclicity of zonal flows in the equatorial atmosphere" [7, p 12], on the TROPEX-74 expedition one of the goals was "... estimation of the wave disturbance parameters in the GATE region and, in particular, in the intratropical convergence zone" [8, Vol 1, p 8], and so on.

The primary concern during the TROPEX expeditions and all of GATE was compilation of synoptic and aerological maps with maximum detail, the analysis of which was not only to confirm the results of the observation data processing at various points, but also to give impetus to subsequent analysis of the characteristic features of the processes in low latitudes. For these purposes the basic data are the atlases of synoptic and aerological maps [2] and the cloud photograph atlas [10].

Before proceeding with a description of the characteristic features of wave processes in the tropics, it is necessary to determine what is to be understood by disturbances (often identified with waves) in low latitudes and what the characteristics of these disturbances are. Usually, by a disturbance we mean an object of synoptic scale, that is, a scale of 1000 km detected against a background of a zonal pattern, in other words, disturbance of the zonal distribution of the corresponding meteorological element or parameter. Here the dimensions of the disturbance from west to east and from north to south approximately coincide. This understanding is unacceptable for the lowest latitudes: large-scale disturbances are anisotropic here, and they are sharply elongated in the zonal direction. The clearest example is the intratropical convergence zone (ICZ): its length is several thousands of kilometers with a width of a few hundred kilometers. (The structure of the ICZ is highly varied and closely related to the nature of the processes in the converging flows [9], that is, the processes occurring on different sides of the ICZ). The anisotropy of disturbances at low latitudes should not be forgotten, especially in cases where the characteristics of disturbances of light nature are compared with those for temperate latitudes.

As is known, GATE lasted 100 days; on 58 days of these 100 days (three phases) more frequent observations were made by special programs. The disturbances having more or less periodic nature, a period of T days, were manifested approximately $n \sim 100/T$ times. If T is several days, then n will be sufficient to talk confidently about the corresponding disturbance and its characteristics. For $T \sim 10$ to 30 days the confidence in the results will be low. Analogous arguments are properly applicable also to space data: the GATE region is elongated longitudinally, approximately 4000 km long; latitudinally it is 2500 km long. Disturbances more than 2000 km in size must be interpreted quite cautiously. This is especially true in that the African continent has a strong influence on the processes in the GATE region; the conditions in the Indian and Pacific Oceans are different. Therefore one of the next goals of studying the characteristic features of atmospheric movements in the tropics is a careful comparison of the results of GATE and the Monsoon experiments in order to discover common features and, primarily, differences of the processes in these regions.

1. Methods of Detecting Wave Disturbances

Characteristically, disturbances having a periodic nature can be divided into two groups. The first group includes those, the period of which is equal to the natural period determined by external factors: the diurnal and annual rotation of the earth. On the basis of the peculiarities of the equations of atmospheric dynamics, in a number of cases a semidiurnal period appears as the natural period. The second group includes waves propagated with defined phase velocities not connected with the mentioned natural periods. These phase velocities, that is to say, the periods are defined as eigenvalues of some operator describing the dynamics of the corresponding atmospheric processes. In the general case the operator is complex, and to facilitate analysis of the broad spectrum of wave movements in the atmosphere simplifications are introduced permitting isolation of waves generated by a defined mechanism: Rossby waves (the gyroscopic effect), gravitational waves (gravitational force), mixed Rossby-gravitational waves (the name itself defines their genesis), and so on.

Various principles are used as the basis for wave classification. The mentioned types of waves are defined by defined physical factors -- rotation of the earth, gravity, and so on. For analysis of the mechanism of atmospheric processes, the cause of the occurrence of certain types of waves plays a no less important role. The occurrence of waves frequently is connected with disturbance of the stability of some process. Three basic mechanisms of loss of stability of the zonal flow in the tropics are distinguished: a) barotropic and baroclinic instability, b) instability caused by the release of heat during cloud formation (for example, CISK), c) instability caused by the presence of heat sources in a flow that is nonuniform with respect to coordinates, especially with respect to z.

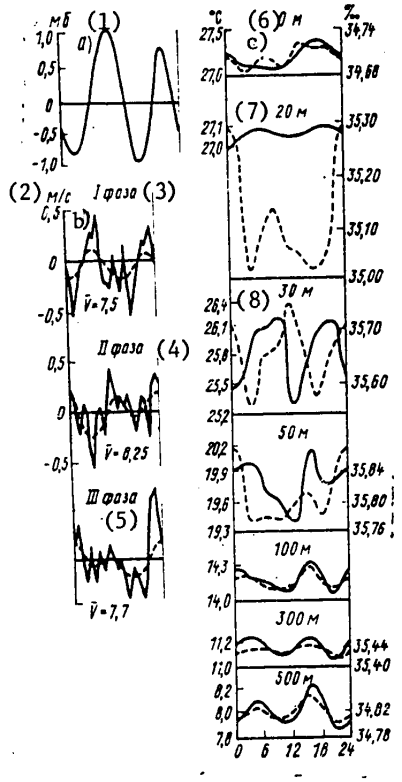

Figure 1. Diurnal behavior of meteorological elements.
a) pressure at sea level; b) modulus of the horizontal wind velocity in the tradewinds zone (the dotted line represents two harmonics of the Fourier series); c) temperature (solid curve) and salinity (dotted curve) on various levels according to the TROPEX-72 and TROPEX-74 data.

Key:

1. millibars
2. m/sec
3. phase I
4. phase II
5. phase III
6. 0 meters
7. 20 meters
8. 30 meters

This division is conditional for two reasons. First, it is not always possible clearly to isolate only one factor causing the generation of a wave, let us say, baroclinic instability (the velocity profile with respect to z or the horizontal temperature gradient). Secondly, other principles can be used as the basis for the classification, for example, the occurrence of disturbances as a result of orography, as a result of a sharp temperature gradient along the flow (land-sea), and so on.

Here, if the appearance of an almost periodic disturbance of the wave type is interpreted as a result of loss of stability of some (or several) mechanism, then the systematic appearance of disturbances must be interpreted as a stable process.

For detection of periodic processes basically two methods are used: 1) direct determination of the amplitude (and sometimes the phase) of the fluctuation of an entirely clear a priori known period (diurnal, annual, semidiurnal). 2) Obscure periods are defined by the application of the appropriate procedure based on using statistical characteristics of a sufficiently long series of observations. These methods are often combined -- the period (quasibiannual zonal wind cycle in the upper troposphere and lower stratosphere) is established approximately by empirical data, then the fluctuation parameters are determined on the basis of statistics. The most widespread method of discovering periodicities is the construction of a spectral density graph (directly or as the Fourier transformation of the correlation function); the peaks are interpreted as the presence of oscillation,with the corresponding frequency.

Oscillation with given frequency in the spectral function theoretically corresponds to a "spike" of the Dirac δ-function type. On the spectral density graph this is never obtained either on the basis of the limited volume of the initial data or because there is no "pure" oscillation with an exact period in nature. An auto-oscillatory mode with variable parameters can exist; the parameter variation alters the oscillation period. (Obviously, this is the situation with the quasibiannual cyclicity of the zonal wind and its three-five-day wave. The nature of these oscillations is still to a great extent unclear.) These facts -- limited nature of the sample and absence of a clear physical period -- lead to "blurring" of the peak on the spectral density graph. Frequently it is very difficult to estimate the effect of each of the factors separately; therefore conclusions about the presence of one clear period or another must be taken with a known degree of precaution.

When processing the data from the TROPEX-72 and TROPEX-74 expeditions and all of GATE, both methods of determining the characteristics of "purely" periodic and quasiperiodic fluctuations of the meteorological element fields were used.

2. Brief Description of the Results of Studying Wave Disturbances

a) Direct Determination of Characteristics (Diurnal and Semidiurnal Periods). According to the data from the stepped-up observations during the expeditions graphs were constructed of the diurnal behavior of in practice all the meteorological parameters. These parameters can be divided into three groups. The first group (Figure 1) includes those which are measured directly -- pressure, temperature, modulus of the horizontal wind velocity, and so on. The second group includes those which are obtained from observation data as a result of processing these data

(averaging, isolation of individual components, summation over defined time intervals) -- zonal and meridional wind velocity components, hourly precipitation totals, and so on (Figure 2). The third group (they are presented in Figure 3) includes parameters calculated by the equations of hydrodynamics. In all of the figures GMT time is used. In order to obtain local time, 2 hours must be subtracted.

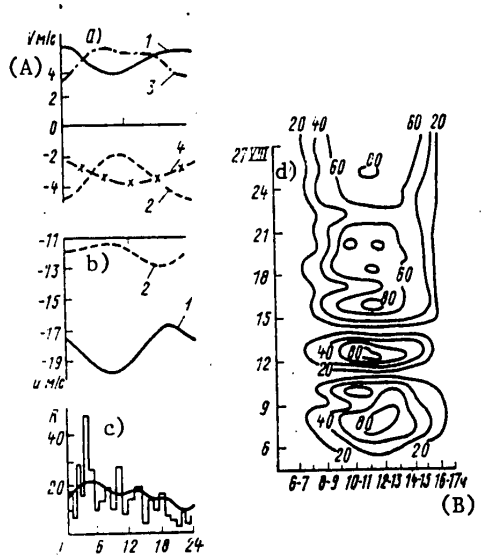

Figure 2. Diurnal behavior of meteorological elements.
a -- meridional component of the wind velocity (1 -- for a latitude of 12° on the 200 millibar level, 2 -- for a latitude of 5° on the 200 millibar level, 3 -- for a latitude of 12° at sea level, 4 -- for a latitude of 5° at sea level); b) zonal component of the wind velocity (1 -- on a ship located at 6.5° north, 20° west; 2 -- on a ship located at 6.5° north, 27° west); c) diurnal behavior of the amount of precipitation in the convergence zone 7°30' north, 20°50' west, the hourly totals were obtained for the averaging period of 10-25 July and 6-21 August 1974. The smooth curve is a representation by three harmonics; d) the hourly sums of the total radiation in the synoptic test area 6-27 August 1974 (cal/cm^2). If vertical sections are taken, then a wave with a period of 3 to 5 days is clearly manifested. The wave amplitude will be low during the morning and evening hours and comparatively high at midday.

Key:
A. V, m/sec
B. hours

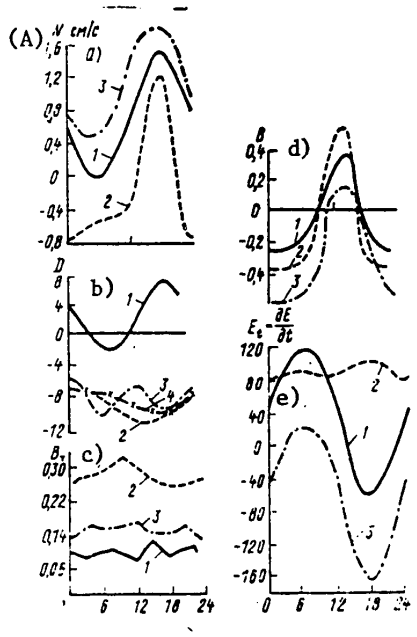

Figure 3. Diurnal behavior of the vertical component of the wind velocity at the 400 mb level (1 -- phase I, 2 -- phase II, 3 -- phase III) (a); diurnal behavior of the divergence (10^6 sec^{-1}) (1 -- on the 200 mb level; 2, 3, 4 -- at sea level for phases I, II and III, respectively) (b); diurnal behavior of turbulent heat exchange (cal/cm^2-min)) at different latitudes (1 -- 10° north, 2 -- 7.5° north, 3 -- 5° north) (c); diurnal behavior of the ocean-atmosphere heat exchange (cal/(cm^2-min)) (1 -- phase I, 2 -- phase II, 3 -- phase III) (d) and diurnal behavior of the energy variation as a result of large-scale movements in phase I in the test area A-B (1 -- in the 1000-200 mb layer, 2 -- in the 1000-700 mb layer, 3 -- in the 700-200 mb layer).

Key:

A. W, cm/sec

Analysis of the diurnal behavior demonstrates the presence of a close relation between the meteorological parameters, which makes it possible more precisely to define the measurement procedure and the procedure for calculating various values and the construction of theoretical models of the circulation mechanism at low latitudes. As an illustration it is possible to present the following fact. The diurnal behavior of precipitation in the vicinity of cloud accumulations has two peaks: during morning hours (0700 to 1200 hours) and evening hours (1900 to 2400 hours); here the morning peak is more intense than the evening peak. On the graph of the diurnal behavior of the divergence (calculated for phase II of GATE) at 1000 and 2200 hours (local time) there is a maximum divergence at sea level.

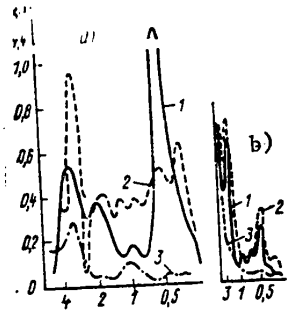

Figure 4. Meteorological element spectra.
a -- Spectra of the measured parameters (1 -- ground pressure (peak in the semidiurnal period region is shown in a different scale as a separate peak), 2 -- wind velocity modulus averaged by the data from three ships located at 7.5° latitude; 3 -- temperature fields); b) -- spectra of the zonal (1) and meridional (2) components of the current velocity and temperature (3) at a depth of 500 meters.

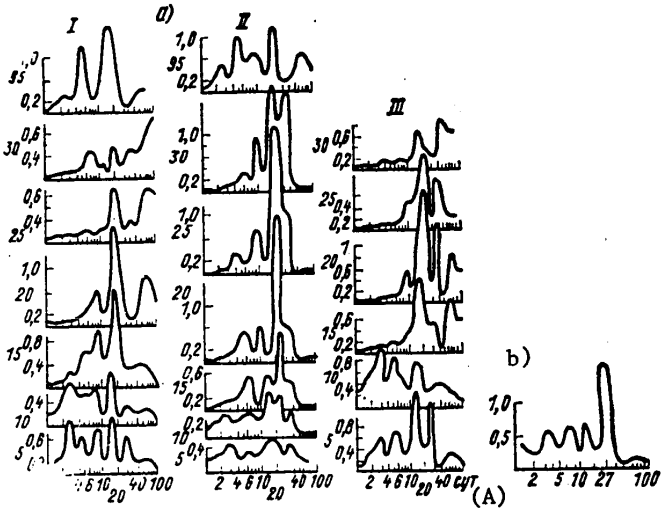

Figure 5. Spectra of the zonal (I) and meridional (II) components of the wind velocity and temperature (III) at different altitudes in the atmosphere (the altitudes are indicated in kilometers on the left) (a) and geomagnetic index spectrum (b)

Key:
A. days

b) Discovery of Periodic Spectral Density Components. The construction of the spectra for different paramenters was started immediately on completion of the TROPEX-72 reconnaissance expedition using data obtained from 11 to 25 July 1972, in the mesometeorological test area (the "Cross" formed by five ships at the following points: 4°56' north, 23°53' west; 9°34' north, 23°39' west; 7°37' north, 18°35' west; 7°31', 23°22' west; 7°19' north, 20°52'). Then the previously constructed spectra were more precisely defined during GATE, and the spectra of other meteorological parameters were determined. As usual, the spectra were constructed in the coordinates $fS(f)/\sigma^2$, ln f (f is frequency, S/σ^2 is the spectral density reduced to the total dispersion (σ^2)). In addition to "compactness" of the graph, in these coordinates the area under the spectral density curve is proportional to the proportion of the dispersion which means it characterizes the proportion of the energy reduced to the corresponding frequency interval.

Figure 4 shows the pressure, air temperature, ocean surface temperature spectra, and the wind velocity modulus. (The periods are indicated in days on the x-axis in all figures where the spectra are presented).

Since one of the key problems of GATE was to study the interaction of the ocean and atmosphere, spectra were constructed for different hydrophysical parameters measured during GATE. Figure 4b shows examples of the spectra of the horizontal components of the current velocity at a depth of 500 meters. The semidiurnal wave in the velocity field is expressed very clearly, more clearly than the diurnal wave; in the temperature field these periods are expressed very weakly.

Figure 5 shows the spectra of different values in the atmosphere.

Attention is attracted by the peak near 4 to 5 days detected in practice on the graphs of the spectral functions of all the parameters, including those not purely meteorological such as, for example, the geomagnetic index (the local characteristic of the magnetic field disturbance). If the 4-day waves in the wind, pressure, temperature and precipitation fields are interpreted as the result of loss of stability of the zonal flow, then why is the geomagnetic index here? Obviously, we are dealing with something more complicated: the 4-day oscillation probably reflects the internal autooscillatory mode characteristic of the atmosphere (and ocean) at low latitudes. If this is so, then it is necessary to obtain it theoretically from the general equations of hydrodynamics, possibly using "magnetic" interactions. How this is done is still unclear. On this level further careful processing of the empirical data for longer time intervals appears to be quite necessary. Perhaps, it will permit clarification of the general mechanism of the autooscillatory mode and formulation of the problem of theoretical research more clearly.

It is also necessary to note that the maximum in the vicinity of T=30 days correlates well with the 27-day zonal circulation index and that the maximum corresponding to 15-16 days is traced at all altitudes to 95 km.

Inasmuch as the 4-day period appears in each element, it must also appear on the mutual spectrum graphs. This is obviously confirmed in Figure 6 in which examples of the mutual spectra of different meteorological parameters are presented.

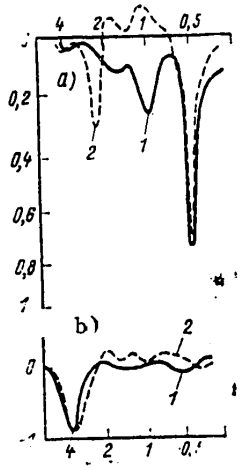

Figure 6. Mutual spectra of meteorological parameters in the layer next to the water.
a -- according to TROPEX-72 data (1 -- precipitation and air temperature, 2 -- sea surface and air temperatures); b) according to TROPEX-74 data (1 -- meridional and zonal wind velocity components, 2 -- meridional wind velocity and air temperature).

c) Approximate Determination of the Characteristics of Long-Period Disturbances. Fluctuations with a period of 7 to 8 days or more cannot in practice be detected by objective methods for a series length of 100 days. Nevertheless, in a number of cases they were observed quite clearly. Let us present three examples. During GATE, especially during phase II (28 July to 16 August), variations in the wind direction from ESE to NE and back with a period of 7-8 days were regularly observed at altitudes of 6-10 km. Possibly, this is a consequence of the passage of inertial gravitational waves with a basic period of 3-4 days. Figure 7a shows graphs of the behavior of the mean diurnal water temperature at various levels. At depths of 50-100 meters a periodicity of 7-8 days is clearly traced. Figure 7b illustrates the time behavior of the latitudinal component at the 75-meter level. A monthly rhythm is to be seen.

It is highly necessary to accumulate a long series so that spectral analysis methods can be accurately applied.

d) Determination of the Phase of the Quasibiannual Zonal Wind Cycle. The study of the quasibiannual cycle requires a special procedural approach. Therefore let us briefly describe the procedure for determining the parameters of this cycle.

Figure 8 shows the mean monthly zonal wind velocities at different altitudes according to the data from several stations located at low latitudes. The periodicity is clearly visible, but one harmonic is inadequate for description of it. The curves can be considered as a realization of a complex random process consisting of periodic components U(t) and noise x(t). The periodic components are "useful" signals.

$$U(t) = \sum_{m=1}^{N} \sum_{k=1}^{K} \left(a_{mk} \cos k \frac{2\pi}{t_m} t + \right.$$

$$\left. + b_{mk} \sin k \frac{2\pi}{t_m} t \right), \qquad (*)$$

where t_m are the basic periods (which can be incompatible with each other);

a_{mk}, b_{mk} are the coefficients of the Fourier expansion in a series with respect to these harmonics.

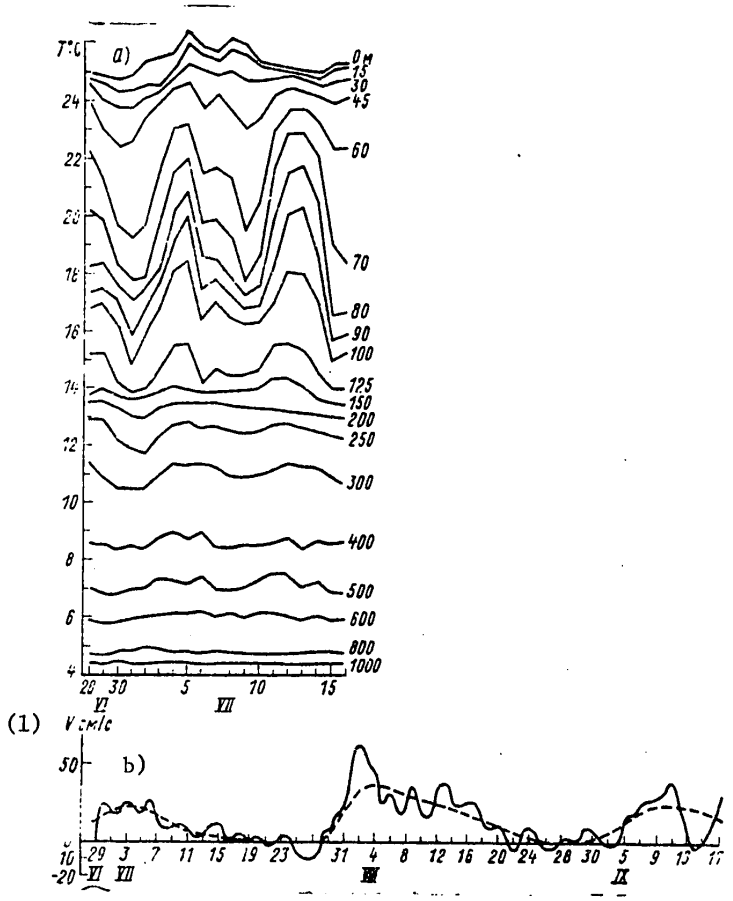

Figure 7. Time behavior of the mean diurnal water temperature at different depths during phase I of GATE (a) the zonal component of the current velocity at a depth of 75 meters (b)

Key:
1. V, cm/sec

The spectral density was calculated by the formula

$$S(k) = \frac{B(0)}{\tau_{max}} + \frac{2}{\tau_{max}} \sum_{q=1}^{\tau_{max}-1} \times$$

$$\times B(q) \cos \frac{2\pi}{\tau} kq + (-1)^k \frac{B(\tau_{max})}{\tau_{max}},$$

where

$$B(\tau) = \frac{1}{N} \sum_{\tau=1}^{N-\tau} u'(t)\, u'(t+\tau)$$

is the correlation function. (It is more correct to insert the factor $1/(n-\tau)$, and not $1/N$ in front of the summation sign. In this case the estimate of B will be unbiased and consistent. However, first, in this case $B(\tau)$ decreases more slowly than the true correlation function; secondly, the presence of τ in the denominator creates additional difficulties when calculating the spectral function as cos-Fourier transformation of the correlation function),

τ_{max} is the maximum value of τ up to which it is possible to consider the values of the correlation function reliable. Usually τ_{max} is determined empirically until the correlation function begins to shake "sharply,"

$t_m = \frac{2\tau_{max}}{m} \Delta t$ is the period; Δt=1 month.

For smoothing, a "hanning" (sic) filter was used:

$$a_N(k) =$$

$$= \begin{cases} \frac{1}{2}\left(1 + \cos \frac{\pi k}{\tau_{max}}\right) & \text{for } k \leqslant \tau_{max}, \\ 0 & \text{for } k > \tau_{max}. \end{cases}$$

Figure 9 shows the correlation functions for $U(\tau)$ and noise. The noise is the difference between $u(\tau)$ and the sum of the oscillations eliminating the greater part of the dispersion. The results of calculating the most probable oscillations for certain points are reduced to a table where the following notation is used: U_0 is the mean value of u; σ_0^2 is the dispersion of the deviations u' in m^2/sec^2; $\sigma_1^2(t_m)$ is the dispersion of the value of $u-U(\tau)$ corresponding to an oscillation with period t_m; $D(t_m) = (\sigma_1^2/\sigma_0^2)100\%$ is the proportion of the decrease in the dispersion as a result of oscillation with a period of t_m; $A(t_m)$ is the oscillation amplitude of the period t_m in m/sec.

From the table it is clearly obvious that U_0 increases with altitude, that is, the east wind becomes stronger; at 9° latitude the energy of the annual oscillation in practice is equal to the energy of the 28-month oscillation; at a latitude of $\pm$18° the quasibiannual cycle is almost not felt at all; only the annual behavior is clearly manifested; at the equator oscillations with periods of 26-27-28 months take in practice the same proportion of the energy (the calculations demonstrated that for t_m=25 months and t_m=29 months the "drawoff" of energy decreases sharply, by 2-2.5 times).

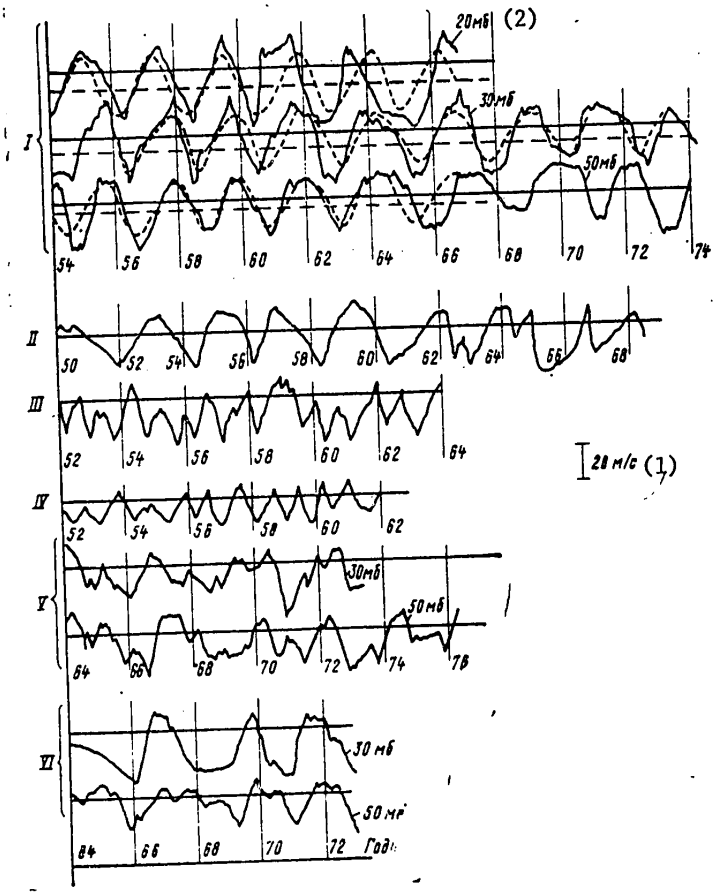

Figure 8. Time behavior of the zonal component of the wind velocity (mean monthly values) for stations located at low latitudes.
I -- Canton Island (≈3° south latitude), 1954-1967, Gan Island (≈2° south latitude), 1964-1974; II -- Howard (≈9° north latitude); III -- Kingston (≈18° north latitude); IV -- Nandi (≈18° south latitude); V -- Trivandrum (≈8° north latitude); VI -- Voznesenіya Island (≈ 8° south latitude).

Key:
1. 20 m/sec
2. millibars

In Figure 8 the dotted line shows the results of representation of the initial data by several terms of a series of the type (*). For example, let us present the formula for u on the 20 mb surface at Canton station:

$$u = -7{,}7 - 13{,}1\cos\frac{2\pi}{27}t - 12{,}2\sin\frac{2\pi}{27}t - 2{,}9\cos\frac{2\pi}{8}t - 1{,}7\sin\frac{2\pi}{8}t.$$

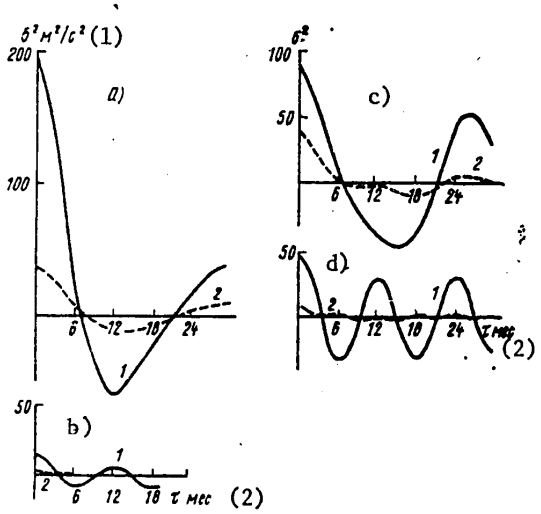

Figure 9. Correlation functions for U(τ) (1) and "noise" (2).
a -- Canton, b -- Nandi, c -- Howard, d -- Kingston

Key:
1. m^2/sec^2
2. τ, months

Of course, the sample volume is insufficient and obviously there is no mechanism realizing an oscillation with an exact period of 26, 27 or 28 months. However, the fact that for this spectral interval there is a clear peak should not raise any doubt. Within the limits of accuracy of the measurements and reliability or the numerical characteristics obtained it is reasonable to assume that the amplitudes of the annual and quasibiannual cycle are equal at latitudes of 6-10°. It is also difficult to consider that it is a random fact that for all three probabilities (50, 30, 20 mb) a period of 27 months turned out to be the most probable. Since the quasibiannual cycle is traced over the entire equatorial zone, this means that this is a manifestation of the global-scale circulation mechanism which can hardly exist independently of other elements of the GAC [general atmospheric circulation]. Therefore, it was important to determine and more precisely define the phases of the quasibiannual cycle during the TROPEX-72 and TROPEX-74 expeditions. A careful analysis of the field u in the upper troposphere and lower stratosphere demonstrated that "... westerly flows of the western phase of the quasibiannual cycle with maximum velocity of about 20 m/sec at 2° south latitude were observed in the 18.5-20.8 km layer. In the 20.8-34.5 km layer there were easterly currents of the

Some Characteristics of Oscillations of the Zonal Component of the Wind Velocity in the Stratosphere

Observation point, coordinates	Parameter	Surface, mb 50	30	20	Observation point, coordinates	Parameter	Surface, mb 50	30	20
Canton (island) 2°46′ S 171°43′W	U_0	−2	−6	−8	Kingston, 17°56′ N, 76°47′ W	U_0	−8		
	σ_0^2	187	298	300		σ_0^2	48		
	σ_1^2 (27)	79	134	143		σ_1^2 (28)	3		
	D (27)	42	55	52		D (28)	9,4		
	A (27)	14.9	18,5	17.9		A (28)	2,1		
						σ_1^2 (12)	37		
						D (12)	77		
						A (12)	8,6		
Howard, 8°56′ N, 79°34′ W	U_0	−2			Nandi, 17°45′ S, 177°27′E	U_0	−5		
	σ_0^2	91				σ_0^2	15		
	σ_1^2 (28)	42				σ_1^2 (26)	2,8		
	D (28)	47				D (26)	19		
	A (28)	9,3				A (26)	1,8		
	σ_1^2 (12)	9,0				σ_1^2 (12)	11,7		
	D (12)	10,0				D (12)	78		
	A (12)	3,0				A (12)	4,8		

quasibiannual cycle with maximum velocities of 40 and 42 m/sec at the 32 and 28 km levels in the vicinity of 7.5° north latitude and 4.5° north latitude, respectively. In the 34.5-38.0 km layer, westerly currents of the new phase of the quasibiannual cycle were noted, which were replaced by easterly currents above 38.0 km. In July and August the westerly phase in the lower stratosphere deteriorated, and only the easterly currents remained in the layer from 18 to 34 km. The rates of descent of the boundaries of the westerly and easterly winds of the quasibiannual cycle are close to normal [7, p 36]. A similar picture was also observed in the summer of 1974: easterly winds in the upper troposphere and lower stratosphere were expressed quite clearly within the boundaries of latitudes 5-12°.

3. Some Characteristics of Tradewinds Circulation

The tradewinds circulation is one of the main elements of the GAC manifested at low latitudes. A detailed analysis of the aerological material obtained during the TROPEX-72 expedition made it possible significantly more precisely to define the structure of the tradewinds circulation both vertically and horizontally. It is especially necessary to note the following facts. In the tradewinds zone in the 600-500 mb layer, a temperature inversion is observed which is called the second tradewinds inversion. This fact is extraordinarily important, for it determines the layered moisture distribution: under the first and second tradewinds inversions are layers close to saturation, and the relatively dry layers are above the inversions.

Calculation of the magnitude of the wind divergence also demonstrated a layered structure -- the presence of two divergence layers immediately under the inversion layers and two convergence layers above these layers. This determines the labile energy and latent heat transport downward -- to the subinversion layers. The materials of the TROPEX-74 expedition fully confirmed the existence of three blocking layers -- two clear inversions and a layer close to isothermy. It turned out that the second tradewinds inversion and the third blocking layer are propagated quite far; they are traced to 15° north latitude and 50° west longitude.

It is characteristic that on approaching the axis of the ICZ, the recurrence rate, intensity and thickness of all three blocking layers decrease. These blocking layers are connected with the general circulation mechanism of tropical latitudes.

The fact that the altitude spectra of the lower boundary of the first tradewinds blocking layer have sharp peaks in the region of diurnal, two-day and 4-5-day periods (Figure 10) speaks in favor of this statement.

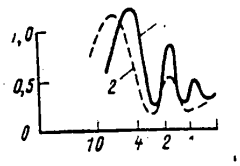

Figure 10. Altitude spectrum of the lower boundary of the first (1) and second (2) tradewinds inversions

Thus, the study of wave disturbances of a synoptic scale during GATE demonstrated a close interrelation of the different mechanisms (tradewinds circulation, ICZ, quasiregular wave movements with a period of a few days, quasibiannual cycle) and the necessity for further study -- complex and comprehensive -- of each of these mechanisms.

BIBLIOGRAPHY

1. Dobryshman, Ye. M. "Wave Motions and the Equatorial Belt (Zonal Model)," METEOROLOGIYA I GIDROLOGIYA [Meteorology and Hydrology], No 1, 1977.

2. KARTY POGODY ATLANTICHESKOGO TROPICHESKOGO EKSPERIMENTA ATEP [Weather Maps of the Atlantic Tropical Experiment GATE], edited by B. S. Chuchkalov, Nos I, II, III, Obninsk, 1977.

3. Lysenko, I. A.; Petrosyants, M. A.; Portnyagin, Yu. I.; Svetogorova, L. V. "Periodic Variations of the Wind Velocity in the Lower Thermosphere, Stratosphere and Troposphere in the Winter," METEOROLOGIYA I GIDROLOGIYA, No 10, 1974.

4. Petrosyants, M. A.; Snitkovskiy, A. I.; Fal'kovich, A. I. "Air Circulation in the Intratropical Convergence Zone," METEOROLOGIYA I GIDROLOGIYA, No 5, 1977.

5. REZUL'TATY METEOROLOGICHESKIKH ISSLEDOVANIY PO MEZHDUNARODNOY PROGRAMME TROPEKS [Results of Meteorological Studies under the International TROPEX Program], edited by V. S. Samoylenko, Moscow, Institut okeanografii AN SSSR, 1975.

6. Sitnikov, I. G. "Problem of Scale Analysis of the Equations of the Dynamics of the Tropical Atmosphere," TRUDY GIDROMETTSENTRA SSSR [Works of the USSR Hydrometeorological Center], No 197, 1977.

7. TROPEKS-72. TRUDY MEZHDUVEDOMSTVENNOY GEOFIZICHESKOY EKSPEDITSII PO PROGRAMME NATSIONAL'NOGO ATLANTICHESKOGO TROPICHESKOGO EKSPERIMENTA [TROPEX-72. Works of the Interdepartmental Geophysics Expedition under the National Atlantic Tropic Experiment Program], edited by M. A. Petrosyants, et al., Leningrad, Gidrometeoizdat, 1974.

8. TROPEKS-74. TRUDY MEZHDUVEDOMSTVENNOY EKSPEDITSII PO PROGRAMME MEZHDUIARODNOGO ATLANTICHESKOGO TROPICHESKOGO EKSPERIMENTA. T. I. ATMOSFERA [TROPEX-74. Works of the Interdepartmental Expeditions under the International Atlantic Tropical Experiment Program. Vol I. Atmosphere], edited by M. A. Petrosyants, et al., Vol II, OKEAN [Ocean], edited by V. A. Burkov, A. A. Rybnikov, Leningrad, Gidrometeoizdat, 1976.

9. Fal'kovich, A. I. DINAMIKA I ENERGETIKA VNUTRITROPICHESKOY ZONY KONVERGENTSII [Dynamics and Energetics of the Intratropical Convergence Zone], Leningrad, Gidrometeoizdat, 1979.

10. GATE REPORT NO 17. REPORT ON THE FIELD PHASE OF THE GARP ATLANTIC TROPICAL EXPERIMENT. METEOROLOGICAL ATLAS. ICSU & WMO, Geneva, 1975.

UDC 551.557:621.396.96

INFORMATIVENESS OF METEOR RADAR USED TO MEASURE THE WIND IN THE UPPER ATMOSPHERE

Moscow METEOROLOGIYA I GIDROLOGIYA in Russian No 5, May 81 pp 109-114

[Article by A. A. Gavrilov, Institute of Experimental Meteorology, manuscript received 8 Jul 80]

[Text]

Abstract: A study is made of the problem of the informativeness of meteor radar (MRLS) used to measure the wind in the upper atmosphere. An algorithm is proposed for evaluating the informativeness of the MRLS radar. An informativeness calculation was performed for specific primary data processing algorithms used on the radar measurements of the drift velocities of meteor trails. It was demonstrated that the most informative for investigation of the mean hourly wind velocity components out of the investigated four primary processing algorithms are the reference frequency transport method and the phase variation rate $d\phi/dt$ measurement method. The informativeness of the phase-time method and the method with fourfold multiplication of the frequency of the received and the reference signals depends on the measured mean values of the wind velocity and decreases with a decrease in them.

The radiometric method of determining the wind velocity is one of the simplest and most convenient. According to the data of [8, 12], radiometeor studies of wind conditions in the lower thermosphere are performed at more than 30 observation stations.

Unfortunately, the use of the results of wind measurements obtained in the MRLS network for meteorological purposes presents defined difficulties inasmuch as up to now no criterion has been proposed for comparing the reliability of the radiometeor measurement data for the wind velocity at the various observation points, and the estimates which have been encountered in the literature [8, 11] are for the most part of a subjective nature.

The development of quantitative criteria for comparing the wind velocity radiometeor measurement data and estimation of the informativeness of the MRLS used to measure the wind in the upper atmosphere are the purpose of this paper.

For selection of the quantitative criterion let us consider the method of processing the meteor trail drift rate measurement results. The basis for the majority of the procedures [8] is harmonic or spectral analysis of the wind velocities V(t) averaged for a defined time interval Δt. The choice of the corresponding averaging interval requires a compromise solution with respect to the random error and bias error.

According to [2], the bias error ΔV_1 of the function V(t) for the averaging interval Δt

$$\Delta V_1 = \frac{\Delta t^2}{24} V''(t). \tag{1}$$

where V"(t) is the second derivative of the velocity, and the random error for the same averaging interval

$$\Delta V_2 = \sqrt{D_{\bar{V}}} = \sqrt{\frac{D_V}{N}}, \tag{2}$$

where $D_{\bar{V}}$ is the sample dispersion,

D_V is the dispersion,

N is the size of the sample.

Traditionally, Δt=0.5 to 1 hour is taken as the averaging interval in the existing procedures.

From (1) when $V=V_0 \sin(\omega_2 t+\phi_2)$, $V_0 \sim 40$ m/sec, $\omega_2=2\pi \cdot 2/T$, T=24 hr, we obtain ΔV_1=0.5 m/sec. For equipment of average sensitivity, for Δt=1 hr the sample size $N \sim 100$, and according to (2) for $D_V=900$ m^2/sec^2 we obtain $\Delta V_2 \sim 3$ m/sec.

The sample mean velocity is calculated for the interval Δt

$$\bar{V} = \frac{\sum_i V_i}{N}, \tag{3}$$

the dispersion

$$D_V = \frac{\sum_i (V_i - \bar{V})^2}{N} \tag{4}$$

and considering (4) by formula (2), the sample dispersion.

According to (2) $D_{\bar{V}}$ depends both on the dispersion of the argument D_V and on the sample size N. Therefore it is reasonable to take the sample mean $\bar{V}$ as the basic unit of comparison of the measurement results obtained at the different stations.

In probability theory [10] in order to estimate the measure of indeterminacy of the random variable x, the concept of entropy H(x) and also the concept of information I_x connected with it are introduced,

$$I_x = H_1(x) - H_2(x), \tag{5}$$

where $H_1(x)$ is the entropy of the system before obtaining the information;

$H_2(x)$ is the entropy of the system after obtaining the information.

Using (2), (5), and considering that the distribution of the wind velocity components for the meteor zone over the course of an hour of observation is subject to a normal law [9], for the quantity of information about the value $\overline{V}$ we obtain:

$$I_{\overline{V}} = \log \overline{\left[\frac{P_2(\overline{V})}{P_1(\overline{V})}\right]}, \tag{6}$$

where $P_1(\overline{V})$ is the a priori distribution density $\overline{V}$ with dispersion D_1 caused by the random structure of the wind field in the lower thermosphere;

$P_2(\overline{V})$ is the aposteriori distribution density with the dispersion $D/N=(D_1+D_2)/N$;

D_2 is the dispersion introduced by the measuring system.

For calculation of the dispersion $D=D_1+D_2$ let us use the formula obtained in [3] for dispersion of the horizontal component of the wind velocity D_r,

$$D = D_r = (D_1 + D_\varphi \overline{V}_y^2 + \Delta u^2 D_h) + 1{,}3 D_R, \tag{7}$$

where D_φ is the dispersion of the distribution of the azimuth of the reflecting points of the meteor trails;

$\overline{V}_y^2$ is the mean value of the square of the orthogonal component of the wind velocity;

Δu is the vertical gradient of the horizontal component of the wind velocity;

D_h is the altitude distribution dispersion of the reflecting points;

D_R is the dispersion caused by the algorithms used to determine the doppler frequency shift.

An estimate was made of the first term of the righthand side of (7) in [13]. In the above-referenced paper [3], the contribution of the second and third terms of the righthand side of (7) to the dispersion of the horizontal component of the wind velocity D_r was estimated. In order to estimate the contribution of the fourth term of the righthand side of (7) to the dispersion D_r let us write the formulas for calculating the radial wind velocity component V_R and the dispersion for the most widely used algorithms for determining the doppler frequency shifts [5, 8]:

$$V_R = \frac{\lambda}{2T}, \quad D_R = \frac{c_1 \lambda^2}{q^2 T^2} \tag{8}$$

for the time-phase method;

$$V_R = \frac{\lambda}{2KT}, \quad D_R = \frac{c_2 \lambda^2}{K^2 T^2 q^2} \tag{9}$$

for the time-phase method with frequency multiplication;

$$V_R = \frac{\lambda}{2}\left(\frac{1}{T} - \frac{1}{T_0}\right), \qquad D_R = \frac{c_3 \lambda^2}{T^2 q^2} \tag{10}$$

for the method of reference frequency transport or the "Stanford" method;

$$V_R = \frac{\lambda}{2 \cdot 2\pi \sqrt{2(n-1)}} \sum_i \frac{\Delta\varphi}{\Delta T}, \qquad D_R = \frac{c_4 \lambda}{(n-1)^2 \Delta T^2} \sum_i \frac{1}{q(t_i)} \tag{11}$$

for the method of measuring the phase variation rate $d\phi/dt$; the linear approximation algorithm (LAA).

Here λ is the MRLS wavelength,

T is the doppler period,

K is the frequency multiplication factor,

c_i is a constant,

T_0 is the shift period,

$q=A/s$ is the relative amplitude of the signal,

A is the amplitude of the signal,

S is the noise amplitude,

t is the radio echo duration,

ΔT is the pulse following period,

n is the number of pulses, $\Delta\phi_n=\phi_n-\phi_{n-1}$,

ϕ_n is the discrete value of the phase.

Averaging D_R in (8) with respect to all values of T and q and considering that T and q are independent, we obtain

$$D_R = \int\int D_R(T, q) P(T) P(q) \, dT \, dq. \tag{12}$$

Here P(T), P(q) are simple distribution densities.

Using the formula obtained in [1, 14] for the amplitude distribution density of the meteor radio echo, for the distribution function of the relative amplitudes we obtain the following expression:

$$P(q) \approx q^{-2}. \tag{13}$$

Considering that the distribution of the wind velocity components for the meteor zone in an hour of observation is subject to a normal law, using (8), we obtain the following expression for the distribution density P(T)

$$P(T) = \frac{\lambda}{\sqrt{2\pi D_1}} \exp \frac{\bar{V}^2}{2D_1} \exp - \frac{\lambda^2}{8 D_1 T^2} ch \frac{\bar{V}\lambda}{2T D_1}. \tag{14}$$

As was demonstrated by Manning [15], for measurements by the radar method the "noticeableness" of the slow and fast drifts of the meteor trails is different. Considering the known dependence of the duration of the radio echo t on the relative amplitude of the signal q: $t=\tau \ln(q/q_0)$, where q_0 is the threshold signal/noise ratio with respect to voltage, let us proceed in (13) from the distribution of the relative amplitudes P(q) to the distribution of the durations of the meteor radio echo P(t):

$$P(t) = \frac{1}{\tau_a} \exp - \frac{t}{\tau}. \tag{15}$$

where $\tau=\lambda^2 D_a/16\pi^2$ is the decay constant for an unpacked trail;

D_a is the ambipolar diffusion coefficient.

Integrating (15) from T to ∞, we obtain F(T) -- the selectivity function of the equipment for various drift velocities

$$F(T) = \exp - \frac{T}{\tau}. \tag{16}$$

An experimental function F(T) was obtained in [4].

The experimental function and the function calculated by (16) agreed satisfactorily for $\tau=0.25$ second.

Substituting values of P(T), F(T), P(q) in (12) we obtain

$$D_R = \frac{B_1(\bar{V}, \tau, D_1)}{q_0^3}. \tag{17}$$

Performing analogous calculations for other methods of determining the doppler frequency shift, we obtain the expression for the dispersion $(D_R)_i$

$$(D_R)_i = \frac{B_i}{q_0^3}. \tag{18}$$

Here the coefficients B_i characterize the accuracy of each of the methods. For a sample size N_i for each of the methods used to determine the doppler frequency shift considering (13), (14), (16), we obtain the following expression:

$$N_i = \int_T \int_q P(T)\,P(q)\,F(T)\,dT\,dq = \frac{N_{ш}(1)}{q_0\,A_i}, \tag{19}$$

Key: 1. noise

where the coefficient A_i reflects the variation of the "noticeability" of the radio echo responsible for the drift.

N_{noise} is the number of cases of radio echo on the noise level $q_0=1$.

Substituting values of D_r, D_R. N from (18), (19) and (7) in (6), for the informativeness $I_{\overline{V}}$ we obtain the following expression:

$$I^i_{\overline{V}} = \log \sqrt{\frac{N_{ш}\,A_i\,D_1}{\frac{1{,}3\,B_i}{q_0} + q_0\,(D_1 + D_в\,\overline{V}_y^2 + \Delta u^2\,D_h)}}, \tag{20}$$

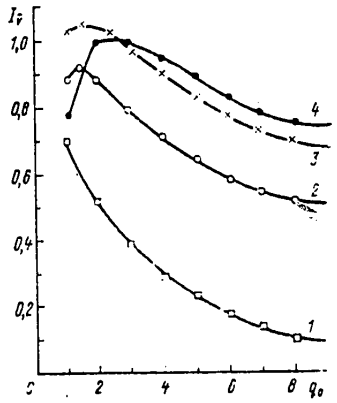

Informativeness $I_{\overline{V}}$ as a function of the threshold amplitude q_0 for the time-phase method (1), the time-phase method with fourfold frequency multiplication (2), the "Stanford" method (3) and the $d\phi/dt$ measurement method (4)

In the figure the relation calculated by (20) for the informativeness $I^i_{\overline{V}}$ in relative units is presented as a function of the threshold value of q_0 for $\overline{V}$=5 m/sec, D_1=400 m^2/sec^2, Δu=0, τ=0.25 sec for four radiometeor data processing algorithms for the drift rates.

As follows from the figure, for all the processing algorithms the curve for the informativeness $I_{\overline{V}}$ as a function of q_0 is characterized by the presence of one peak for small values of q_0 and quite slow decrease in $I_{\overline{V}}$ with an increase in q_0.

The maximum value of I_{AS}^{V} is reached when the denominator in (20) approaches the minimum. From the condition of the minimum of the denominator it is possible to find the optimal value of the relative threshold q_0. The values of q_0 that are optimal for several values of the wind velocity distribution parameters and two values of the decay constant of the meteor radio echo amplitudes are presented in Table 1. For example, for the method of measuring $d\phi/dt$, the value of q_0 of the optimal relative threshold varies within the limits of 1.23 to 2.4, which differs significantly from the value of $q_c=5.9$ presented in [6, 7].

For the same parameters for a value of $q_0=2$ according to (20), the informativeness I_{AS}^{V} was calculated. The values of I_{AS}^{V} in relative units are presented in Table 2. It is obvious from this table, the most informative are the "Stanford" method and the method of measuring $d\phi/dt$. The informativeness of the time-phase method and the methods of frequency multiplication depends on the measured mean values of the wind velocity and decreases with a decrease in them.

Table 1

Processing algorithm	D_1, m^2/sec^2			
	400	1600	400	1600
	Radio echo with τ=0.25 sec		Radio echo with τ=0.125 sec	
Measurement of $d\phi/dt$ (LAA)	1.94	1.23	2.4	1.49
"Stanford" f_0=40 hertz	1.49	<1	1.5	<1
Time-phase	<1	<1	<1	<1
Time-phase with frequency multiplication K=4	1.36	<1	1.38	<1

Table 2

Processing algorithm	$\bar{V}$, m/sec	D_1, m^2/sec^2			
		400	1600	400	1600
		Radio echo with τ=0.25 sec		Radio echo with τ=0.125 sec	
Measurement of $d\phi/dt$ (LAA)	-	1.0	1.06	0.93	1.05
"Stanford"	5	1.02	1.06	1.0	1.04
f_0=40 hertz	50	1.02	1.06	1.0	1.05
Time-phase with	5	0.89	1.01	0.82	0.96
frequency multiplication	50	1.02	1.04	1.0	1.01
K=4					
Time-phase	5	0.65	0.83	0.48	0.73
	50	0.96	0.94	0.87	0.87

Table 3

D_1, m^2/sec^2	Processing algorithm			
	Measurement of $d\phi/dt$ (LAA)	"Stanford" f_0=40 hertz	Time-phase with multiplication K=4	Time-phase
	$D_{procedural}/D_{experimental}$ %			
400	54	31	28	18
1600	31	21	20	17

Using (7), it is also possible to estimate the contribution of the horizontal component D_r to the dispersion as a result of procedural factors. The results of the calculation by (7) for $\Delta u=0$ are presented in Table 3. In this table the value of $D_{procedural}/D_{experimental}$ reflects the contribution resulting from procedural factors to the experimentally determined dispersion.

From the data in Tables 1, 2, 3 and the figure it is possible to draw the following conclusions:

1) For defined mean values of the wind velocity it is preferable to use the "Stanford" method and the method of measuring $d\phi/dt$.

2) For determination of the wind velocity dispersion it is preferable to use the time-phase method of determining the doppler frequency shifts.

In conclusion, it must be noted that the proposed method of estimating the informativeness is being introduced into scientific research practice at the Institute of Experimental Meteorology. The developed algorithm for calculating the quantity of information about the measured wind velocity based on calculating the increase in entropy of a random variable can be used to estimate the reliability of the data from observations of other meteorological elements.

BIBLIOGRAPHY

1. Bel'kovich, O. I. STATISTICHESKAYA TEORIYA RADIOLOKATSII METEOROV [Statistical Theory of Meteor Radar], Kazan, Izd-vo KGU, 1971.

2. Bendat, Dzh.; Pirsol, A. IZMERENIYE I ANALIZ SLUCHAYNYKH PROTSESSOV [Measurement and Analysis of Random Processes], Moscow, Mir, 1974.

3. Gavrilov, A. A. "Wind Velocity Dispersion in the Lower Thermosphere by the Results of Radar Measurements of the Meteor Trail Drift," GEOMAGNETIZM I AERONOMIYA [Geomagnetism and Aeronomy], Vol 19, No 6, 1979.

4. Gavrilov, A. A.; D'yachenko, V. A.; Il'ichev, Yu. D.; Portnyagin, Yu. I. "Estimation of Systematic Errors in Wind Measurements by the Radio Meteor Method," TRUDY IEM [Works of the Institute of Experimental Meteorology], No 2(47), 1974.

5. Kashcheyev, B. L.; Nechitaylenko, V. A. "Problems and Means of Automating Observations and Processing Radio Meteor Data," TRUDY VSESOYUZNOGO SOVESHCHANIYA PO ISSLEDOVANIYU DINAMICHESKIKH PROTSESSOV V VERKHNEY ATMOSFERE [Works of the All-Union Conference to Study Dynamic Processes in the Upper Atmosphere], Moscow, Gidrometeoizdat, 1976.

6. Lizogub, V. V. "Phasometric Studies of Radio Signals and the Problems of Automating Their Processing in Meteor Doppler Radar," author's review of dissertation for the scientific degree of Candidate of Sciences, Khar'kov, 1977.

7. Lizogub, V. V.; Nechitaylenko, V. A. "Optimal Threshold of a Digital Phase Meter in a Meteor Doppler Radar," RADIOTEKHNIKA [Radio Engineering], No 42, Khar'kov, 1977.

8. Portnyagin, Yu. I.; Shprenger, K.; Lysenko, I. A., et al. IZMERENIYE VETRA NA VYSOTAKH 90-100 km NAZEMNYMI METODAMI [Measuring the Wind at Altitudes of 90-100 km by Ground Methods], Leningrad, Gidrometeoizdat, 1978.

9. Pokrovskiy, G. B.; Starostin, V. M.; Teptin, G. M. "Distribution of the Pulsating Wind Velocities in the Meteor Region of the Atmosphere," IZV. AN SSSR. FIZIKA ATMOSFERY I OKEANA [News of the USSR Academy of Sciences. Physics of the Atmosphere and Ocean], Vol 5, No 6, 1969.

10. Pugachev, V. S. VVEDENIYE I TEORIYU VEROYATNOSTEY [Introduction to Probability Theory], Moscow, Nauka, 1968.

11. Spizzikino, A. "Measuring the Wind by Radar Measurements of Meteor Trails over Europe," TERMOSFERNAYA TSIRKULYATSIYA [Thermospheric Circulation], Moscow, Mir, 1975.

12. Barnes, A. A. "Status Report on Radar Meteor Wind and Density Measurements," BULL. AMER. METEOROL. SOC., Vol 54, No 9, 1973.

13. Justus, C. G. "Distributions and Structure of Irregular Winds Near 100 km," J. GEOPHYS. RES., Vol 75, 1970.

14. Kaiser, T. R. "Radio Echo Studies of Meteor Ionization," PHIL. MAG. SUPPL., Vol 2, 1953.

15. Manning, L. A.; Peterson, A. M.; Willard, O. G. "Ionospheric Wind Analysis by Meteoric Echoes Techniques," J. GEOPHYS. RES., Vol 59, No 1, 1954.

UDC 551.(501.771+507.2)

CALCULATING THE HUMIDITY OF THE AIR ABOVE THE SEA BY AIR AND WATER TEMPERATURE

Moscow METEOROLOGIYA I GIDROLOGIYA in Russian No 5, May 81 pp 114-117

[Article by T. F. Masagutov, Institute of Experimental Meteorology, manuscript received 30 Jun 80]

[Text]

Abstract: On the basis of analyzing marine hydrometeorological data from the TROPEX-72 expedition (about 1500 observations) the relation was obtained for the relative humidity of the air as a function of the water-air temperature gradient in the presence of unstable stratification. It is demonstrated that considering the relation obtained it is possible to construct a more exact method of calculating the water vapor pressure in the air by comparison with the known ones.

The existing manuals for weather stations and outposts on merchant vessels [2] do not provide for measuring the humidity of the air. At the same time it is known that knowledge of this value (or at least estimates of it) is extraordinarily important to studying many atmospheric processes over the ocean in tropical latitudes.

The methods of calculating the humidity of the air by indirect data can be found in references [1, 3]. However, as will be demonstrated below, the accuracy of these methods of estimation turns out to be quite low as applied to tropical latitudes. In this paper an improved procedure is proposed for calculating the humidity of the air over the ocean in tropical latitudes.

Calculation Procedure

The empirical fact of the existence of a correlation between the temperature Θ_a and the humidity of the air e_a has been established in reference [1]. If we begin with the formula

$$e_a = f e_H(\Theta_a), \tag{1}$$

which is in essence a determination of the relative humidity of the air, it is clear that there will be a high correlation between e_a and Θ_a only in the case of approximate constancy of the value of f. Here the value of $e_H(\Theta_a)$ is the

saturated water vapor pressure in the air. The correspondence between the water vapor pressure in the air e_a and the air temperature Θ_a is illustrated by the graph presented in Figure 1. The curve on this graph is taken from reference [1] and approximately corresponds to the value of a relative humidity f=81%. In the figure it is obvious that for a typical air temperature over the ocean in tropical latitudes of 27°C, the error in determining the humidity of the air e_a by curve 1 will be ± 5 mb. At the same time, the characteristic value of the water-air water vapor pressure gradient, according to the data from the TROPEX-72 expedition, is about 8 mb. It is clear that the accuracy of determining the humidity of the air by the procedure of [1] is insufficient in the case where non-averaged data on the nature of variation of the humidity field in the water layer of the atmosphere are needed. In practice, calculation of the water vapor pressure in the air also by the method proposed in [2] leads to the same errors. Therefore we shall limit ourselves to referencing it.

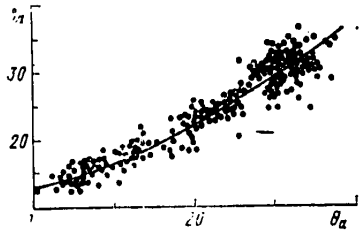

Figure 1. Empirical dependence of the water vapor pressure in the air on the air temperature according to the data from the TROPEX-72 expedition

Results Characterizing the Mean Value of the Relative Humidity as a Function of the Water-Air Temperature Gradient

ТРОП-ЭКС-72 (1)	(2) Градации перепада температуры, °С: 0—0,5	0,6—1,0	1,1—1,5	1,6—2,0	2,1—2,5	2,6—3,0	3,1—3,5	3,6	f%
(3) II фаза (11—25 июля)	76,5 69—84 (48)	79,3 68—87 (151)	80,9 65—88 (189)	89,9 64—93 (114)	87,3 67—95 (66)	88,6 80—95 (45)	92,6 87—96 (32)	91,8 86—96 (11)	82,4 64—96 (656)
(4) III фаза (6—21 августа)	76,7 70—86 (55)	77,6 65—91 (247)	78,7 66—92 (222)	84,5 65—94 (79)	88,6 78—91 (28)	90,2 87—96 (16)	90,3 84—96 (13)	93 93 (2)	79,4 65—96 (731)
(5) За две фазы	76,5 69—86 (103)	78,2 65—91 (398)	79,7 65—92 (411)	83,5 64—94 (193)	87,6 67—95 (94)	89,0 80—96 (61)	91,9 84—96 (45)	92,0 86—96 (13)	80,8 64—96 (1387)

Key:
1. TROPEX-72
2. Temperature gradient gradations, °C
3. Phase II (11-25 July)
4. Phase III (6-21 August)
5. For two phases

Let us show how it is possible to increase the accuracy of calculating the air humidity somewhat by indirect data. It is known that when precipitation falls in the tropics, the air temperature drops. As a rule, the relative humidity of the air rises, and the water temperature changes insignificantly. It turned out that the indicated behavior of the relative humidity of the air in general depends not on the variation of the absolute air temperature but only on the water-air temperature gradient (the water temperature varies very little).

In order to establish the quantitative nature of the function $f(\Delta\theta)$, the corresponding analysis was made of about 1500 pieces of data from standard hydrometeorological observations on the TROPEX-72 expedition. The obtained results are presented in the table. The gradations for the water-air temperature gradient at 0.5°C were taken from the condition that the errors in determining $\Delta\theta$ are $\pm$0.2°C when measuring by an aspiration psychrometer on ships. For each gradation the mean value of the relative humidity and the extremal dispersion within the limits of each interval $\Delta\theta$ were determined; the latter was indicated in the tables as the mean value. The number of cases falling into an individual gradation is presented in parentheses.

Beginning with the results presented in the table, it is possible to draw the conclusion that the most probable value of the relative humidity for $\Delta\theta \geq 1.5$ to 2.0°C depends to a significant degree on the maximum recurrence rate of the water-air temperature difference in the given region.

The results obtained permit us to propose the following procedure for calculating the water vapor pressure in the air: the most probable value of the relative humidity is determined by the measured temperature gradient $\Delta\theta$ from the table, and corresponding calculations are performed by formula (1).

Comparison of the Calculation Procedures

The proposed procedure for calculating the humidity of the air is suitable only in the case of unstable stratification in the water layer of the atmosphere ($\Delta\theta>0$). Otherwise ($\Delta\theta<$) and for neutral (or close to neutral) stratification ($\Delta\theta\approx$) it is not possible to establish any laws between the relative humidity and the temperature gradient. Therefore for $\Delta\theta\leq 0$ to calculate e_a it is recommended that formula (1) be used, setting f=81% (that is, the Malevskiy-Malevich procedure be used [1]).

Let us compare the calculations of e_a by the Malevskiy-Malevich method and by the given procedure. Independent (not used when obtaining the empirical function $f(\Delta\theta)$) data from the "Typhoon-75" and TROPEX-72 (phase I) expeditions were selected for comparison. Considering what has been stated above, only cases were used where the condition $\Delta\theta \geq 1.5$°C was satisfied during the measurements, and the minimum distance of the ship from the shore was about 300 km.

The results of the calculation by the compared and given procedure are presented in Figure 2. As can be seen from the figures, the dispersion of the data decreased during the calculation by the proposed procedure by approximately twofold and, in addition, the systematic error in determining the value of e_a occurring on the basis of specific peculiarities in the behavior of the relative humidity of the air above each specific region in practice disappeared.

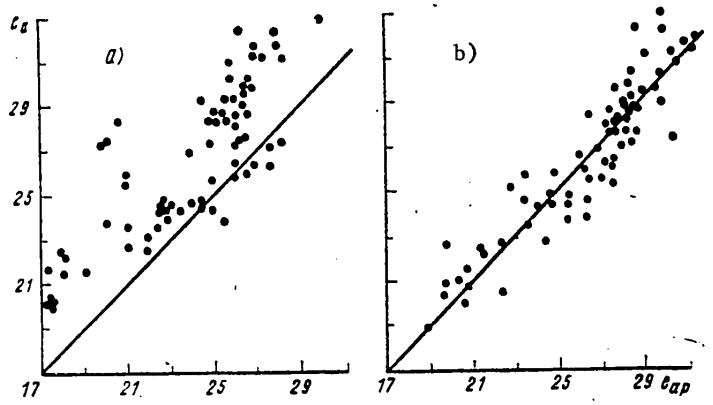

Figure 2. Graphs of the correlation of the water vapor pressure in the air calculated by the procedure from [1] (a) and by the given procedure (b)

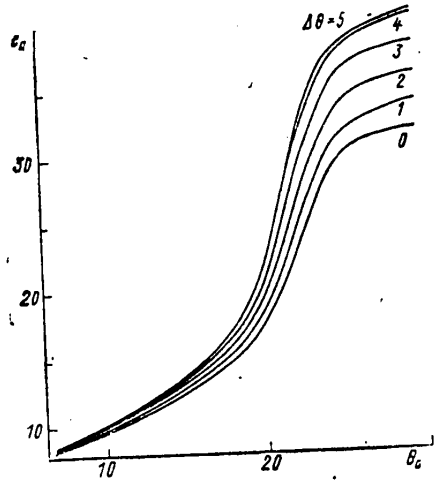

Figure 3. Nomogram for calculating the humidity of the air by the water-air temperature gradient ($\Delta\theta$) and the air temperature θ_a

The nomogram for calculating the water vapor pressure in the air e_a by the measured temperature gradient $\Delta\theta$ and the air temperature θ_a is presented in Figure 3.

In addition, for calculating e_a with the same accuracy it is possible to use the approximation formulas

$$e_a = \begin{cases} 0{,}76\,(1 + 0{,}06\,\Delta\theta)\,e_n(\theta_a) & \text{for } \Delta\theta > 0 \\ 0{,}81\,e_n(\theta_a) & \text{for } \Delta\theta \leqslant 0. \end{cases}$$

They can turn out to be useful in the case of the necessity for computer processing of mass observation data.

BIBLIOGRAPHY

1. Malevskiy-Malevich, S. P. "Determination of the Bowen Ratio Above the Ocean," METEOROLOGIYA I GIDROLOGIYA [Meteorology and Hydrology], No 9, 1973.

2. NASTAVLENIYE GIDROMETEOSTANTSIYAM I POSTAM [Manual for Hydrometeorological Stations and Outposts], No 9, Part III, Leningrad, Gidrometeoizdat, 1971.

3. Snopkov, V. G. "Calculating the Humidity of the Air Above the Sea by the Water-Air Temperature Difference," METEOROLOGIYA I GIDROLOGIYA, No 2, 1980.

UDC 551.501

APPLICATION OF A COMPUTER GRAPH FOR VISUAL REPRESENTATION OF HYDROMETEOROLOGICAL DATA ARCHIVES

Moscow METEOROLOGIYA I GIDROLOGIYA in Russian No 5, May 81 pp 117-119

[Article by R. I. Kofman, Candidate of Geographic Sciences A. V. Monakhov, All-Union Scientific Research Institute of Hydrometeorological Information -- World Data Center, manuscript received 29 Sep 80]

[Text]

Abstract: A general description is presented of the hardware and software making up the developed output system for producing hydrometeorological data microfilm on the EVM YeS [Unified Computer System]. For graphical representation of the data, the "Karat" microfilm unit is used which is distinguished by speed of obtaining the image, precision, and short machine-time requirement. In practical work graphical displays of archive data can be used to monitor the data and represent the data or calculation results in visual form when performing scientific research work.

Two examples of visual display of data taken from the archive magnetic tapes are presented.

With the development of computer engineering, a trend is being observed toward the accumulation of large volumes of archive hydrometeorological data on magnetic tapes. Here certain problems usually connected with the accumulation, storage and processing of archive data, for example, monitoring the data, are complicated and require additional efforts for their solution.

The computer graph must be considered as a useful tool when solving these problems. In many cases it is expedient to represent the data contained in the archive visually, in the form of specially selected displays. Inspection of these displays permits detection of some of the errors in the data.

Graphical displaying of data can be useful also in other respects. Data (initial or the results of calculations) which is represented graphically, frequently is more viewable than the same data represented in the form of tables with numbers. It is possible that the methods of visual (graphical) representation of data will help in generalizing the materials from hydrometeorological observations which already are available and continue to be accumulated in large quantity.

In this article some of the results of the work done at the VNIIGMI-MTsD [All-Union Scientific Research Institute of Hydrometeorological Information-World Data Center] to improve the data representation techniques are discussed. In particular, a system has been developed for outputting hydrometeorological data on microfilm. This system will make it possible to output data in graphical and text forms on microfilm from the EVM YeS [Unified Computer System].

The system includes the following:

The YeS-1022 computer, Minsk-32 computer;

Karat microfilm output unit;

Standard equipment for photochemical processing of microfilm;

A set of graphical programs "GRAFOR-YeS";

Applied programs for outputting hydrometeorological data on microfilm.

The image is output on a 24×18 mm frame at a speed of 6-12 frames per minute depending on the complexity of the image. During the operation of the system it is possible to see the image on the screen of a cathode-ray tube (a special graphical display), and also after developing the photographic film, on the microfilm reader or simply by the naked eye; it is possible to obtain enlarged images by ordinary photographic printing and to obtain originals for offset printing. The high resolution of the "Karat" unit makes it possible to obtain images with a large number of fine details. It is necessary to note the high output rate which permits us to obtain a large number of images on microfilm -- on the order of hundreds and thousands in a few hours of operation. This property of the equipment is especially useful for graphical representation of hydrometeorological data archives, for these archives contain a large volume of materials. Another method which also permits the problem of graphical representation of large volumes of archive hydrometeorological data to be solved -- output on a graphical display -- is more expensive than output on microfilm, and it does not permit the images to be retained.

Let us discuss the used hardware and software in more detail. The EVM YeS Computer is used in the system to perform calculations and assemble the image constructing program in "Karat" instructions. Direct output on microfilm is handled by a "Minsk-32" computer, to which the "Karat" is connected. Communication between the computers is realized by magnetic tape. The operating principle and characteristics of the "Karat" are presented in [1]. Standard 35-mm "Mikrat-300" perforated photographic film is used for taking the pictures. The film is chemically processed in accordance with the All-Union State Standards on series equipment which usually is used for microfilming.

The basis for the software of the system is the set of graphical programs GRAFOR adapted to the EVM YeS computer [2]. The GRAFOR complex consists of a large number of subroutines which execute various graphical functions, for example, the construction of a segment of a straight line, symbols and more complex elements. The GRAFOR complex for the EVM YeS computer is constructed so that almost none of the programs depend on the device which is used to construct the images. The

characteristic features of this output device are taken into account in a special driver program. Therefore the software includes the "Karat" driver. The driver converts the operators of the GRAFOR machine language to instructions for the "KARAT." As a result of production necessity (obtaining of aerological information tables TAE-16A) the "KARAT" is at the present time connected to the "Minsk-32" computer. Therefore two auxiliary routines have been developed, one of which converts the instruction format and magnetic tapes of the EVM YeS to the "Minsk-32" format, and the second directly controls the output to the "Minsk-32" computer, that is, it finds the file and frame number on the magnetic tape indicated in the assignment, it reads the data off the magnetic tape and outputs the data to the "Karat."

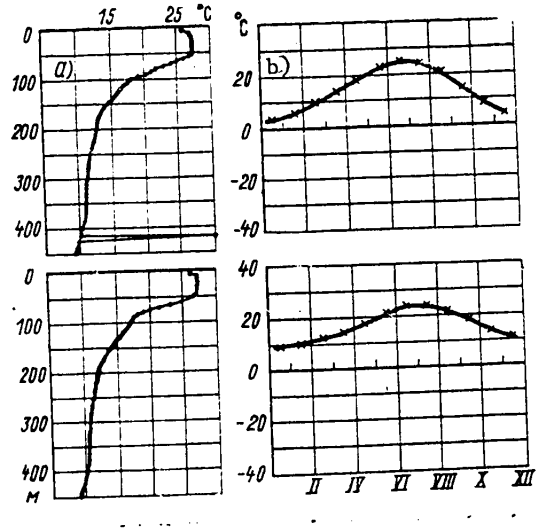

Fragments of two computer-synthesized microfilms: a) with bathythermogram images, b) with graphs of the annual behavior of air temperature

Since the GRAFOR complex consists of individual subroutines, a master program is needed to output the data in the form of an image. Input of the assignment, input of the data and calling of the GRAFOR subroutines to construct the images are organized in the master program. The programs for constructing the figures presented here are such master programs. The package of programs (and GRAFOR subroutines) for constructing the image of archive hydrometeorological data is still undergoing development.

Let us present two examples of visual representation of data from two different archives. The first example pertains to oceanographic data. A magnetic tape with an archive of bathythermographic observations performed during GATE was taken for visual display. Each bathythermogram is represented in the archive by a group of numbers corresponding to the water temperatures at defined depths.

A program was written which made it possible to obtain microfilm with images of individual bathythermograms, as shown in Figure a. The arrangement of the data on the graphs, that is, the form of the bathythermograms and also the form and content of the accompanying text were selected arbitrarily and theoretically can be different. On the bathythermogram in the upper part of Figure a, distortion caused by an error in the data on the archive magnetic tape can be seen.

Thus, data contained in the archive on the magnetic tape were converted to microfilm containing a graphical representation of the same data.

As a result of oceanographic operations under the GATE program, magnetic tapes were obtained for the materials of approximately 10,000 bathythermographic observations. These data are stored on three magnetic tapes in accordance with the three GATE phases. Considering the speed of output of the images to microfilm and the compactness of such data representation, it would be possible to obtain all of the data from the bathythermographic observations of the three phases of GATE in graphical form without extraordinary expenditures.

For the second example, climatic data were used -- the mean values (norms) for many years of the mean monthly air temperature on the earth's surface at nodes of a $5\times10^{\circ}$ grid of the northern hemisphere in 1931-1960. These data are a component part of the archive of monthly air temperature anomalies for the earth's surface. Part of the data in this archive containing the norms for the mean monthly air temperature were entered on the magnetic tape of the EVM YeS computer. Using the written program, the data were output to microfilm in the form of graphs of the annual behavior representing variations of the mean monthly values of the air temperature for each node of the coordinate grid. Thus, a microfilm was obtained with 664 graph frames (see Figure b). Each frame, in addition to the graph, contains the required reference information. Examination of the microfilm makes it possible to ascertain regular variation of the form of the graphs as a function of the geographic position of the corresponding node of the grid. Significant distortions are not seen on the graphs; this indicates absence of gross errors in the data. A total of about 1.5 hours of machine time were required to create this microfilm, that is, output the data from the computer.

The "Karat" microfilm output unit is manufactured in small series, but it is possible to use already existing units. For this purpose, by using the software described in the article (or other software providing for the assembly of the "Karat" programs in the required format) a magnetic tape must be prepared on the EVM YeS computer and sent, for example, to the computer center at the VNIIGMI-MTsD, where the "Karat" is located for output on microfilm. It must be added that the program for shaping the image can be checked out on a plotter (for which the "Karat" driver is replaced by the plotter driver during checkout). It is natural that this method is expedient only when it is necessary to construct a large number of images, but the created system is also designed for this use.

BIBLIOGRAPHY

1. Avdeyev, V. S., et al. "'Karat' Output Unit for Outputting Graphical and Alphanumeric Data from a Computer to Microfilm," ELEKTROMETRIYA [Electrometry], No 1, 1976.

2. Bayakovskiy, Yu. M.; Mikhaylova, T. N.; Mishakova, S. T. "GRAFOR: Set of FORTRAN Graphical Programs," No 1, preprint No 41, Institute of Applied Mathematics of the USSR Academy of Sciences, Moscow, 1972.

REVIEW OF MONOGRAPH BY V. V. BOGORODSKIY AND V. P. GAVRILO: 'LED. FIZICHESKIYE SVOYSTVA. SOVREMENNYYE METODY GLYATSIOLOGII' [ICE. PHYSICAL PROPERTIES. MODERN METHODS OF GLACIOLOGY], LENINGRAD, GIDROMETEOIZDAT, 1980, 384 pages

Moscow METEOROLOGIYA I GIDROLOGIYA in Russian No 5, May 81 p 120

[Review by O. V. Boykova]

[Text] The science of ice developed in the 19th Century. In the middle of the 20th Century considerable information was accumulated on the glaciation area, the mass and properties of ice. The first large paper that generalized the accumulated materials was the monograph by B. P. Veynberg LED [ICE], which was published in the 1940's. Books were later published by N. N. Zubov, I. S. Peschanskiy, V. V. Bogorodskiy, Yu. P. Doronin and D. Ye. Kheysin, P. Khobbs and other authors in which the studies and analysis of the properties of ice found reflection.

In the reviewed reference monograph by V. V. Bogorodskiy and V. P. Gavrilo, an entire series of new data on ice has been classified, on the basis of which many physical phenomena originating in the ice covers such as the propagation of electromagnetic waves, sound emission of deforming ice, characteristic infrared and microwave radiation, and so on are deeply and comprehensively explained. The monograph reflects the results of research performed using modern physical methods based on the achievements of radio engineering and electronics.

The book consists of eight chapters. Seven of them actually discuss all of the basic properties and characteristic features of the structure of ice: geographic location and morphology, atomic-molecular structure, thermodynamic and mechanical properties, seismoacoustics, electrical and optical properties. One of the chapters is on modern radiophysical methods of investigating ice covers and the peculiarities of performing experiments and observations. Ice terms, the principles of standardizing methods of testing ice and extracts from the Construction Norms and Rules (SNiP) are presented in the Appendices.

The new book on ice by V. V. Bogorodskiy and V. P. Gavrilo is a timely, necessary publication. This book, which generalizes recent achievements in studies of the ice covers by Soviet and foreign scientists, is a valuable reference which will help everyone involved in studying the problems of ice science to become oriented with respect to the new information on ice for use of this information in present and future practical solutions.

It must be noted that the paper contains not only broad, varied reference material on the parameters and properties of the ice covers, but also a qualitative theoretical analysis of the investigated phenomena which is combined well with specific characteristics and a large number of figures.

The reference monograph undoubtedly will be useful to meteorologists, hydrologists, oceanologists and specialists involved in planning, design and construction in polar regions.

SEVENTY-FIFTH BIRTHDAY OF YEVGENIYA SEMENOVNA SELEZNEVA

Moscow METEOROLOGIYA I GIDROLOGIYA in Russian No 5, May 81 p 121

[Article by Colleagues, Friends and Students of Yevgeniya Semenovna Selezneva]

[Text] Yevgeniya Semenovna Selezneva, doctor of geographic sciences, professor, famous specialist in the field of atmospheric physics, celebrated her 75th birthday on 12 December 1980.

Ye. S. Selezneva began work at the Main Geophysics Observatory imeni A. I. Voyeykov in 1927. In 1934 she completed her post graduate studies under the direction of professor P. A. Molchanov; then for a number of years her scientific activity in the field of agroclimatology developed at Pavlovskaya Aerological Observatory. The problems of cloud microstructure, the physical processes of cloud formation, the structure of the wind field, aerological research -- this was the basic sphere of her interests.

In 1957-1960, Yevgeniya Semenovna was an active participant in the IHY [International Hydrological Year] and the IQSY [International Year of the Quiet Sun], organizer of new types of observations of the chemistry of precipitation and condensation nuclei. Under her guidance and with her personal participation a great deal of work was done to organize observation station networks to observe condensation nuclei and gather atmospheric precipitation samples, for analysis and generalization of the obtained material. She created the presently existing network for observations of precipitation chemistry, numbering about 70 stations. The results of this work are used for many practical purposes. The studies in this area have acquired special significance in connection with studying the global background of atmospheric pollution.

Ye. S. Seleznev is the author of more than 100 scientific papers, including five monographs, one of the co-authors of the well-known KURS METEOROLOGII [Course in Meteorology] edited by P. N. Tverskiy and the book ATMOSFERNYYE AEROZOLI [Atmospheric Aerosols] -- a generalization of research in the field of condensation nuclei containing unique material on the distribution of the nuclei in the free atmosphere over various parts of the Soviet Union.

Yevgeniya Semenovna has trained dozens of specialists, who have graduated from Leningrad State University where she successfully combined pedagogical activity with scientific research work for more than 20 years. More than 10 people have defended their candidate's dissertations under her direction.

The combination of enormous theoretical knowledge with large-scale experimental work has made her a respected scientific authority and won her recognition not only among Soviet meteorologists, but also abroad. For many years Ye. S. Selezneva was a member of the International Commission on Atmospheric Chemistry and Global Air Pollution of the International Geodetics and Geophysics Union and a member of the working group of the WMO. Yevgeniya Semenovna has been awarded three orders and several medals for many years of fruitful work.

At this time Ye. S. Selezneva, who is enjoying a deserved rest, is continuing to publish her scientific papers. She maintains scientific relations with the observatory, she directs the work of postgraduates, and consults with co-workers on the problems of atmospheric chemistry and general meteorology.

We wish Yevgeniya Semenova good health and active scientific work for many years to come.

HIGH AWARD

Moscow METEOROLOGIYA I GIDROLOGIYA in Russian No 5, May 81 p 121

[Unsigned Article]

[Text] By order of the Presidium of the Supreme Council of the USSR, 13 March 1981, the rank of Hero of Socialist Labor was conferred on Soviet Antarctic Expedition Chief, Deputy Director of the Arctic and Antarctic Scientific Research Institute of the USSR State Committee on Hydrometeorology and Monitoring of the Natural Environment, Doctor of Geographic Sciences Yevgeniy Sergeyevich Korotkevich with presentation to him of the Order of Lenin and the "Sickleand Hammer" Gold Metal for great service in the study and exploitation of the Antarctic.

CONFERENCES, MEETINGS, SEMINARS

Moscow METEOROLOGIYA I GIDROLOGIYA in Russian No 5, May 81 pp 121-126

[Article by V. G. Azanovskiy, A. P. Zhilyayev, Yu. G. Slatinskiv. V, B. Kiselev, L. R. Son'kin, N. A. Shestakova]

[Text] The fifth conference of directors of the computer subdivisions of the USSR State Committee on Hydrometeorology was held in Rostov-na-Donu from 30 October to 3 November 1980. Its work was participated in by 37 people from 24 scientific research institutions and the UGKS administration.

The conference was opened by GKhI director A. M. Nikanorov. N. A. Yakshin (USSR State Committee on Hydrometeorology) gave a report on the preliminary results of the work to improve the efficiency of utilizing computers at the NIU and the UGKS in 1980 and the prospects for creating an information computer center network in 1981-1985. L. A. Timokhin (VNIIGMI-MTsD) told about the principles and plans for the construction of an automated base and data bank on the environment. V. P. Krylov (ZapSibNII) shared experience in creating an automated data processing system for the regional hydrometeorological center using modern communication media and computers. G. Ya. Venetskiy (TsKB GMP) analyzed the operation of the automated system for delivering data to the branch ACS. L. A. Timokhin told about starting up a new phase of the system for operative current and forecasted weather information support.

In the reports by the participants in the conference it was noted that the work started several years ago on creating an IVTs [Information Computer Center] network is continuing successfully. In 1980 alone, three new IVTs were converted to independent budget -- in the Transcaucasus, Polvozh'ye [the Volga region] and the Far East. Planned work has also continued on reequipment of the information computer centers that have already been built with hardware and procedural materials. A number of new documents regulating work planning, hardware and software for the activity of the information computer center have been developed and prepared for introduction. In order to increase the operating efficiency, a branch procedural seminar was held on problems of the production-finance activity of the information computer centers of the USSR State Committee on Hydrometeorology on independent budget.

At the same time, the conference participants noted that a number of NIU and UGKS are giving insufficient attention to the problems of the creation and support of the activity of regional algorithm and program libraries. The quality of the developed programs still does not always correspond to the requirements of the current standards.

In the adopted resolution, a number of primary goals were formulated with respect to the further development of the information computer center network and improvement of the operation of these centers. In particular, it was recommended that the UGKS and NIU directors introduce a production quality control subsystem for the output of the computer subdivisions of the USSR State Committee on Hydrometeorology in the first half of 1981 with the help of the VNIIGMI-MTsD.

The expansion and publication of a collection of computer subdivision certificates in which the basic activity of the subdivisions, for example, the data volume, list and processing times, would be reflected. It was recommended that the computer center of one of the republic UGKS be charged with the functions of a base center for problems of the development, experimental operation and introduction of automated operative data processing systems.

V. G. Azanovskiy, A. P. Zhilyayev,
Yu. G. Slatinskiy

An interational WMO conference PA-VI on the development of methods of forecasting unfavorable meteorological conditions leading to high atmospheric pollution levels was held in Leningrad from 17 to 20 November 1980. The conference was held in accordance with a resolution of a meeting of the European Regional Organization (PA-VI) of the WMO. The Main Geophysics Observatory imeni A. I. Voyeykov was responsible for holding the conference. The USSR State Committee on Hydrometeorology organized an organizational committee (chairman Ye. P. Borisenkov), and the WMO secretariat organized an international program committee (chairman M. Ye. Berlyand).

The work of the conference was participated in by 69 specialists from 14 countries: Belgium, Hungarian People's Republic, German Democratic Republic, Denmark, Italy, Norway, Polish Peoples Republic, Portugal, USSR, Federal Republic of Germany, France, Czechoslovakia, Sweden and Yugoslavia.

GGO [Main Geophysics Observatory] director Ye. P. Borisenkov opened the conference. Vice Chairman of the USSR State Committee on Hydrometeorology V. G. Sokolovskiy and WMO representative A. S. Zaytsev welcomed the participants to the conference.

During the work of the conference 25 reports were heard, including 11 from the USSR.

In the report by M. Ye. Berlyand (USSR) "On basic principles of forecasting atmospheric pollution" a study was made of the great possibilities for forecasting development connected with the use of the results of theoretical and experimental studies of the propagation laws of impurities from various types of sources as a function of meteorological factors. Two basic approaches are noted, one of which is based on the empirical-statistical models of the impurity distribution, and the other, on the solution of the atmospheric diffusion equation. In the report it was demonstrated that the second approach is more prospective. A study was made of the results of the developments in numerical and statistical forecasting methods at the Main Geophysics Observatory. A discussion was presented of the papers on forecasting meteorological conditions defining high atmospheric pollution levels, and the prospects for their development were investigated. M. Ye. Berlyand also stated arguments to the effect that further development of the methods of pollution forecasting is to a significant degree connected with the joint use of various methods when developing the forecasting schemes. In particular, it appears prospective to combine forecasting methods

based on numerical integration of the diffusion equation and atmospheric boundary layer theory with forecasting the characteristics of background air pollution and the mean diurnal concentrations, and the use of statistical and synoptic developments.

W. Klug (Federal Republic of Germany) investigated two types of meteorological situations leading to an increased air pollution level. The first type included episodes with low wind velocities and stable stratification. This situation is frequently caused by the presence of a powerful anticyclone. Low sources located near the sampling point make the primary contribution to pollution. Another situation is characterized by high wind velocities, wind direction that is stable in time, absence of precipitation and powerful precipitation inversion. This arises on the periphery of a stationary anticyclone. Here the impurity is transported from remote industrial sites.

M. Ye. Berlyand, Ye. L. Genikhovich and R. I. Onikul (USSR) devoted their report to calculation of the integral concentration distribution characteristics over the territory of a city and their use in short range atmospheric pollution forecasting. This report contained a discussion of the results of analyzing the impurity propagation process from an area source. Here, an area source is understood as a set of a large number of point sources having approximately identical altitude and discharge parameters. A study is made of the meteorological conditions for which high air pollution levels can form in the city.

In a report by K. Ye. Gronskey (Norway) a study was made of the basic requirements on the dangerous air pollution warning system in areas of various types; the problems of predictability of impurity content in the air were discussed.

The participants in the conference held a broad discussion of the problems of developing statistical and synoptic air pollution forecasting methods for cities. A survey of the papers in this area was presented in a report by L. R. Son'kin (USSR). Papers on statistical forecasting from various countries of the world were investigated. The conclusion was drawn that the most prospective were schemes which take into account the physical laws of the propagation of impurities in the atmosphere and the actual manifestation of relations between concentrations and meteorological parameters by observation data in specific cities. Such schemes have been developed in the USSR with the application of pattern recognition and successive graphical regression techniques. It was noted that it is very useful to utilize synoptic analysis in forecasting air pollution in cities.

G. Finzi (Italy) demonstrated a statistical atmospheric pollution forecasting scheme developed for Milan. The autoregression model and logarithmic regression method for determining impurity concentrations in the air based on meteorological predictors were used simultaneously in this scheme. A generalized characteristic of air pollution for the city as a whole was investigated as the predictant. Synoptic situations are taken into account. Conclusions were drawn that it is expedient to make broad use of meteorological predictors in the schemes and that the application of the autoregression model alone is not effective. In another report by G. Finzi (coauthored with G. Bakki) a study was made of the possibilities of more precise forecasting of wind velocity under complex orographic conditions of Milan considering atmospheric circulation at the 500 gPa surface level.

The report by V. B. Kiselev and T. P. Ivleva (USSR) was on the method of formation of most informative complex predictors for forecasting increased atmospheric pollution levels. The maximum informative predictors obtained were used for the construction of a scheme to forecast harmful impurity content in the air of cities based on successive graphical regression.

Yu. Bubnik and F. Gesek (Czechoslovakia) discussed a statistical atmospheric pollution forecasting scheme developed for various parts of Czechoslovakia based on a set linear regression technique. The regression equations were calculated for given meteorological situations which obviously determined the relative success of the schemes.

V. K. Petrenko and V. I. Chernyayeva (USSR) presented results from the development of an atmospheric pollution forecasting scheme using the method of successive graphical regression by data for a large city. Sets of meteorological parameters formulated by the authors were presented which define the growth of the concentration of impurities created by individual sources within the city.

L. M. Neronova and L. V. Tikhomirova (USSR) devoted their report to the problem of synoptic forecasting of meteorological conditions determining atmospheric pollution. Assuming that the atmospheric pollution level is determined by three factors -- synoptic processes, thickness of the thermodynamic mixing layer and wind velocity in this layer, the authors consider the possibilities of forecasting these conditions. They gave primary attention to forecasting the vertical wind velocity and temperature distribution in the boundary layer of the atmosphere. For this forecast, the 925 mb map introduced into practice by the USSR Hydrometeorological Center was used.

In the report by L. R. Son'kin, et al. (USSR) results are presented from a study of the synoptic conditions of the formation of long periods of increased atmospheric pollution. Situations are isolated which in the overwhelming majority of cases determine the growth of the impurity concentrations over the course of several days.

B. B. Goroshko (USSR) investigated the problem of regulating harmful discharge into the atmosphere. The scientific grounds and primary principles of the development of measures for short term reduction of discharge during periods of unfavorable meteorological conditions are discussed.

R. Berkovich and L. Pram (Denmark) familiarized the participants in the conference with the results of modeling diffusion in the boundary layer of the atmosphere using the turbulent diffusion coefficient which depends on the wave number (that is, on the size of the vortex). The proposed method permits explanation of some of the fine effects observed in a flume, for example, an increase in maximum concentration in the spray with removal from the source.

D. Sepeshi (Hungarian Peoples Republic) discussed an air pollution forecasting model for a city based on consideration of discharge from two basic types of sources -- area (less than 50 m high) and high-altitude. First a study was made of the qualitative relation between the discharge and the ground concentration by data on the discharge, the air pollution and meteorological measurements. The model was tested for prediction of the propagation of sulfur dioxide discharge under the conditions of the city of Pécs (in the southern part of Hungary). The transport of the sulfur dioxide from area sources was simulated using a quasistationary box model.

In a report by G. Dietze (German Democratic Republic) a study was made of the short-range air pollution forecasting technique presently employed by the Meteorological Service of the German Democratic Republic. This technique considers the wind direction and velocity and the Ulig stability classification.

A number of brief reports were also heard given by A. A. Gorchiyev and R. M. Rafiyev (USSR), I. A. Shevchuk, L. I. Vvedenskaya and O. P. Andrakhanova (USSR), I. V. Koroleva and K. E. Tserfas (USSR), S. Bodin (Sweden), L. Pram and R. Berkovich (Denmark).

The participants in the conference discussed a WMO technical note prepared by M. Ye. Berlyand "Atmospheric Pollution Forecasting." This document, which contains more than 300 pages of text, discusses and generalizes studies of the given problem in various countries of the world. Consideration is given to results discussed in more than 250 publications. The physical principles of atomospheric pollution forecasting, numerical, statistical and synoptic forecasting methods, problems of predicting unfavorable meteorological conditions determining intense concentration growth and also regulation of atmospheric discharge were investigated. The prospects for further development of research were formulated.

On the final day of the meeting, its participants discussed a draft of proposals for the development of methods of predicting unfavorable meteorological conditions leading to high atmospheric pollution levels. In the draft an analysis is made of the modern state of the art with respect to research in atmospheric pollution forecasting, and the direction of future research is defined. The necessity for concentrating efforts on the development of methods of operative determination of meteorological parameters important to atmospheric pollution forecasting, pollution potential forecasting, the development of combined forecasting scheme and methods of regulating discharge during periods of unfavorable meteorological conditions was noted. The conference requested that the secretary take the necessary steps to organize an international conference on problems of atmospheric pollution forecasting in 1984.

The conference promoted the expansion and strengthening of international cooperation and development of mutual understanding among the specialists of European countries with respect to one of the urgent problems of environmental protection. The conference participants came out in favor of further expansion of international cooperation in the field of the development and introduction of atmospheric pollution forecasting methods.

V. B. Kiselev, L. R. Son'kin

A concluding meeting of specialists of the USSR and the Peoples Republic of Bulgaria participating in the joint development of a procedure for general evaluation and prediction of the quality of water coming from the territories of cooperating countries was held in Yalta from 11 to 14 November 1980. At the meeting the results of many years of joint work were investigated, and the structure of the final joint report was agreed on. Representatives of the Sevastopol' division of the GOIN [State Institute of Oceanography], the Odessa division of Economics and Ecology of the Sea of the Marine Hydrophysical Institute of the Ukrainian SSR Academy of Sciences, the All-Union Scientific Research Institute of Economics and Control of Water Management and the All-Union Scientific Research Institute of Water Protection of the USSR Ministry of Water Management participated in the conference on the Soviet side.

At the meeting it was noted that the efforts of specialists from the USSR and the Peoples Republic of Bulgaria have done a great deal of work to implement the working plan of scientific and engineering cooperation in the field of environmental protection and efficient use of natural resources. The participants in the meeting discussed the materials obtained and final versions of the developed water quality forecasting procedures. The methods of estimation and prediction of the chemical runoff of rivers flowing into the Black Sea were also investigated. A great deal of attention was given to a method of forecasting water protection measures to prevent negative effects on the quality of water flowing into the sea from the territories of cooperating countries.

A substantiation of the criteria for evaluating the physical chemical characteristics of the water of the Black Sea, including the salinity of the water in the western part of the sea, the gas regime elements (oxygen, hydrogen sulfide, active pH reaction) and nutrient salts (phosphates, nitrites, silicates) was prepared within the framework of joint cooperation by the Sevastopol' division of the State Institute of Oceanography. A description of the water by individual areas of the western part of the sea was also compiled. The Odessa division of Economics and Ecology of the MGI [Marine Hydrophysical Institute] of the Ukrainian SSR Academy of Sciences presented procedural principles of economic-ecologic normalization of the discharge of pollutants into sea water. The scientific research institutions of the USSR Ministry of Water Management developed procedures for forecasting water protection measures to prevent negative effects on the quality of water coming from territories of cooperating countries as a result of implementing a number of ameliorative measures. Procedures for predicting the quality of discharge into the sea from Soviet and Bulgarian enterprises were also investigated. The Bulgarian side also presented a chemical runoff forecast for the Danube river into the Black Sea and a procedure for general evaluation of water quality in the Black Sea region for inclusion in the joint report.

In the adopted resolution the participants in the meeting expressed satisfaction with the work done.

A. P. Zhilyayev, Yu. G. Slatinskiy

A meeting of the Scientific Council of the USSR Hydrometeorological Center was held from 5 to 9 January 1981. The results of the scientific work of the institute in 1978-1980 were summed up at the meeting. The plenary session was preceded by sectional meetings at which more than 40 reports and communiques were heard.

Primarily the results of the work under the GKNT coordination program were reported at the plenary session.

In the report by corresponding member of the USSR Academy of Sciences Ye. N. Blinova, a study was made of a method of hydrodynamic long range forecasting of meteorological elements based on a more precise description of heat influxes from radiation. A procedure for predicting clouds and albedo for the Northern Hemisphere improved by including PGEP data and artificial earth satellite information was discussed. Results were presented from numerical experiments in long-range forecasting of deviations of the mean monthly ground air temperatures and the temperatures of the 500 mb surface for the Northern Hemisphere from the norm.

Improvement of the methods of long-range forecasting based on expanding the exchange of information about the state of the atmosphere and ocean was discussed in a report by Sh. A. Musayelyan and V. P. Sadokov. The authors developed the theoretical principles of including nonadiabatic factors in the simplest thermodynamic model of the atmosphere and ocean. A study was made of the possibilities of improving the analysis procedure and the method of adiabatic forecasting of the mean monthly temperature of the middle troposphere averaged over large regions. The prospectiveness of asymptotic methods in problems of long-range weather forecasting was noted.

S. A. Mashkovich and I. V. Trosnikov discussed the results of numerical experiments with respect to finite-difference and spectral models of general atmospheric circulation. Using the finite-difference model, experiments were performed in reproduction of the atmospheric circulation of the Northern Hemisphere for different seasons, and the energetics and spectra of atmospheric movements reproduced by the model were analyzed. Numerical experiments in the study of the effect of vertical and horizontal resolution in the model, inaccuracies in the initial data, the role of waves of a subnetwork scale, and so on were performed on a spectral model using the complete equations.

A report by N. I. Zverev was devoted to the synoptic method of weather forecasting for the month based on considering heat exchange of the underlying surface with the atmosphere and empirical laws of general atmospheric circulation. A procedure was proposed for predicting the five-day temperature anomaly for all five-day periods of the month.

D. A. Ped' reported on the results of studies aimed at developing objective principles of a seasonal weather forecasting technique. A procedure for determining the seasonal boundaries, calculation of their expected beginning and establishment of predictors of future seasons were proposed. In addition, a statistical method of forecasting the air temperature anomaly for the seasons in the cold part of the year for Siberia and the Far East was developed.

N. A. Bagrov told about the studies made of irregular fluctuations of atmospheric circulation over the territory of the USSR. Large temperature and precipitation anomalies were isolated, their characteristic features and conditions of occurrence were analyzed. The report discussed the construction principles, and results were presented from evaluating statistical schemes for forecasting the height of the 500 mb surface H_{500}, the temperature and precipitation for the month and the season up to one year ahead.

A. A. Vasil'yev, K. G. Abramovich, N. P. Shakina investigated a procedure for semi-automated calculation of the forecasting map of special phenomena. The study of the processes of the occurrence of turbulent layers and zones, convective belts in atmospheric fronts was investigated, and more exact statistical relations were presented for predicting glaciation.

M. Ya. Ratsimor and M. V. Rubinshteyn reported on the results of improving the procedure for automated forecasting of the height of the lower cloud boundary and the meteorological visibility for 1 to 3 hours at Moscow airports.

V. D. Zhupanov, Yu. K. Fedorov and N. A. Shestakova discussed the basic aspects of constructing an information system to support automated forecasting of aircraft landing conditions developed as applied to minicomputers.

A report by Ye. S. Ulanova was devoted to the development of a method of forecasting grain crop yields in the basic economic regions where they are grown three to four months ahead and also the writing of a "Handbook for Agrometeorological Forecasting."

Ye. G. Popov and P. Yu. Kharchenko reported on a refined method of calculating water inflow into the Vilyuyskoye reservoir and a developed method of predicting the side inflow into the planned GES-Sh hydroelectric power plant.

Co-workers of the VNIIGMI-MTsD, the All-Union Scientific Research Institute of Agricultural Microbiology, the Voronezh Higher Military Aviation School, the Far Eastern Scientific Research Institute, the Main Geophysics Observatory, the Institute of Applied Geophysics and the Central Aerological Observatory participated in the concluding session of the Scientific Council.

N. A. Shestakova

NOTES FROM ABROAD

Moscow METEOROLOGIYA I GIDROLOGIYA in Russian No 5, May 81 pp 126-127

[Article by B. I. Silkin]

As is reported in SCIENCE, Vol 209, No 4462, 1980, Stanford Research Institute (Palo-Alto, California, USA) has developed a new method of tracking hurricanes using a high-frequency wave, large-aperture radar.

The instrument has high resolution. It operates in the frequency range between 6 and 30 megahertz. The rated azimuthal beam width of the radar on a frequency of 15 megahertz is 0.5°, which is achieved by an antenna assembly consisting of 256 individual antennas arranged over a space of 2.5 km.

Ionospheric reflections of the signal offer the possibility of receiving an echo from targets more than 3000 km away. A target 3 by 15 km can be picked up about 2000 km away.

The received signal, after being converted, gives 84 individual doppler spectra for each of the specific time intervals from which the average spectrum is derived. By the doppler frequency shift of different echos it is possible to determine the speed of the surface current in the sea and the wind direction above it and also the wind velocity and wave height.

The first such experimental device made it possible to track hurricane Anita with high precision across the Gulf of Mexico for about 5 days. This led to the construction of detailed maps of the surface wind field with respect to individual sections up to 200 km from the center of the hurricane.

The trajectory of the hurricane was calculated. The calculation was verified with sufficient accuracy by data from the National Hurricane Study Center gathered by complex traditional methods. When the hurricane was traveling in the vicinity of 26° North Latitude, it approached the EB-71 meteorological buoy installed there by the National Administration for Ocean and Atmosphere Studies. This made it possible to compare the measurement data gathered by the meteorological buoy equipment with the information obtained by the new high-frequency radar.

The differences in measuring the wind direction were only 7°, the differences in its velocity were 0.4 m/sec, and in wave height, 0.5 meters, which in general does not exceed 10% of the measured value.

The new procedure confirmed its advantages, which consist in a high degree of resolution, the significance of the area encompassed by it and continuity of information flow. By using this procedure it is possible to gather data (and what is especially important, data on the initial phase of development of the hurricane) which serve as a valuable supplement to the meteorological data received from satellites, ground stations and laboratory aircraft.

AMBIO, Vol IX, No 5, 1980, reports that as a result of the industrial revolution, the amount of lead entering the earth's atmosphere from industrial sources has increased from approximately 20 to 400,000 tons per year in the last century. During the same period, the industrial discharge of sulfur dioxide into the air increased approximately from 13 to 190 million tons/year. The content of such heavy metals as zinc, copper, cadmium, silver and mercury in the atmosphere has also increased to a significant degree. The greater part of all of these polluting agents enter the natural environment from the economically developed regions of the Northern Hemisphere -- North America and Europe.

It was recently established that even in such regions remote from industrial areas such as Antarctica, the mean atmospheric concentration of a number of heavy metals coming from anthropogenic sources is 4 to 10 orders higher than aerosols coming from two basic natural sources -- dust of land origin and sea foam. The study of this problem became possible as a result of developing a method of analyzing snow and ice layers deposited in the glaciers of Greenland and Antarctica since the beginning of the industrial age. The relation between their chemical composition and the composition of the atmosphere has been proven. A comparison of the data on these two regions is especially significant in view of the fact that 90% of the discharge of anthropogenic pollutants into the air takes place in the Northern Hemisphere and must be felt first of all in Greenland, for the equator plays the role of a barrier for tropospheric exchange of air masses between the hemispheres.

It has now been discovered that the lead concentration in the surface layer of snow in Antarctica is only about 20×10^{-12} g/g of snow (that is, 20 mg of lead per thousand tons of snow). For silver the corresponding value is a total of 5×10^{-13} g/g of snow, which is 500 micrograms of silver per 1000 tons of snow. Even in samples of especially pure snow obtained artificially under laboratory conditions, the pollution level usually is higher.

Reliable data on the pollution of the ice and snow of Greenland with lead, zinc and cadmium and also sulfates now encompass the last 800 years, and with mercury, 250 years. They demonstrate that the content of all of the substances remained approximately on the same level until about 1940. Then judging by everything, the lead content tripled, and the zinc content possibly doubled. At one Greenland station, evidence of tripling of the sulfate content after 1960 has been noted.

However, it is necessary to consider that samples were gathered at remote points from each other, and pollution as a result of recent expeditionary activity is not entirely excluded. Finally, some distortion of the data under the effect of volcanic activity in Iceland is possible.

Analysis of one sample of Greenland ice, the age of which is estimated at 3000 years, indicates an extremely low lead content in the atmosphere of that era; it is less than 1×10^{-12} g/g.

For Antarctica there are reliable data on the lead, zinc, copper, cadmium and silver and also sulfate content in its snow and ice gathered at one point of the deep region of the southern part of the continent. They encompass the last one hundred years. In spite of significant fluctuations within this time interval, the present content of all of the mentioned substances in the snow is very close to that observed 100 years ago. Thus, the proposition is confirmed that the heavy metals and sulfate concentrations in the atmosphere over the remote regions of the Southern Hemisphere have not in practice changed as a result of human activity in a hundred years. Among the natural causes of fluctuations of the chemical composition of the atmosphere, volcanic activity is noted in first place. In Anarctica, just as in Greenland, the lead and zinc content curve for the last 100 years coincides closely with the curve characterizing volcanic activity. Variations in the sulfur concentration in the snow and ice of Antarctica immediately after the largest eruptions in the Southern Hemisphere -- the Krakatau volcano in 1883 and Agunga in 1963 -- are especially noticeable.

OBITUARY OF ISAY GRIGOR'YEVICH GUTERMAN (1911-1981)

Moscow METEOROLOGIYA I GIDROLOGIYA in Russian No 5, May 81 pp 127-128

[Article by Colleagues of Isay Grigor'yevich Guterman]

[Text] Soviet aeroclimatology has suffered a severe loss; a great scientist, doctor of geographic sciences, professor Isay Grigor'yevich Guterman died on 26 February 1981, at the age of 71.

I. G. Guterman was born on 18 February 1911, in the city of Pochep in Bryansk Oblast, where he began work as a weather station observer. On graduation from Moscow Hydrometeorological Institute in 1937, he was recommended for postgraduate studies, and for a number of years he successfully combined study with work on Arctic expeditions. He participated in the rescue of the "Chelyuskin," in the first high-latitude expedition on the icebreaker "Sadko." A student of P. A. Molchanov, he organized the first regular launches of radiosondes under polar night conditions. The cold front study that he made by sounding at increased frequency became a classic and became a firm part of textbooks on weather forecasting.

During World War II I. G. Guterman headed the hydrometeorological division of the operative section of army headquarters.

From 1945 to 1955, I. G. Guterman directd the observation section at the Central Aerological Observatory. With his characteristic energy and inquisitiveness, he became involved with the improvement and introduction of new methods and means of aerological observations, especially radiosonde observations. He was initiator and author of the application of the active target in the radar system for tracking radiosonde flights, organizer of launching sonde meteorographs to an altitude of 35 km with three temperature gages, as a result of which the conditions of overheating of the temperature receiver in the middle stratosphere were established.

In 1955 I. G. Guterman was invited to the newly created Scientific Research Institute of Aeroclimatology, at which the innovative and organizational talent of the scientist was fully manifested for a quarter of a century. The first aeroclimatic references and atlases in 22 volumes in the country were created here with the most active participation of I. G. Guterman. There were 65 publications studying air currents above the earth out of his total of 110 works. The monograph on this topic RASPREDLENIYE VETRA NAD SEVERNYM POLUSHARIYEM [Wind Distribution over the Northern Hemisphere) became thesubject of a doctor's dissertation, and for successful scientific

pedagogical activity, in 1961 I.G. Guterman received the rank of professor. During the flourishing of I. G. Guterman's activity a cycle of reference publications "Materials on Climate and Circulation of the Free Atmosphere" and aeroclimatic atlases of different regions of the earth and also a new aeroclimatic reference for the USSR, the first phase of which was concluded by the publication of 12 volumes, was created under his direction.

In the last decade I. G. Guterman worked on the creation of a model of the earth's atmosphere. The unique archive of aeroclimatic characteristics collected under his direction competes successfully with foreign analogs with respect to completeness of content, cost effectiveness and popularity.

A distinguishing feature of the scientific activity of I. G. Guterman was his close relation to practice evolving from profound knowledge of the requirements of various national economic organizations.

I. G. Guterman generously shared all of his many years of experience and knowledge with numerous students and colleagues, the exactingness for which was based on the special exactingness of himself. I. G. Guterman was an example of wholehearted devotion to the cause which he served until he drew his last breath.

The party and government valued the services of I. G. Guterman in World War II and in peacetime work highly, awarding him the order of the "Symbol of Honor" and a number of medals.

Everyone who knew I. G. Guterman mourns the death of this great scientist, a man of inexhaustible energy and great modesty. They will remember him that way forever.

10,845
CSO: 1864/10

- END -